IRE Transactions

on Microwave Theory and Techniques

Volume MTT-4 **JULY, 1956** Number 3

TABLE OF CONTENTS

PUBLISHED BY THE

essional Group on Microwave Theory and Techniques

IRE PROFESSIONAL GROUP ON

MICROWAVE THEORY AND TECHNIQUES

The Professional Group on Microwave Theory and Techniques is an association of IRE members with professional interest in the field of Microwave Theory and Techniques. All IRE members are eligible for membership and will receive all Group publications upon payment of the prescribed annual assessment of $2.00.

PGMTT Chapters

Baltimore	H. E. Schrank
Boston	Walter Rotman
Buffalo-Niagara	Frank Pelton
Albuquerque-Los Alamos	Sheldon H. Dike
Long Island	Robert Wegenroth
Philadelphia	S. M. King
Los Angeles	C. W. Chandler
Chicago	Clarence Arnow
Northern New Jersey	T. N. Anderson
San Francisco	K. Tomiyasu

IRE TRANSACTIONS®

on Microwave Theory and Techniques

Published by the Institute of Radio Engineers, Inc., for the Professional Group on Microwave Theory and Techniques, at 1 East 79th Street, New York 21, New York. Responsibility for the contents rests upon the authors, and not upon the IRE, the Group, or its members. Price per copy: IRE PGMTT members, $1.25; IRE members, $1.85; nonmembers, $3.75. Annual subscription price: IRE members, $8.50; colleges and public libraries, $12.75; nonmembers, $17.00.

Address all manuscripts to Theodore S. Saad, Sage Laboratories, 30 Guinan St., Waltham, Mass.

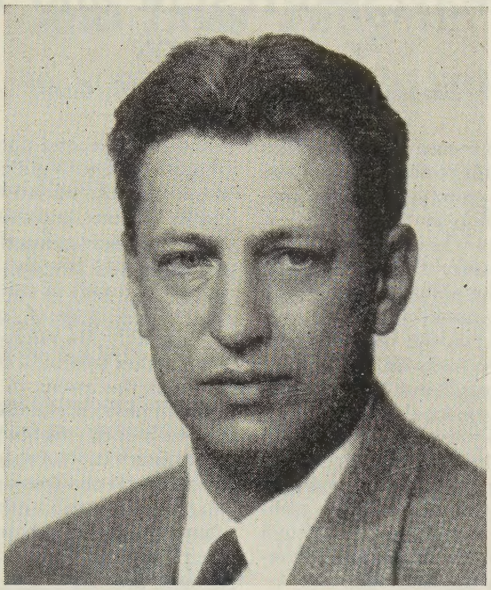

E. L. Ginzton

Born in Russia in 1915, in Ekaterinoslav, now Dnepropetrovsk, Edward L. Ginzton came to the United States when he was 13. He attended the University of California, receiving the B.S. and M.S. degrees in electrical engineering. With the encouragement and assistance of Dr. F. E. Terman, he transferred to Stanford University for graduate work in radio engineering, receiving the E.E. degree in 1938 and the Ph.D. degree in 1940, after specializing in the study of negative feedback and the theory and application of stabilized negative impedances.

In 1939 he was a research associate in the Physics Department of Stanford University working with Prof. W. W. Hansen, Russell and Sigurd Varian, and Prof. D. L. Webster on the development of the klystron tube and its application in microwave systems. In 1940, he moved with this project and some of the personnel to the Garden City Research Laboratories of Sperry Gyroscope Company. He remained there throughout the war, successively becoming assistant project engineer, project engineer, and research engineer, in charge of the Microwave Research Department from 1942 to 1945, and the head of the Microwave Research and Tube Research Laboratories from 1945 to 1946. The work at this time included the development of microwave measurement techniques and instruments, of special Doppler radar systems for MTI applications, and early experimentation with Doppler navigation. He made two trips to Europe as a result of this work. The first, in 1944, was sponsored by OSRD to exchange information between the United States and England about Doppler radar, klystrons, and microwave measurement techniques. The second, in 1945, was sponsored by the Vacuum Tube Development Committee to study and evaluate wartime klystron developments.

In 1946, after the end of World War II, as assistant to Prof. W. W. Hansen, he returned to Stanford University to help form the Microwave Laboratory. In 1949 he was appointed Professor of Electrical Engineering and Applied Physics, and after the death of Dr. Hansen he was made Director of the Microwave Laboratory.

The Stanford Microwave Laboratory, under Dr. Ginzton's direction, undertook the development of the high power pulsed klystron which became a key element in the construction of the Stanford Billion Volt Linear Electron Accelerator. This machine, started under the direction of W. W. Hansen after the completion of a 10-foot pilot model, occupied a large fraction of the activities of the Laboratory until completed in 1952 and has since become a prominent tool in nuclear physics research.

Since the completion of the 200-foot Linear Electron Accelerator, Dr. Ginzton has participated in the development of several other specialized linear electron accelerators. These include a six million volt X-ray machine, designed for cancer therapy that is currently being used for experimental treatment.

As a member of the Physics and Electrical Engineering Departments, he supervises the research work of graduate students in the fields that bridge physics and engineering. His students have been engaged in many aspects of microwave research, especially in studies of high power tubes, linear electron accelerators, and their application in medical and biological research problems.

Dr. Ginzton has been active in Varian Associates from the early planning period that preceded the formation of this electronics firm. Since the formal organization in 1948, he has served on its Board of Directors, taking an active part in formulating the policies of the company.

Dr. Ginzton has published many papers in the field of electronics and microwave applications and is the sole or joint inventor of approximately 50 patents on klystron tubes, klystron circuits, radar systems, microwave measuring devices, linear electron accelerators, and electronic computing circuits. He teaches graduate courses in microwave measurements and is presently writing a text on that subject. He is a member of Sigma Xi, Tau Beta Pi, Eta Kappa Nu, and in 1951 was made a Fellow of the IRE for his contributions to the development of the high power pulsed klystron.

Microwaves—Present and Future

E. L. GINZTON
Stanford University, Stanford, Calif.

Many of us are so immersed in the ever-narrowing branches of electrical engineering that it is difficult to take stock of the accomplishments in the field as a whole or to visualize the possibilities and limitations of future developments. For those of us engaged in teaching and research, and who expect to remain in the field, such an assessment is necessary if we are to guide our students properly and anticipate the probable roles of our own specialties. I will review briefly present-day microwave applications indicating some of the spectacular developments during the past twenty years and try to make an appraisal of potential limitations in microwave research *per se*, and point to a possible profitable avenue of research for the future.

Since 1940, microwave research has received a tremendous emphasis because of the obvious usefulness of this part of the electromagnetic spectrum for radar and communication systems. In the span of a relatively few years, microwave techniques have reached a high degree of development, although many practical unsolved problems remain in the specific requirements of commercial and military applications.

Current microwave applications, preponderantly supported by the military needs are necessarily governed by the "hide and seek" game imposed by international competition, as well as conflicting defense and offense objectives. Despite these general complications, the technology has already reached a high degree of perfection and future refinements will be governed only by their economic justification. For example, in radar applications, unlimited transmitter power at any wavelength can be made available and amplification of microwave signals at a noise level within a factor of 3 or 4 of perfection is now within reach as was recently demonstrated by traveling-wave tube research. Although much can be done to improve the reliability and the intelligence handling capacity of microwave communication systems, these are also a matter of economic justification as the technical solutions can be foreseen clearly. Further improvements in the range of communication systems, especially in the underdeveloped areas of the world, can be anticipated from the future development of forward-scatter techniques.

A number of new navigational systems, for both air and sea use, depend upon microwave developments. These range from the conceptually simple, but practically complicated, systems such as the instrument landing systems for airport traffic control and distance measuring equipment, to the imaginative devices which employ the Doppler effect to measure the ground speed of an aircraft and, by integration, its position. The basic principles for such systems have been thoroughly explored; it would seem to be only a matter of time before a new era in navigation accuracy is reached when these integrated systems are designed and developed to meet the various specific transportation service needs. For instance, it is easy to see that the Sage system, currently being installed for military use, has obvious extensions to commercial navigation for the location, control, and piloting of aircraft over the territorial limits of the United States.

Concurrently, microwaves, as a tool of basic research, have permeated a number of natural sciences. The spectroscopic research, so popular immediately after the end of World War II, has produced quantities of information about the molecular world, just as the knowledge of the atomic structure has resulted from the use of spectroscopy in the visual region. The early experiments were inspired by their intrinsic value, but today numerous applications are arising in other branches of physics, chemistry, and communications. For example, we are upon the threshold of new frequency and time standards, based upon the frequency of certain molecular transitions. Since these depend upon the interaction of a limited number of particles, the frequency can be expected to remain more constant than the period of the earth's rotation. These "atomic clocks" in turn, make other scientific experiments and applications feasible: one can think of repeating the Michelson-Morley experiment to test the theory of general relativity; the possibility also exists of using the Doppler effect to establish completely new types of navigation instruments.

Similarly, the microwave paramagnetic resonance phenomenon makes possible a clearer insight into the chemical bonding between the atoms in complicated molecules, an important topic in physics, chemistry, and other sciences. Microwave application of this technique in biological science may make possible observation of reactions of normal living organisms to environmental changes such as the effect of irradiation or drugs.

There are many other applications of microwaves, too numerous to mention here. To illustrate one possibility, consider their use in the linear electron accelerator. The power from a radar-type transmitter is made to flow simultaneously with electrons in specially designed disk-loaded waveguides; the acceleration of the electrons can be obtained without the use of high voltages. For example, an S band one megawatt source can produce 6 mev electrons in the distance of six feet, a one megawatt X band source can produce the same energy in two feet, and a 200 foot waveguide using 400 megawatts of S band power can produce one billion volts. The size and their relative simplicity make these machines practical for applications in industrial radiography, X ray and electron treatment of cancer, for the cold sterilization of food and drugs, and for other specialized applications. The high energy machines, such as the Stanford 220 foot accelerator, make many experiments in nuclear physics possible.

It is evident that the present microwave knowledge has created many applications undreamed of 20 years ago. The number of applications and their economic value will continue to grow, both in number and diversity, as components, techniques, and general know-how become universally available and understood. However, despite the daily invention of novel applications, we must not become complacent. From the history of scientific development, one can generalize that every new field of research has a finite half-life, perhaps not too different from 50 years. Thus, we must assume that research *per se* must come to an end. How soon? 10, 15, 20 years: certainly not much longer.

Keeping the importance of *basic research* in mind, those of us who have specialized in this field must anticipate either more prosaic engineering applications or a change to some other branch of science. Many will remain to explore and exploit the possibilities for which the foundation is now laid. Some will turn to the applications of microwaves in allied sciences, such as nuclear physics or biology.

Some will think of exploring the higher regions of frequency lying beyond the microwaves—to try to bridge the gap between the radio and infra-red radiation. For those of us who were educated at the time when conventional radio engineering was maturing into a sound branch of engineering, there is a parallel here. As the radio engineer sought higher and higher frequencies, the study and development of the microwave region was a natural evolution. Thus, the generation of submillimeter waves, lying in the wavelength range of 100–1000 Angstroms, or between 300 and 3000 kmc, appears as fascinating and promising today, as the microwave region appeared in 1936. Now, as then, there are many practical difficulties, challenging to the imagination and ingenuity of human skill but which offer, for the scientific adventurer, unknown rewards.

Rapid Measurement of Dielectric Constant and Loss Tangent

D. M. BOWIE AND K. S. KELLEHER†

Summary—The problem of evaluating dielectric constant and loss tangent by the short-circuited-waveguide technique has been encountered continually in recent years in the study of artificial dielectric media and radome materials. In general, practical measurements have involved materials with low loss and dielectric constants less than 10. The analytical method normally applied to data on such materials requires laborious computation. The available graphical methods have not completely eliminated computation and have provided answers of unsatisfactory accuracy.

The present paper describes rapid graphical techniques for evaluating dielectric constant and loss tangent from the quantities normally measured with the slotted line, using samples of arbitrarily chosen length. It begins with equations previously derived for the case of low-loss media. By use of a new parameter, the relationship between dielectric constant and the measured shift in standing-wave minimum is plotted in such a way that all possible values of dielectric constant within any predetermined range are read directly from the graph with no computation whatsoever. A graph can be readily prepared to apply over a full range of frequency to all sizes of rectangular waveguide.

With the dielectric constant known, a simplification in determining the loss tangent is possible, using half-wavelength samples. The loss tangent is obtained by direct recourse to a graph of loss tangent as a function of the standing wave ratio.

Dielectric Constant Measurement

Introduction

THE SHORTED-LINE method[1–4] for determining dielectric constant now utilized in many laboratories for evaluation of dielectric materials used in radomes, lenses, and other microwave components necessitates lengthy computational procedures after each experimental measurement. However, there is a method, introduced here, which reduces the time and eliminates all computation by using a graph for evaluation of the dielectric constant. This graph does not include the effect of loss in the dielectric, which has been treated at length,[4] but returns to the more common problem of dielectric materials of low loss. It has greatest similarity to graphs published by Redheffer,[3] but offers several advantages over that presentation.

In previous graphical methods, the ambiguity introduced by the cyclic nature of the tangent function, rather than being clearly expressed in a cyclical line set, was required to be introduced by repeatedly adjusting a parameter-value (usually one of length), each adjustment yielding a possible value of K_e. This has usually resulted in obscuring the relation between sample length and the order of ambiguity present. A second limitation is that the plotting range has sometimes been directly related to the ratio of sample length to wavelength, which for a given wavelength places an upper limit on length of sample which can be accommodated by lines within a given rectangular plotting region. The present method, without these inherent limitations, is adaptable to any selection of sample lengths. This is a useful feature in testing samples of artificial dielectrics, where long samples are needed in order that a sample contain a sufficient number of *inclusions*, on which the effective dielectric constant depends.

In the determination of dielectric constant, it is desirable to utilize a single graph showing the relationship between the dielectric constant and a measured quantity. Moreover, the dielectric constant should be read from the graph to an accuracy of better than 1 per cent, preferably to an accuracy of 0.5 per cent. A final requirement, peculiar to this particular problem, is that ambiguity in the dielectric constant value should be evident from the graph alone, and not require recomputation. It is felt that the graph described in this paper adequately satisfies all of these conditions.

Restrictions on the use of the graph are identical to those imposed in the method mentioned[3] in that the graph holds only for a fixed value of the parameter p, where p equals $(\lambda/\lambda_c)^2$, and holds for sample length of discrete values, arbitrarily selected. Subject to these conditions, the graph yields, to the desired degree of accuracy, all possible solutions for the dielectric constant within any preset limits. The philosophy behind this graph will be thoroughly discussed in order that it can be reproduced by the reader or extended to greater values of dielectric constant than had been encountered in the authors' work in the derivation of the graph.

Since we are considering only low-loss material, we begin with the two expressions given by Dakin and Works:[2]

$$\frac{-\lambda_g \tan 2\pi(x_0/\lambda_g)}{2\pi d} = \frac{\tan \beta_2 d}{\beta_2 d} \tag{1a}$$

$$K_e = \frac{1/\lambda_c^2 + (\beta_2 d)^2/(2\pi d)^2}{1/\lambda_c^2 + 1/\lambda_g^2} \tag{2a}$$

where λ_g and λ_c are guide wavelength and cutoff wavelength, respectively, β_2 the propagation constant in the dielectric sample, d the length of the sample, and x_0 the measured quantity shown in Fig. 1.

† Melpar, Inc., Falls Church, Va.

[1] S. Roberts and A. von Hippel, "A new method for measuring dielectric constant and loss in the range of centimeter waves," *J. Appl. Phys.*, vol. 17, pp. 610–619; June, 1946.

[2] T. W. Dakin and C. N. Works, "Microwave dielectric measurements," *J. Appl. Phys.*, vol. 18, pp. 789–796; September, 1947.

[3] R. M. Redheffer, "Technique of Microwave Measurements," McGraw-Hill Book Co., Inc., New York, N. Y., p. 625; 1947.

[4] R. M. Redheffer, R. C. Wildman, and W. O'Gorman, "The computation of dielectric constants," *J. Appl. Phys.*, vol. 23, pp. 505–508; May, 1952.

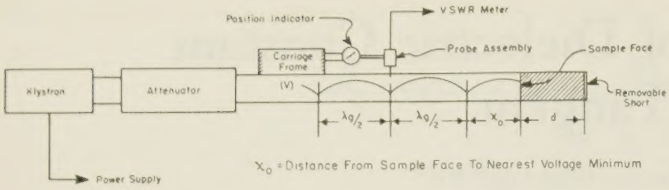

Fig. 1—Diagram of test apparatus with measured distances shown.

Analysis of Equations—Selection of Parameters

In order to clarify the above equations, in preparation for their expression in graphical form, two substitutions are made. The constant β_2 is replaced by its definition: $\beta_2 = 2\pi/\lambda_{gs}$, where λ_{gs} is the wavelength within the sample in the guide, and the parameter $p = (\lambda/\lambda_c)^2$ is introduced. In this way these equations are obtained in the following form:

$$\frac{\lambda_{gs}}{\lambda_g} = \frac{-\tan 2\pi(x_0/\lambda_g)}{\tan 2\pi(d/\lambda_{gs})} \tag{1b}$$

$$K_e = (1 - p)(\lambda_g/\lambda_{gs})^2 + p. \tag{2b}$$

Eq. (1b) clearly expresses the phase relationship across the air-sample interface in terms of existent wavelengths. The value of x_0 is limited by its definition to the range: $0 < x_0 < \lambda_g/2$; the value of d is limited to the maximum length of sample which the guide will accommodate; the ratio λ_{gs}/λ_g has values in general less than 1.

It has been arbitrarily decided that the final graph will use fixed values of the parameter $p = (\lambda/\lambda_c)^2$ and sample length d. For these fixed values, it is possible to solve the first equation for the measured quantity x_0 in terms of a new parameter: $q = \lambda_g/\lambda_{gs}$. Since p is a constant, the second equation gives the dielectric constant K_e directly in terms of the parameter q. Eliminating this parameter between the two expressions produces the desired relationship between the dielectric constant and the measured quantity.

The choice of sample length, d, can be used to minimize the difficulty caused by ambiguity inherent in rf dielectric constant measurements. If the approximate working range of K_e is known, a value of d can be found which will produce a single cycle of values of x_0 vs q; larger values of length will produce more than a single cycle, in which case a single value of x_0 corresponds to more than one value of the parameter q. The approximate limit of sample length, d', which presents no ambiguity between given maximum and minimum values of dielectric constant, is given by the following formula:

$$d' \leqq 0.6\lambda_g/\sqrt{K_e(\max) - K_e(\min)}.$$

In cases where estimates of the dielectric constant are not feasible, it is necessary to make two measurements using different sample lengths and to use the value of K_e which occurs in agreement for the two lengths. With this procedure, no prior knowledge of dielectric constant is needed. For convenience in testing, sample lengths can be made to be integral multiples of the narrow dimension of the test waveguide.

Method of Construction of Graphs

The procedure for obtaining K_e consists, first, in graphically recording values of x_0 vs assumed values of the parameter $q = \lambda_g/\lambda_{gs}$, for preselected values of d and λ_g expressed as their ratio. The choice of p, of course, determines λ_g. This preselection determines values of both the arguments, x_0/λ_g and d/λ_{gs}, in (1b). A sufficient number of q values are assumed to make feasible a graph of x_0 vs q over a preselected working range of the latter parameter.

The relationship between the dielectric constant K_e and the parameter q, expressed in (2), can be utilized in tabular form, together with the graph of (1), to yield x_0 vs K_e values for plotting. However, it has been found convenient to graph the function $K_e(q)$ of (2), and utilize this graph as an intermediate step in obtaining the final graph.

Once the graphs of (1) and (2) are obtained over the same interval of the parameter q, it is possible to obtain trial dielectric constant values directly from measured values. It is possible to see, for a single measured value, all possible values of dielectric constant within the range plotted. These two relationships could be used in the form of separate graphs on the same grid, but to facilitate evaluation, they have been combined into a single graph expressing the relationship between the measured quantity, x_0, and the unknown, K_e.

Discussion of Graph of x_0 vs K_e

Fig. 2 is an illustrative graph of the relationship: x_0 vs K_e for four values of sample length. For practical reasons, these values are integral multiples of the length $\lambda_c/4$. The value of the parameter p, the square of the ratio of wavelength to cutoff wavelength, was assumed to be 0.400.

It might be noted that curves have common points where $x_0 = 0$ and K_e equals 2.0 and 4.0. No particular significance should be attached to this feature, since the existence of common points arises from the mathematics, in that all sample lengths are multiples of the same unit; the fact that these points have even integral values is due to the value of p chosen. It is worth noting that in the interval of one cycle for the unit sample length, the order of ambiguity present for any integral multiple length is equal to the multiple itself.

Because of the mathematically indirect relationship between curves for different sample lengths, each should be considered individually. They have been plotted together to facilitate the determination of dielectric constant when more than one value of sample length is used. Different weights of line are used, one for each sample length. This set of curves will *not* permit interpolation for values of d intermediate to those for which curves are plotted. A discontinuity is present between any two curves, even between those which intersect at

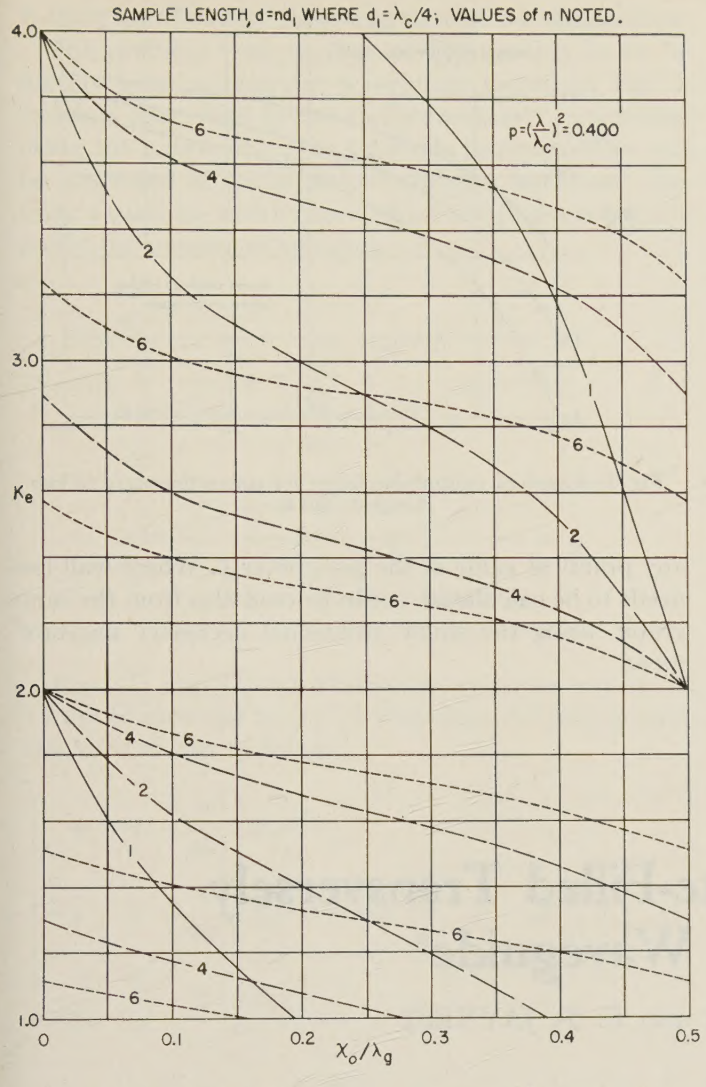

Fig. 2—Graph of dielectric constant vs measured quantity for four arbitrarily chosen sample lengths.

$x_0=0$ and thus give the illusion of being contained in the same mathematical surface. For this reason samples should be cut exactly to a length for which curves are available.

Practical Application of Fig. 2

While the method of evaluation places no inherent restriction on sample dimensions or on frequency, certain relationships must be used in order that the curves of Fig. 2 be valid. It is first necessary to choose the source frequency and waveguide dimensions so that the parameter p is equal to 0.400. This parameter, which is the square of the ratio of free-space wavelength to cutoff wavelength, sets the value of frequency for use with a given size of waveguide. If this value of p cannot be obtained with available equipment, or if for any other reason another value is desired, a modification of Fig. 2 is required.

An additional restriction is that the curves of Fig. 2 have been plotted only for sample lengths equal to integral multiples of $\lambda_c/4$, which in turn equals one-half the wide dimension of the waveguide. Other values of sample length relative to waveguide width would require further computation. However, this involves (1) only, since the length d does not enter into (2).

The above relationship of sample length to waveguide size can be used advantageously by making the waveguide inside dimensions in the ratio of exactly 2 to 1. Samples can then be cut as cubes whose edge is equal to the narrow dimension of the waveguide cavity. Two such cubes, placed side by side in the guide, form a sample corresponding to curve 1 of Fig. 2; additional samples are added to utilize the other curves. The use of cubical samples permits investigation of sample uniformity, since each cube can be inserted in any one of several orientations.

A method utilizing an adjustably mounted dial indicator circumvents several steps in the processing of data by allowing x_0 values to be read directly. This consists in merely presetting the dial indicator coupled between the probe assembly and the carriage frame to read the minimum positive value of $(N\lambda_g/2-d)$, N a positive integer, with the probe assembly resting on a voltage minimum and the sample removed. With this input, the dial indicator will read x_0 directly when, with a sample of length d in place, the probe assembly has been moved to the nearest voltage-minimum position. The range of both the dial indicator itself and that of its mounting adjustment need to be greater than $\lambda_g/2$. With this provision it is necessary only to tabulate values of dial input setting, one value for each sample length to be used.

Loss-Tangent Measurement

For evaluation of loss tangent of samples by the shorted-line method, Dakin and Works[2] give the following general expression, pertaining to the sample medium.

$$\text{Tan } \delta_2 = \frac{\Delta x}{d}\left[\frac{(1/\lambda_c^2 + 1/\lambda_g^2) - 1/\lambda_c^2 K_e}{1/\lambda_c^2 + 1/\lambda_g^2}\right] \times \frac{\beta_2 d[1 + \tan^2 (2\pi x_0/\lambda_g)]}{\beta^2 d(1 + \tan^2 \beta_2 d) - \tan \beta_2 d}, \quad (3)$$

where Δx equals the width of the standing-wave *minimum* at twice the minimum-power value (3 db above minimum indicated on swr square-law-calibrated meter), d the length of the sample, and K_e the dielectric constant of the material.

By making the substitutions: $\beta_2=2\pi/\lambda_{gs}$ and $p=(\lambda/\lambda_c)^2$, this expression is reduced to the formula:

$$\tan \delta_2 = \frac{\Delta x}{d}(1 - p/K_e) \quad (4)$$

for the case where $d=n\lambda_{gs}/2$, n being an integer, and λ_{gs} the wavelength in the sample in the waveguide. With these values of sample length, $\Delta x/d$ has its minimum value and the remaining factors in the general expression (3) are insensitive to sample length.

Sample lengths for which (4) holds can be computed by use of the expression:

$$\lambda_{gs} = \lambda/\sqrt{K_e - p}. \tag{5}$$

Allowed values of sample length can be expressed directly in terms of the same measurable parameters as

$$d = \frac{n\lambda}{2\sqrt{K_e - p}}, \quad n \text{ being any integer.} \tag{6}$$

Wall loss, which is a function of waveguide parameters only, is obtainable by applying (4) to the empty guide in question, for which case $K_e = 1$ and d becomes the distance from the short to the null position. Wall loss is eliminated by subtracting the value of tan δ_2 thus obtained from the value of tan δ_2 obtained with the sample in place.

A graph, from (4), facilitating evaluation of loss tangent from the value of $\Delta x/d$ measured for a sample of specified length and known K_e value is included as Fig. 3. Interpolation on this graph will permit evaluation for any practical value of the parameter p. Where wall loss needs to be calculated, it can be read also from the same graph, using the single additional necessary measurement.

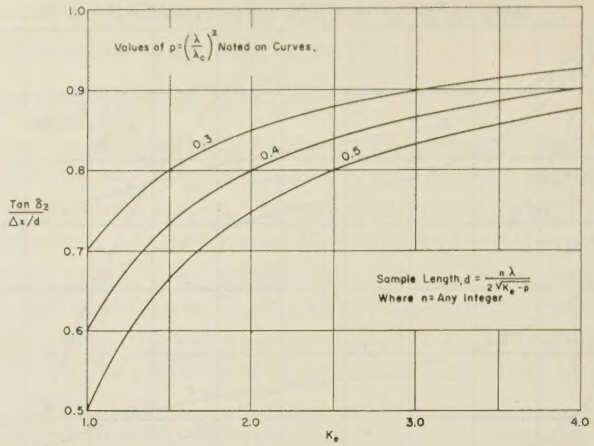

Fig. 3—Graph of multiplying factor for converting $\Delta x/d$ to loss tangent, tan δ_2.

Propagation in Ferrite-Filled Transversely Magnetized Waveguide*

P. H. VARTANIAN† AND E. T. JAYNES‡

Summary—**A solution to the problem of propagation of higher modes in a transversely magnetized ferrite-filled rectangular waveguide has been found. The solutions to the problem are expressed in the form of four rigorous nonlinear algebraic equations which characterize the problem and are ready for numerical solution. The dependence of the fields in the direction of magnetization is the same as for the classical modes.**

WE SHALL consider the problem of propagation in a rectangular waveguide which is completely filled with ferrite and magnetized transversely to the direction of propagation.

This problem is becoming of more interest as lower loss ferrites are developed. As these very low-loss ferrites become available, a class of devices depending on the ability of a dc magnetic field to change the propagation constant within a waveguide will become practical. With the transverse field geometry, these devices will operate at low field values far from gyromagnetic resonance. They will be characterized by transverse fields which are distorted by the applied magnetic field. This will make this geometry useful in field displacement devices such as isolators and radiators.

We shall hence find the fields and propagation constants for the modes in this particular ferrite geometry. They will be characterized by parameters which continuously vary with increasing magnetic field from the classical TE and TM modes into a new set of modes having fields and propagation constants which are magnetically controllable.

Gamo[1] and Kales[2] have investigated the case of the longitudinally magnetized filled cylindrical waveguide. Van Trier[3] has solved the case of the TE_{10} mode in the transversely magnetized waveguide and found that the new mode is a TE mode with a distorted transverse field dependence. Mikaelyan[4] and recently Chevalier,

* This paper was presented orally at URSI Symposium on Electromagnetic Wave Theory, University of Michigan, Ann Arbor, Mich., June 22, 1955. The work was done at the Electronic Defense Lab., of Sylvania Electric Products, Inc., under Signal Corps Contract No. DA-36-039-sc-31435, and at Stanford University.

† Electronic Defense Lab., Mountain View, Calif.
‡ Stanford Univ., Stanford, Calif.

[1] H. Gamo, "The Faraday rotation of waves in a circular waveguide," *J. Phys. Soc. Jap.*, vol. 8, p. 176; March, 1953.
[2] M. L. Kales, "Modes in waveguides containing ferrites," *J. Appl. Phys.* vol, 24, p. 609, May, 1953.
[3] A. A. Van Trier, Th. M., paper presented orally at meeting of Amer. Phys. Soc., Washington, D.C.; April, 1952.
[4] A. L. Mikaelyan, "Electromagnetic waves in a rectangular waveguide filled with a magnetized ferrite," *Doklady*, A.N. USSR, vol. 98, p. 941; October, 1954.

Kahan, and Polacco[5] have also worked on the problem.

The problem then, is that of propagation in an infinitely long rectangular waveguide shown in Fig. 1, which is filled with ferrite and transversely magnetized along the x direction. The solutions to the problem will be expressed in terms of four rigorous nonlinear algebraic equations which characterize the problem and are ready for numerical solution.

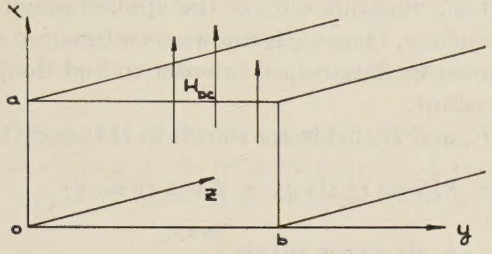

Fig. 1—Coordinate system.

Eqs. (1) and (2) are Maxwell's equations written in a form to show the tensor permeability. All field quantities vary as exp $(j\omega t-\gamma z)$.

$$\begin{bmatrix} 0 & \gamma & \frac{\partial}{\partial y} \\ -\gamma & 0 & -\frac{\partial}{\partial x} \\ -\frac{\partial}{\partial y} & \frac{\partial}{\partial x} & 0 \end{bmatrix} \begin{bmatrix} E_x \\ E_y \\ E_z \end{bmatrix} = -j\omega\mu_0 \begin{bmatrix} 1 & 0 & 0 \\ 0 & \mu & -jK \\ 0 & jK & \mu \end{bmatrix} \begin{bmatrix} H_x \\ H_y \\ H_z \end{bmatrix} \quad (1)$$

$$\begin{bmatrix} 0 & \gamma & \frac{\partial}{\partial y} \\ -\gamma & 0 & -\frac{\partial}{\partial x} \\ -\frac{\partial}{\partial y} & \frac{\partial}{\partial x} & 0 \end{bmatrix} \begin{bmatrix} H_x \\ H_y \\ H_z \end{bmatrix} = j\omega\epsilon \begin{bmatrix} E_x \\ E_y \\ E_z \end{bmatrix} \quad (2)$$

The elements in the permeability tensor are known,[6] given the applied magnetic field and frequency. For zero applied field, μ becomes unity and K zero. It is important to note that the tensor properties of the ferrite are limited to the y-z plane, that is, the plane perpendicular to the applied field.

From Maxwell's equations we derive the relations for the transverse fields in terms of the longitudinal fields.

$$E_y = \frac{1}{k_{1x}^2}\left(j\omega\mu_0\frac{\partial H_z}{\partial x} - \gamma\frac{\partial E_z}{\partial y}\right) \quad (3)$$

$$H_x = \frac{1}{k_{1x}^2}\left(j\omega\epsilon\frac{\partial E_z}{\partial y} - \gamma\frac{\partial H_z}{\partial x}\right) \quad (4)$$

$$E_x = \frac{-1}{k_{1y}^2}\left(j\omega\mu_0\mu\frac{\partial H_z}{\partial y} + \gamma\frac{\partial E_z}{\partial x} - \omega\mu_0 K\gamma H_z\right) \quad (5)$$

$$H_y = \frac{-1}{k_{1y}^2}\left(j\omega\epsilon\frac{\partial E_z}{\partial x} + \gamma\frac{\partial H_z}{\partial y} - jk^2 K H_z\right) \quad (6)$$

where

$$k_{1x}^2 = \gamma^2 + k^2 \qquad k^2 = \omega^2\epsilon\mu_0$$

$$k_{1y}^2 = \gamma^2 + k^2\mu$$

It is seen that these are of the usual form except that the E_x and H_y relations have extra terms proportional to H_z. Physically this is the rotational effect of the ferrite, that is, electrons in the ferrite driven in the z direction are caused to precess and generate a field in the perpendicular plane. We shall work with the E_z and H_z fields and the transverse fields can then be found from these equations.

The two differential equations which E_z and H_z must satisfy are obtained from Maxwell's equations.

$$\omega\epsilon\left[\frac{j\gamma X}{k_{1x}^2 k_{1y}^2}\frac{\partial^2}{\partial x\partial y} + \frac{K}{k_{1y}^2}\frac{\partial}{\partial x}\right]E_z + \left[\frac{1}{k_{1x}^2}\frac{\partial^2}{\partial x^2} + \frac{\mu}{k_{1y}^2}\frac{\partial^2}{\partial y^2} + \mu - \frac{k^2K^2}{k_{1y}^2}\right]H_z = 0 \quad (7)$$

$$\left[\frac{1}{k_{1y}^2}\frac{\partial^2}{\partial x^2} + \frac{1}{k_{1x}^2}\frac{\partial^2}{\partial y^2} + 1\right]E_z + \omega\mu_0\left[\frac{j\gamma X}{k_{1x}^2 k_{1y}^2}\frac{\partial^2}{\partial x\partial y} - \frac{K}{k_{1y}^2}\frac{\partial}{\partial x}\right]H_z = 0 \quad (8)$$

where $X=\mu-1$.

There are three interesting cases here. For zero applied field, the first term in the first equation and second term in the second equation, are zero since X and K are zero. The remaining expressions reduce to the usual forms for the classical TE and TM modes. Secondly if there is no variation of the fields in the x direction, then the TE_{no} modes found by Van Trier[3] having a distorted transverse dependence and a magnetically controllable propagation constant result. The third case is the general one, of all the other higher order modes.

The fact that the tensor properties are limited to the y-z plane suggests the form of the solutions shown in (9).

$$E_z = f(y)\sin\frac{m\pi x}{a}; \qquad H_z = g(y)\cos\frac{m\pi x}{a}. \quad (9)$$

[5] A. Chevalier, T. Kahan, and E. Polacco, "Propagation des ondes electromagnetiques dans un milieu gyromagnetique anisotrope, contenu dans un guide rectangulaire," *Compt. Rend. (Paris)*, vol. 240, pp. 1323–1324; March, 1955.

[6] C. L. Hogan, "The ferromagnetic Faraday effect at microwave frequencies and its applications," *Bell Sys. Tech. J.* vol. 31, pp. 1–31; January, 1952.

Hence the x dependence of the fields remains unaltered by the ferrite. Substituting this form of fields into the differential equations, the x dependence drops out and we are left with two second order linear differential equations in f and g. The determinantal equation for these two equations is

$$\left[\frac{\partial^4}{\partial y^4} + B\frac{\partial^2}{\partial y^2} + C\right]\begin{Bmatrix} f \\ g \end{Bmatrix} = 0 \tag{10}$$

where B and C depend on the propagation constant, frequency, and applied field. Thus the functions f and g may be represented as a sum of four independent trigonometric or exponential functions.

We will choose solutions consisting of products of two trigonometric functions each having a different argument, ry and qy.

$$\begin{Bmatrix} \sin \\ \cos \end{Bmatrix} ry \begin{Bmatrix} \sin \\ \cos \end{Bmatrix} qy.$$

This particular form is suggested by the requirement that the fields reduce to the usual TE and TM modes for the case of zero applied field. Hence we would expect that r would go to $n\pi/b$ and q to zero for zero applied field. As an example, a plot for small values of q of sin ry cos qy is shown in Fig. 2. It is seen that fields described by this function are distorted towards one side of the waveguide as the magnetic field is applied. As in the case of the TE_{no} modes this may result in a Poynting vector which on one side of the guide is opposite to the direction of propagation. This may be thought of as a uniform Poynting vector with a superimposed circulating energy.

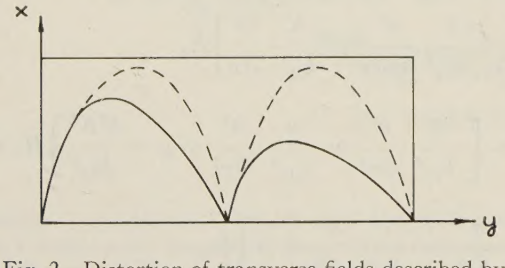

Fig. 2—Distortion of transverse fields described by sin ry cos qy for small q.

Substituting any of these four solutions in (10) yields two relations which must be satisfied by the unknowns r and q.

$$\gamma^2 = \left[-k^2\left(\frac{1+\mu_e}{2}\right) + \left(\frac{1+\mu}{2\mu}\right)\left(\frac{m\pi}{a}\right)^2\right] + r^2 + q^2 \tag{11}$$

$$r^2q^2 = \frac{k^4(\mu_e-1)^2}{16} + \left(\frac{m\pi}{a}\right)^2\frac{k^2}{2}\left[1-\left(\frac{1+\mu}{4\mu}\right)(1+\mu_e)\right] + \left(\frac{X}{4\mu}\right)^2\left(\frac{m\pi}{a}\right)^4 \equiv F^2 \tag{12}$$

and

$$\mu_e = \frac{\mu^2 - K^2}{\mu}.$$

For zero applied field the propagation constant shown in (11) goes to the usual form since the μ and μ_e become unity, r goes to $(n\pi/b)$ and q vanishes, as we postulated when choosing the form of the solutions. A further relation between r and q, (12), states that their product squared is a function only of the applied magnetic field and frequency. Hence q is known as a function of r, and only r must be determined in order to find the propagation constant.

The E_z and H_z fields are shown in (13) and (14):

$$E_z = R[S \sin ry \sin qy + T \cos ry \sin qy + \sin ry \cos qy] \sin \frac{m\pi x}{a} \tag{13}$$

$$H_z = L[M \sin ry \cos qy + N \cos ry \sin qy + P \sin ry \sin qy + \cos ry \cos qy] \cos \frac{m\pi x}{a}. \tag{14}$$

The boundary condition on the E_z field at $y=0$ required the cos cos term to be identically zero. At $y=b$ the boundary conditions require the quantity in the bracket in (13) to be zero.

The H_z field in (14) must satisfy the boundary condition specified by

$$\left(\frac{\partial H_z}{\partial y} + \frac{j\gamma K H_z}{\mu}\right)_{y=0,b} = 0. \tag{15}$$

This magnetic boundary condition is most easily found by requiring that E_x be zero at the walls. Note that this boundary condition is different from the usual in that an extra term is present. Substituting (14) into (15) yields two equations which along with the one equation from the E_z fields gives 3 equations in 6 unknown amplitudes and the quantity r. We hence need 4 more relations which are found by substituting the E_z and H_z fields into one of the original longitudinal differential equations. This can be manipulated into a set of 4 nonlinear algebraic equations in four unknowns.

$$\frac{G - J\tan rb \cot qb}{J - G\tan rb \cot qb} = \frac{G\tan qb - \phi(-1, P, -M)}{J\tan qb - \phi(P, -1, -N)} \tag{16}$$

$$\left(-r + Pq + M\frac{j\gamma K}{\mu}\right)\sin rb \cos qb + \left(Pr - q + N\frac{j\gamma K}{\mu}\right)\cos rb \sin qb + \left(-Nr - Mq + P\frac{j\gamma K}{\mu}\right)\sin rb \sin qb = 0 \tag{17}$$

$$\phi(N, M, P) = GK \tag{18}$$

$$\mu(Mr + Nq) = -j\gamma K \tag{19}$$

where

$$G = k_{1y}^2\left(k_{1x}^2 - \frac{B}{2}\right) - \left(\frac{m\pi}{a}\right)^2 k_{1x}^2$$

$$J = -2Fk_{1y}^2$$

$$\phi(u, v, w) = 2F\mu[j\gamma X(ur + vq) + Kk_{1x}^2 w].$$

The unknowns here are the three magnetic field amplitudes and r. The electric amplitudes are known in terms of these parameters. The theory leading to these equations has been rigorous and they are now ready for solution by numerical methods or by approximation techniques.

It can be shown that there are no pure TE or pure TM modes allowed in the magnetized case. A similar result was found by Gamo and Kales in their treatment of the longitudinally magnetized cylindrical waveguide. This is physically reasonable since the transverse magnetic fields for the TM modes now generate longitudinal fields through the rotational nature of the ferrite and thus TM modes would not be expected. Maxwell's equations permite TE modes only for modes with zero x dependence and these are Van Trier's TE_{no} modes.

In conclusion we have derived a set of four nonlinear equations whose solution determines a rigorous solution to the problem of propagation in a transversely magnetized ferrite-filled waveguide. The fields can be expressed in the form of products of two trigonometric functions with arguments which are asymptotic to $n\pi y/b$ and 0 in the limit of zero applied field. The product of these arguments is dependent only on the magnetic field and frequency.

Currents Excited on a Conducting Surface of Large Radius of Curvature

JAMES R. WAIT†

Summary—**The nature of the electromagnetic field of an antenna in the vicinity of a surface of large radius of curvature is discussed. Assuming a spherical surface, the solution for a dipole source in the form of the Watson residue series is transformed to a more rapidly converging series which is preferable at short distances. Using this result, numerical data is presented in graphical form for the currents induced on the spherical surface. The curves are applicable to both a stub and slot antenna mounted on the conducting surface.**

IN THE VICINITY of a flush-mounted radar antenna for aircraft, the fuselage is a smooth conducting surface having large radii of curvature. It is of interest to know how the current distribution excited on this curved surface differs from that on a perfectly flat surface. It is the purpose of this paper to investigate this problem by simulating the curved surface in the vicinity of the antenna by a spherical surface.

The starting point is to consider the fields of a radial electric dipole located on a perfectly conducting sphere of radius a. Choosing a spherical coordinate system (r, θ, ϕ), the dipole is located at $r=a$ on the polar axis and the sphere is bounded by $r=a$. As is well known,[1] the solution of this problem can be expressed in a radial mode series involving half-order Bessel function whose arguments are ka where $k=2\pi/$wavelength. Unfortunately, this representation which is often called the *harmonic series* is very poorly convergent if ka is large compared to unity. In fact, something of the order of $2\,ka$ terms are required to evaluate the field at any point in space. It was first shown by Watson in 1918 that the radial mode or harmonic series could be transformed to the angular mode or residues series.[1] This Watson representation is highly convergent in certain regions of space, namely, deep in the geometrical shadow of the source. However, when the observer is in the space near the dipole source, the series becomes poorly convergent.

It is the principal task in this paper to derive an alternative expansion which is particularly suitable for calculating the surface currents excited on the spherical surface when θ is small and ka is large.

The fields of the dipole can be expressed in terms of a scalar function v as follows:[1]

$$E_r = \left(k^2 + \frac{\partial^2}{\partial r^2}\right)(rv)$$

$$E_\theta = \frac{1}{r}\,\frac{\partial^2}{\partial r \partial \theta}\,(rv)$$

$$H_\phi = -\,i\epsilon\omega\,\frac{\partial v}{\partial \theta} \qquad (1)$$

where $\epsilon = 8.854 \times 10^{-12}$ and the time factor $\exp(i\omega t)$ has been omitted. The surface current density I, in amperes/meter, on the spherical surface has only a radial component. It is given by

$$I = H_\phi]_{r=a}$$

† Natl. Bur. of Standards, Boulder, Colo.

[1] H. Bremmer, "Terrestial Radio Waves," Elsevier Pub. Co. Amsterdam, Holland; 1949.

Using the residues-series representation for v developed by Van der Pol and Bremmer[1] it is easy to show that

$$I = I_0 U \tag{2}$$

where I_0 is the current density for a sphere of infinite radius or a flat surface and

$$U = [2\pi i x^{2/3}]^{1/2} \sum_{q=0}^{\infty} \frac{\exp[-i\tau_q x^{2/3}]}{2\tau_q} \tag{3}$$

where $x = (kd)^{3/2}/ka$ with $d = a\theta$. The coefficient τ_q is the qth root of

$$H_{2/3}^{(2)}[1/3(-2\tau_q)^{3/2}] = 0 \tag{4}$$

where $H_{2/3}^{(2)}[z]$ is the Hankel function of the second kind of order $\frac{2}{3}$ and argument z. The roots of the Hankel function are tabulated by Watson.[2] Eq. (3) is an approximation valid for a, large compared to both the wavelength and the distance d, from the source to the observer.

Following a crucial suggestion of Dr. H. Bremmer[3] U is now expressed as a Bromwich contour integral as follows

$$U = \frac{1}{2\pi i} g^{1/2} e^{-5\pi/6} \cdot \int_{c-i\infty}^{c+i\infty} \frac{e^{sg}}{s^{1/2}} \frac{H_{1/3}^{(2)}\left[\frac{(-2i)^{3/2}}{3} s^{3/2}\right]}{H_{2/3}^{(2)}\left[\frac{(-2i)^{3/2}}{3} s^{3/2}\right]} ds \tag{5}$$

where $g = x^{2/3}$ and c is some positive real constant. It can be verified by the theory of functions that the sum of the residues at the poles of the integrand leads back to the series representation for U in (3). Symbolically the above equation can be written

$$LU = \frac{g^{1/2} e^{-i5\pi/6}}{s^{1/2}} \frac{H_{1/3}^{(2)}\left[\frac{(-2i)^{3/2}}{3} s^{3/2}\right]}{H_{2/3}^{(2)}\left[\frac{(-2i)^{3/2}}{3} s^{3/2}\right]} \tag{6}$$

where the operator L indicates that the right-hand side of this equation is the Laplace transform[4] with respect to g of U.

It is now proposed to obtain a series formula for U in positive powers of g by developing LU in an asymptotic expansion in power of $1/s$. In order to develop the Hankel functions[2] in their asympotic expansions, it is necessary to assure that the phase of the argument lies within the range -2π to π. Noting that s will range in values from $+i\infty$ to $-i\infty$ it is desirable to multiply the arguments of the Hankel functions in (6) by $e^{-3i\pi}$.

[2] G. N. Watson, "Theory of Bessel Functions," 2nd ed., 1945.
[3] Private communication.
[4] R. V. Churchill, "Operational Methods in Engineering," McGraw-Hill Book Co. Inc., New York, N.Y.; 1944.

Using the identity[2]

$$\frac{H_{1/3}^{(2)}[z]}{H_{2/3}^{(2)}[z]} = e^{i\pi} \frac{H_{1/3}^{(2)}[ze^{-3i\pi}]}{H_{2/3}^{(2)}[ze^{-3i\pi}]} \tag{7}$$

it follows that

$$LU = (g/s)^{1/2} e^{i\pi/6} \frac{H_{1/3}^{(2)}[-i^{1/2}(2s)^{3/2}/3]}{H_{2/3}^{(2)}[-i^{1/2}(2s)^{3/2}/3]}. \tag{8}$$

Denoting $-i^{1/2}(2s)^{3/2}/3$ by Z, the following asymptotic expansions[2] are now valid:

$$H_{1/3}^{(2)}(Z) = \left(\frac{2}{\pi Z}\right)^{1/2} e^{-i(Z-(5\pi/12))} \sum_{m=0}^{\infty} \frac{(-1)^m (1/3, m)}{(2iZ)^m} \tag{9}$$

and

$$H_{2/3}^{(2)}(Z) = \left(\frac{2}{\pi Z}\right)^{1/2} e^{-i(Z-(7\pi/12))} \sum_{m=0}^{\infty} \frac{(-1)^m (2/3, m)}{(2iZ)} \tag{10}$$

with

$$(\nu, m) = \frac{(\nu + m - 1/2)!}{m!(\nu - m - 1/2)!}.$$

It then follows that

$$\frac{H_{1/3}^{(2)}(Z)}{H_{2/3}^{(2)}(Z)} = e^{-i\pi/6}\left[1 + \frac{i}{6Z} - \frac{7}{72Z^2} - i\frac{7}{72Z^3} + \cdots\right]. \tag{11}$$

The desired asymptotic expansion is then given by

$$LU = (\pi g)^{1/2}\left[\frac{1}{s^{1/2}} - \left(\frac{i}{2}\right)^{1/2} \frac{1}{4s^2} + i\frac{7}{64s^{7/2}} + \left(\frac{1}{2i}\right)^{1/2} \frac{21}{128s^5} + \cdots\right]. \tag{12}$$

Employing the basic relation[3]

$$\frac{1}{s^\nu} = \int_0^\infty \frac{g^{\nu-1}}{(\nu-1)!} e^{-gs} dg = L\frac{g^{\nu-1}}{(\nu-1)!} \tag{13}$$

it now readily follows that

$$U = 1 - \frac{\pi^{1/2}}{8}(1+i)g^{3/2} + \frac{i7}{120} g^3 + \frac{\pi^{1/2} 7(1-i)}{2048} g^{9/2} + \cdots \tag{14}$$

or

$$U = \left[1 - \frac{\pi^{1/2}}{8} x + \frac{7\pi^{1/2}}{2048} x^3 + \cdots\right] - i\left[\frac{\pi^{1/2}}{8} x - \frac{7}{120} x^2 + \frac{7\pi^{1/2}}{2048} x^3 + \cdots\right] \tag{15}$$

where $x = (kd)^{3/2}/ka$.

It can be seen that as d tends to zero or a tends to infinity, the value of U approaches unity corresponding to the dipole on a flat conducting surface.[5]

The series, which can be called the 3rd order curvature corrected series, converges adequately for x less than about 1.5. Writing

$$U = |U| e^{-i\Phi}$$

then $|U|$ and Φ are the amplitude and phase lag, respectively, of the correction factor U. Numerical values are computed from (15) and shown plotted in Fig. 1 for x ranging from 0.1 to 3. Values of $|U|$ and Φ obtained from the residue series formula in (3) are also shown on Fig. 1. The agreement between the two sets of curves is excellent unless x exceeds about 2.0. When x is of the order of 0.1 or less, greater than 100 terms in the residue series are required to obtain three figure accuracy, whereas only the term in x need be retained in the curvature corrected series for U. At larger values of x, say greater than 2 or 3, only several terms in the residue series are required, whereas the curvature corrected series would be very poorly convergent.

Although the preceding theory was developed explicitly for a radial electric dipole source, the results are directly applicable to the current excited on a spherical surface by a narrow slot or its equivalent magnetic dipole. Eq. (2) relating the current I on the curved surface to the current I_0 on a flat surface is only strictly valid in the broadside direction from the narrow slot as indicated in the inset in Fig. 1. If kd is much greater than unity, however, the equation is also valid in other directions from the slot. It can now be expected that the mutual impedance Z_m between any two slots oriented for other than minimum coupling on a spherical surface of large radius of curvature a is related to the mutual impedance Z_{0m} for the same slots on a flat surface by the formula

$$Z_m \cong UZ_{0m}.$$

In this case, d is taken as the distance between the centers of the slots.

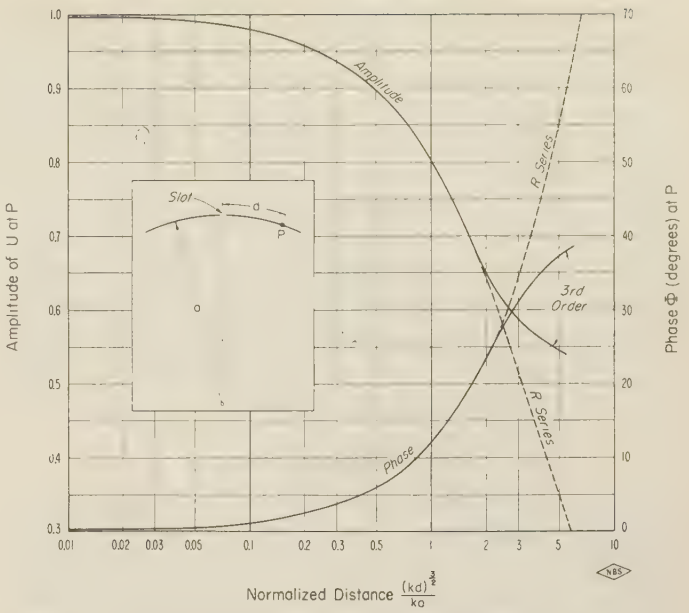

Fig. 1—The ratio of the current induced by a slot on a curved surface to that on a flat surface.

[5] Bremmer, *loc. cit.*, has developed expansion formulas, similar to (15), which are expressed in powers of a factor δ which is approximately proportional to the complex refractive index of the sphere, which in the present analysis is effectively infinite.

A Note on Noise Temperature

PETER D. STRUM†

Summary—**The effective noise temperature of the output impedance of a lossy passive network at an arbitrary noise temperature connected to one or more resistive loads at arbitrary noise temperature lies between the highest and the lowest of these noise temperatures, as determined by the losses between the output terminals and the loads. The determination of the effective noise temperature of a gas-discharge noise generator over a wide frequency range is simplified by the substitution of a loss measurement for the more difficult noise temperature measurement. For minimum-noise radar applications care must be used in considering the excess noise of crystal mixers and gas-discharge duplexers. The influence of galactic radiation on a receiving system is such that there is an optimum frequency in the region of 200 to 600 mc for minimum "operating noise figure." Typical examples of radio-astronomy measurements are amenable to analysis of the type given. Finally, several corrections to measured noise figure are analyzed.**

† Ewen Knight Corp., Needham Heights, Mass. Formerly at Airborne Instruments Lab., Mineola, N.Y.

Introduction

THE OUTPUT noise power of many widely used devices is conveniently expressed in terms of an equivalent noise temperature—that is, the temperature of a passive resistor that would generate an equivalent available noise power. In the case of directional antennas and gas-discharge noise generators, the term noise temperature is accurately applied because, in one case, the antenna is directed into space, which

may have wide temperature variations, and in the other case, the magnitude of the noise output is proportional to the electron temperature of the gaseous discharge. In the case of a crystal mixer, the term noise temperature is often used for describing the output noise ratio as a fictitious normalized temperature.

This paper will deal with the effective noise temperature of a lossy passive network that has internal noise sources and is connected to loads at arbitrary temperature. Noise generators, crystal mixers, and receiving systems are typical of such networks. The application of the analysis to the computation and measurement of noise figure will also be given.

Noise Temperature

The term noise temperature, when used in the dimensionless or normalized sense, is defined as the ratio of the available noise power at the output of a device to the available thermal noise power that the device would yield if its output impedance were at standard room temperature, 290° Kelvin. This normalized noise temperature is sometimes called noise-temperature ratio or output noise ratio. In other circumstances noise temperature is assigned a value in the Kelvin temperature scale.[1] To distinguish between these two applications of the term noise temperature, the following expression is used:

$$t = \frac{T}{290} \tag{1}$$

where t is the normalized noise temperature, T is noise temperature in the Kelvin scale, and 290° Kelvin is the reference temperature that has been standardized for noise-figure considerations.

In cases where normalized noise temperature is different from unity, it is convenient to deal with excess noise, $t-1$. It should be noted that the excess noise may be greater or less than zero; however, because it is usually considered to be greater than zero, the term excess noise is used.

Transmission Line Analog

The noise temperature of the output resistance of a resistive pad connected at its input to a resistive generator, either of which may be at an arbitrary noise temperature, can be computed with the aid of a transmission line analog. Consider the pad to be a uniform transmission line having losses equally divided between series resistance and shunt conductance, thus having a resistive characteristic impedance. Such a transmission line fed by a resistive generator is shown in Fig. 1. The generator is at normalized noise temperature t_g, and the transmission line (or pad) is at normalized noise temperature t_p and has an attenuation constant α. The effective excess noise "seen" when looking to the left at

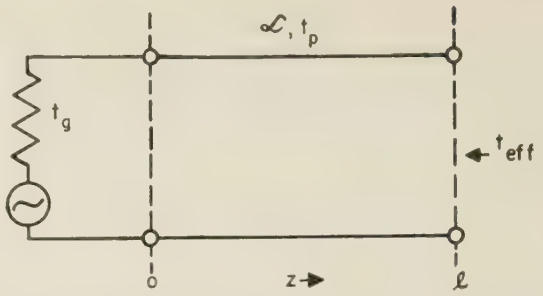

Fig. 1—Transmission-line analog of noisy, or "hot," pad.

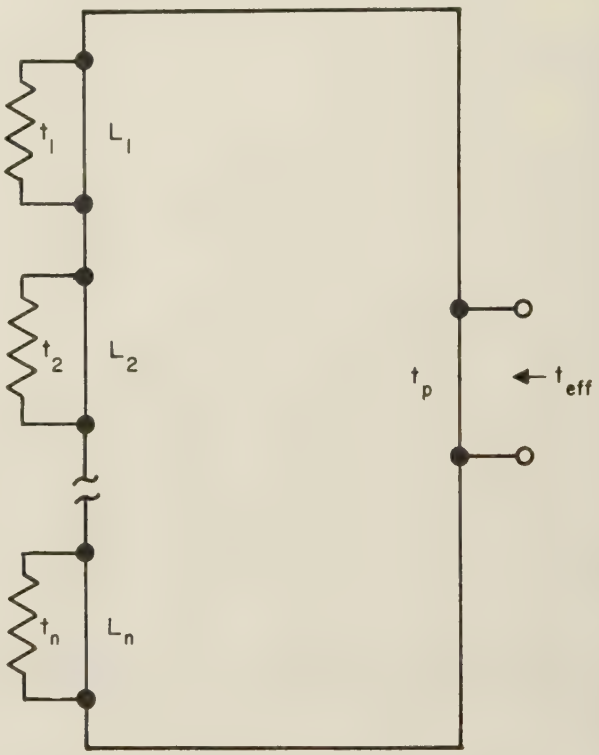

Fig. 2—Noisy pad matched to an arbitrary number of noisy terminations.

any point z in Fig. 1 can be determined on the basis of transmission-line theory, if one bears in mind that noise powers add linearly [hence the factor 2 in the exponentials of (2)] and that excess noise can be otherwise treated like a signal. Therefore,

$$(t_{eff} - 1)_z = (t_g - 1)e^{-2\alpha z} + (t_p - 1)(1 - e^{-2\alpha z}). \tag{2}$$

If one then traverses all z from 0 to 1, one "sees" the excess noise of the generator gradually modified by the loss and excess noise of the transmission line until at $z=1$ the excess noise is that of the generator attenuated by the total loss plus that of the line reduced by that fraction lost into the generator. Thus at $z=1$

$$t_{eff} - 1 = (t_g - 1)/L + (t_p - 1)(1 - 1/L) \tag{3}$$

where L is the total loss in power ratio.

Fig. 2 shows a lossy network to which an arbitrary number of resistive loads is connected. In the network of Fig. 2, t_n is the normalized noise temperature of the nth load resistance, t_p is the normalized noise temperature

[1] See "Standards on electron devices: methods of measuring noise," Proc. IRE, vol. 41, pp. 890–896; July, 1953.

of the resistive components of the pad, and L_n is the loss from the output terminals to the nth load resistor when the output terminals are fed by a generator of resistance equal to the image impedance of the pad at the output terminals. The result given in (3) can be expanded to apply to the multiterminal network of Fig. 2. The expression then becomes[2]

$$t_{eff} - 1 = (t_1 - 1)/L_1 + (t_2 - 1)/L_2 + \cdots (t_n - 1)/L_n$$
$$\text{If } t_1 = t_2 = \cdots t_n + (1 - L_1^{-1} - L_2^{-1} - \cdots L_n^{-1})(t_p - 1). \quad (4)$$

$$t_{eff} - 1 = [(t_1 - 1)/L_1](1 + L_1/L_2 + \cdots L_1/L_n) + (1 - L_1^{-1} - L_2^{-1} - \cdots L_n^{-1})(t_p - 1). \quad (5)$$

It should be noted that in (4) and (5) it may seem possible for the factor containing $(1 - L_n^{-1})$ to become negative. This eventuality is impossible in a passive network, however, because the total gain cannot exceed unity.

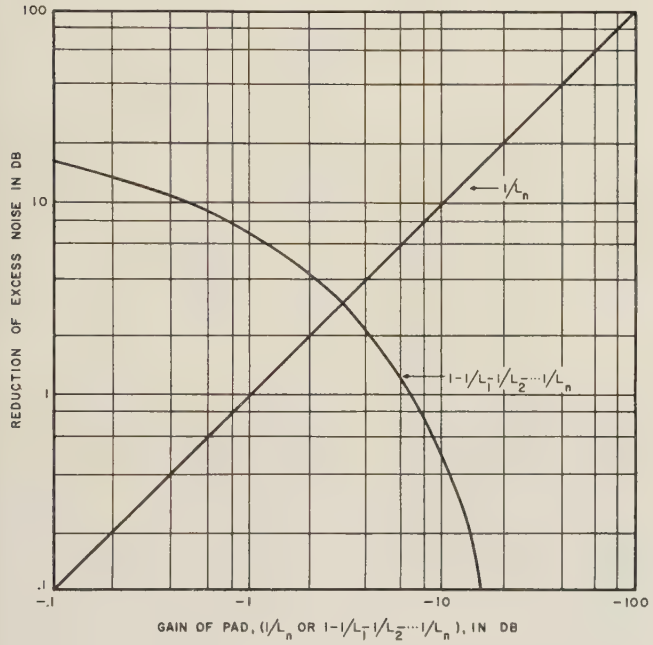

Fig. 3—Reduction of excess noise as a function of loss of pad.

Fig. 3 shows the reduction in excess noise as a function of the losses of the pad in db. In the case of the function $(1 - L_1^{-1} - L_2^{-1} - \cdots L_n^{-1})$ where two or more losses are to be considered, the gains $(1/L_n)$ should be summed. If this summed gain is then converted to decibels, it can be used to enter the abscissa of Fig. 3.

Applications of Analysis

Noise Generators

There are two types of standard noise generators in widespread use at the present time: gas-discharge noise generators and temperature-limited diode noise generators.

[2] This general result agrees with the two particular cases given by W. L. Pritchard, "Notes on a crystal mixer performance," Trans. IRE, vol. MTT-3, pp. 37–39; January, 1955.

In the usual gas-discharge noise generator, t_n is near unity, t_p is large (normalized electron temperature of discharge), and the loss to be considered is the loss induced by the ionized gas. Such a noise generator usually has a matched termination on one end. From (3) it is seen that nearly the entire excess noise will be available at the output provided the induced loss is sufficiently great. In fact, the effective excess noise may seem to be several times larger than the excess noise of the discharge if the receiver under test has appreciable response at more than one channel. In the general case involving responses at several sidebands, the relationship is

$$t_{eff} - 1 = (1 - L_1^{-1})(t_p - 1) + (1 - L_2^{-1})(t_p - 1)r_2 + \cdots (1 - L_n^{-1})(t_p - 1)r_n \quad (6)$$

where L_n is the loss through the discharge at the frequency of the nth response of the receiver and r_n is the relative power response of the receiver at the nth response. If the loss through the discharge is uniform at all response bands, (6) will reduce to

$$t_{eff} - 1 \cong (1 - L^{-1})(t_p - 1)B_0/B_u \cong (t_p - 1)B_0/B_u, \quad L \gg 1 \quad (7)$$

where B_0 is the total bandwidth of the receiver including all sidebands and B_u is the bandwidth of the useful channel.

Temperature-limited diode noise generators are well known to have an excess noise of $20IR$, where I is the temperature-limited diode current and R is the resistive component of impedance. For superheterodyne measurements, again, multiple responses should be considered, in which case

$$t_{eff} - 1 = 20I(\tau_1 R_1 + \tau_2 R_2 r_2 + \cdots \tau_n R_n r_n) \quad (8)$$

where τ_n is a transit-time reduction factor and R_n is the effective resistive component of impedance at the plane of the diode current. At low frequencies all R_n may be equal, but at uhf where there may be a significant distance between the diode and its termination, R_n may be quite variable.

The effect of imperfect (nonunity) swr is usually insignificant in the gas-discharge noise generator because the dissipative match is provided by the "hot" gas column. In the diode noise generator nonunity swr has a first-order effect on accuracy inasmuch as the resistive component of impedance at the plane of the diode current determines the excess noise directly.

Crystal Mixer

Eq. (4) can be applied to a crystal mixer. In this case L_n is the loss from the IF terminals to the nth pair of rf terminals. For ordinary noise-figure considerations, t_n is unity and t_p is the crystal noise temperature. For a high-Q mixer, L_1 is the loss to the signal terminals, and $L_2, L_3, \cdots, L_n$ are sufficiently great that they can be considered to be infinite. In a broad-band mixer, the

losses to the signal and the image terminals are equal; therefore, L_1 and L_2 are equal to the fundamental conversion loss. In certain broad-band mixers, the higher-order sidebands are reasonably well matched; therefore, L_3 and L_4 are the losses to the lower and upper sidebands of the second harmonic of the local-oscillator frequency, and so forth. Usually conversion loss for the second harmonic is greater than that for the fundamental by about 4 to 6 db, and conversion loss for the third harmonic is higher than that for the second by about 6 to 8 db, and so forth. If reasonably good matches are achieved at these high-order sidebands, a significant reduction in noise temperature can occur. However, since the fundamental conversion loss is also dependent on these terminations, receiver noise figure may either rise or fall as a function of the terminations.[3,4]

TR Switch

The duplexer in a microwave receiver usually incorporates a tr switch in which a keep-alive current is maintained. Since the keep-alive discharge is similar to that utilized in gas-discharge noise generators, it is apparent that excess noise may be introduced from this source if there is coupling to the rf circuit. Coupling between the keep-alive discharge and the rf circuit is usually specified in terms of interaction loss, which is the loss introduced into the signal path by the discharge.

Noise figure with keep-alive current will be

$$F_{ka} = L_i F + L_{rk}(1 - L_i^{-1})(t_D - 1)(B_0/B_u) \qquad (9)$$

where F_{ka} is noise figure with keep-alive current, L_i is interaction loss, L_{rk} is the loss from the rf input terminals to the plane of the keep-alive interaction, F is noise figure without keep-alive current, t_D is the noise temperature of the discharge, B_0 is the total bandwidth including all sidebands that are matched to the antenna, and B_u is the useful bandwidth.

To estimate the magnitude of the increase in noise figure that may occur, typical values can be assumed for the excess noise of the discharge and the interaction loss, 16 db above thermal noise and 0.1 db, respectively. On the basis of the assumed values, the excess noise from the discharge is 0.9 or 1.8, depending on whether B_0/B_u is 1 for a high-Q tr switch or 2 for a broadband tr switch. If the assumed values of excess noise and interaction loss occur in actual receivers, a significant increase in noise figure may be experienced.

In certain receiver installations, it may be desirable to incorporate a simple means for checking noise figure. For such an application, it may be possible to use the keep-alive discharge or a discharge directly across the rf gap as a standard source of noise.

Receiving System

The foregoing concepts can be applied to noise figure of a receiving system. In particular, these concepts are applicable to a receiver whose antenna is effectively at a temperature other than room temperature. Typical examples of such receivers are radar and radio-astronomy receivers. It has been well established that the apparent temperature of the sky varies widely, whereas the earth and black-body radiators on the earth exhibit a temperature near 290° Kelvin.[5] Since the term noise figure is standardized in such a way that the excess noise of a receiver is referred to the available noise from a resistor at room temperature (290° Kelvin), it is desirable to use the term "operating noise figure" to define the sensitivity of a receiver in its normal operating environment.[6] For a single-band receiver, operating noise figure can be defined as

$$\begin{aligned} F_{op} &= S_i N_{290}^{-1} S_0^{-1}[(F-1)N_{290} + N_a] \qquad (10)\\ &= F + t_a - 1 \end{aligned}$$

where S_i is the available input signal power, N_{290} is the available noise power from a resistor at 290° Kelvin, S_0 is the available output signal power referred to the input, and N_a is the available noise power from a resistor at the effective antenna temperature. If a broad-band mixer is matched to the antenna at sidebands other than the desired signal frequency, this relation will be altered as follows:

$$\begin{aligned} F_{op} &= F + (t_a - 1)(1 + L_1 L_2^{-1} + L_1 L_3^{-1} + \cdots L_1 L_n^{-1}) \qquad (11)\\ &= F + (t_a - 1) B_0/B_u \end{aligned}$$

where L_n has the same definition as applied to the crystal mixer above, and F is the noise figure of the receiver and includes all effects that result from $B_0/B_u > 1$

[3] P. D. Strum, "Some aspects of mixer crystal performance," Proc. IRE, vol. 41, pp. 875–889; July, 1953.

[4] In passing, it should be noted that care should be exercised in using quoted specifications on noise temperature for crystal mixers. Standard noise-temperature test sets, for example, measure S-band crystal noise temperature at a power level of 0.5 mw and most other crystals at a power level of 1 mw. Most microwave receivers use a local-oscillator power of about 0.3 milliwatt. The noise temperature of a mixer crystal may, therefore, be less than that quoted by the manufacturer in many cases. A functional relationship between excess crystal noise and local-oscillator power has been found experimentally to be

$$t_x - 1 \cong KP^n,$$

where P is the absorbed local-oscillator power, K is an arbitrary constant, and n lies between 1 and 2, 1.3 being a typical value. Other factors that must be considered when determining mixer noise temperature are excess local-oscillator noise and the variation of crystal noise with frequency. See Strum, *op. cit.*, Fig. 9.

[5] J. L. Lawson and G. E. Uhlenbeck, "Threshold Signals," vol. 24, Rad. Lab. Ser., McGraw-Hill Book Co., Inc., New York, N.Y.; pp. 103–108; 1950.

H. V. Cottony and J. R. Johler, "Cosmic radio noise intensities in the vhf band," Proc. IRE, vol. 40, pp. 1053–1060; September, 1952.

J. D. Kraus and E. Ksiazek, "New Techniques in radio astronomy," *Electronics*, vol. 26, pp. 148–152; September, 1953.

H. I. Ewen, "Radio waves from interstellar hydrogen," *Scientific Amer.*, vol. 189, pp. 42–56; December, 1953.

J. L. Pawsey and R. N. Bracewell, "Radio Astronomy," Oxford Univ. Press, New York, N.Y.; 1955.

[6] The concept of "operating noise figure" was introduced by North.

D. O. North, "The absolute sensitivity of radio receivers," *RCA Rev.*, vol. VI, pp. 332–343; January, 1942.

D. O. North and H. T. Friis, "Discussion on 'noise figures of radio receivers'," Proc. IRE, vol. 33, pp. 125–127; February, 1945.

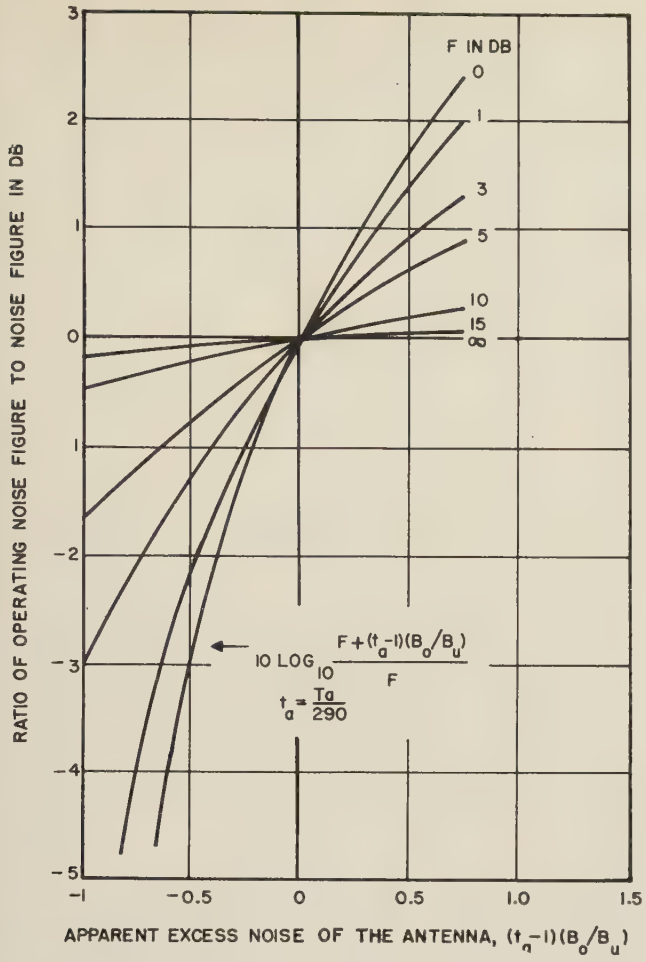

Fig. 4—Ratio of operating noise figure to noise figure.

except for the effect of antenna temperature. Fig. 4 shows the relation of (11).

It should be noted that the operating noise figure as defined in (10) and (11) gives directly a basis for comparison of the abilities of receivers to detect a fixed magnitude of signal power available from the antenna. This case is analogous to the radar case in which a fixed magnitude of echo power is available at the antenna terminals and to the radio-astronomy case in which a fixed magnitude of celestial noise power is available at the antenna.

It should be noted that this result is considerably different from that obtained by using "effective noise figure," as defined by Goldberg.[7,8] Effective noise figure, according to Goldberg's definition, compares the excess noise of the receiver with the noise of a resistor at the temperature of the antenna as follows:

$$F_{eff} = 1 + (F - 1)/t_a. \qquad (12)$$

It should be noted that this relation does not give a direct measurement of the ability of a receiver to detect a signal power of fixed magnitude. As an example of the confusion that may occur, consider a receiver having a 10 db noise figure and an antenna oriented in such a way that t_a equals 0.33. The operating noise figure of such a receiving system will be 9.7 db, the 0.3 db improvement resulting from the fact that less over-all system noise is available in this case in comparison with the room-temperature case. A fixed magnitude of signal power will be slightly more easily discerned in this receiving system than would be the case if the antenna were at room temperature. If, however, one computes effective noise figure, the result will be 14.5 db. Such a result might imply that a particular signal will be less easily discerned. In this case, it is necessary to remember that, for a fixed signal power, the input signal-to-noise ratio is larger by a factor t_a^{-1} than in the room-temperature case.

The concept of operating noise figure gives a basis for including the effects of galactic noise on the receiving system.[5] Galactic noise is usually specified in terms of an apparent temperature, which is applied to the background radiation received from outer space. This background noise has a smooth spectrum, which varies at a rate somewhat greater than with the inverse square of frequency (about $f^{-2.5}$). Discrete noise sources may have much higher noise temperatures than the background, but they are confined in angle of arrival, and may usually be disregarded as sources of interference.

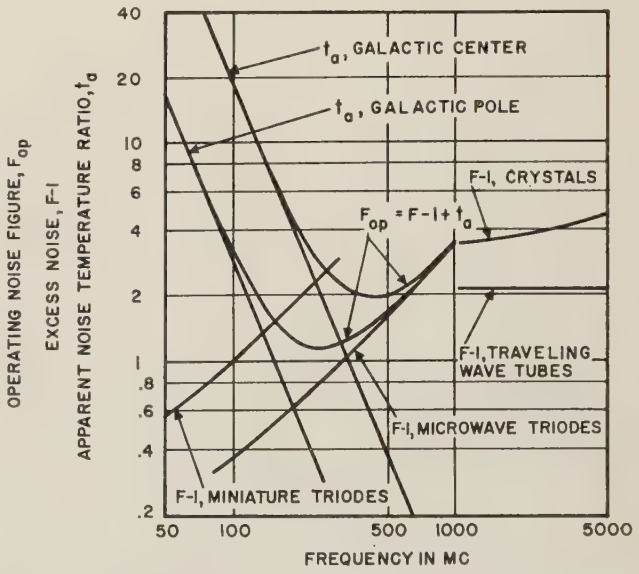

Fig. 5—Influence of galactic noise on operating noise figure.

Fig. 5 shows normalized galactic noise temperature as given by Ewen[5] plotted together with the excess noise of some typical receivers (as specified by their first-stage active circuit elements). It is seen that good microwave triodes provide the best obtainable noise figures at frequencies less than about 1,000 mc. At these frequencies, however, the galactic noise has a pronounced effect on operating noise figure. For these particular receiver types an optimum frequency for mini-

[7] H. Goldberg, "Some notes on noise figures," Proc. IRE, vol. 36, pp. 1205–1214; October, 1948.

[8] Lawson and Uhlenbeck, *loc. cit.*, applied the term "effective noise figure" to the "operating noise figure."

mum operating noise figure is seen to be in the region of 200 to 600 mc. For Fig. 5, it is assumed that the antenna beam is highly directional. If an appreciable portion of the beam intercepts earthbound black-body radiators at about 290° Kelvin, the effective antenna temperature will lie between the galactic noise curve and the horizontal line at unity; and the optimum frequency will be lower. In Fig. 5, man-made interference and atmospherics are not considered, though they are frequently important at frequencies below the ultra-high frequencies.

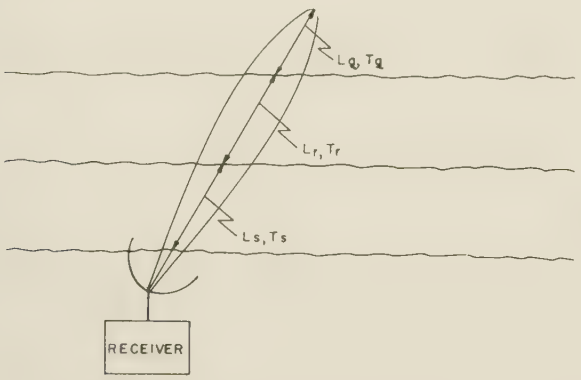

Fig. 6—The radio-astronomy situation.

Radio Astronomy

Galactic and other extraterrestrial noise, besides being forms of interference in certain receiving systems, are subjects of study for radio astronomers. Fig. 6 shows the radio-astronomy situation. The antenna beam intercepts one or more regions that have different values of loss and noise temperature. By solving (4) at successive boundaries, starting at the farthest, the net result at the receiver can be determined. If a narrow-angle source is also to be considered, a correction must be made for the reduced relative solid angle. Several cases can be cited.

The simplest is the case in which the beam of a directive antenna is directed through a semi-infinite absorbing medium at a temperature that is to be measured. In this case, the antenna will effectively exhibit th temperature of the absorbing medium.

Another case is similar to the first except that an absorbing medium is interposed between the antenna and the medium of interest. Such a case occurs when observations are made at frequencies at which the ionosphere exhibits absorption. The ionosphere should then be assigned an effective loss and temperature to permit corrections to be made to the observations. Other such cases occur whenever two or more absorbing mediums in space fall along the center of the antenna beam.

A particularly interesting case is met in observations of the absorption line of galactic hydrogen at 21 cm. In such observations a radio star beyond the hydrogen may raise the background radiation over an appreciable frequency range. At frequencies other than resonance frequencies, the hydrogen is virtually loss-free, or "transparent." At 21 cm, the resonance frequency, the hydrogen becomes highly absorptive, or "opaque." Besides the absorption aspect of the 21 cm line, in directions where background radiation is small, the effective temperature will be raised by radiation from the hydrogen at 21 cm. The 21 cm radiation from galactic hydrogen, first observed by Ewen and Purcell in 1951, has opened one of the largest avenues presently being explored by the astronomers.[9]

It is of interest to note that the image response, which is considered a nuisance in most applications, can be used to improve the sensitivity of a receiver in the measurement of "white" noise, or noise that has negligible difference in magnitude at the two principal sidebands of the local-oscillator frequency. That is, a receiver with equal image and signal responses will be 3 db more sensitive in detecting a single white noise source than a comparable receiver having image rejection. For instance, a two-channel receiver having a 10 db noise figure when rated on the basis of one useful channel would effectively have a 7 db noise figure when used to measure "white" noise. In this case, the factor $B_0B_u^{-1}$ is unity instead of two. If the signal and image channels are sufficiently close together, this fact can be used in measurements of sloping spectra such as that of the galactic radiation.

It was brought to my attention by Ewen that there frequently is the situation in which a weak white noise source is to be detected in a strong background of white noise. In such a case the advantage of the image response is reduced and may virtually disappear, depending upon the relative magnitudes of the background noise and the excess noise of the receiver according to the three following cases:

1) If the background noise is much greater than the excess receiver noise, receiver characteristics such as image rejection, noise figure, and the like have relatively little influence on the output signal-to-noise ratio; therefore, there is little sensitivity advantage in admitting the image sideband.

2) If the background noise is much smaller than excess receiver noise, virtually the full 3-db advantage is obtained.

3) If background noise and excess receiver noise are comparable, there will be a sensitivity advantage between zero and 3 db.

Noise Figure Measurement

Whenever noise figure is measured utilizing a generator at a temperature different from room temperature (when not intentionally emitting excess noise), the

[9] H. I. Ewen and E. M. Purcell, "Radiation from hyperfine levels of interstellar hydrogen," *Phys. Rev.* vol. 83, pp. 881–883; August 15, 1951.

numerical result will be in terms of operating noise figure unless a correction is made for the temperature of the noise generator. The difference between operating noise figure and noise figure in Fig. 4 can be used as a correction to the measured noise figure. The reading from Fig. 4 should be subtracted from the result that is obtained from the measurement. A typical case in which this sort of correction is important is that of environmental testing of receiving equipment. If the environmental testing is done at elevated or reduced temperature the following results can be obtained: 1) If the noise generator is at the ambient temperature imposed upon the receiving equipment, the resulting noise figure will be an operating noise figure, and the correction should be made to give noise figure, and 2) if the receiving equipment is at the environmental test temperature, but the noise generator is at room temperature, no correction is required. In the case of an amplifier with extremely low noise figure, the resulting temperature changes that occur when a noise generator is allowed to warm up become important and must be considered if accurate results are to be obtained. For instance, from Fig. 4 it is seen that for an amplifier with a 1 db noise figure, there is a correction of about 0.1 db for each 10 degrees at temperatures near room temperature.

When a broad-band noise generator is used to measure the noise figure of a superheterodyne receiver in which the mixer is matched to the antenna at sidebands other than the signal frequency, the apparent excess noise is higher than for the single-channel case. For the broad-band receiver, the apparent excess noise is that given by (6) and (7). The result given in (6) and (7) has been used frequently in the past to the extent that the image frequency has been considered. From the plot in Fig. 7, it is seen that significant errors may result if the upper and lower sidebands of the second and third harmonics are not considered. In considering Fig. 7, however, it should be noted that few mixer structures have sufficiently broad response characteristics to require the full correction that is indicated. It is intended here only to indicate that the possibility exists for such corrections. In waveguide structures it may be necessary to consider modes other than the dominant mode when considering the effects of these high-frequency sidebands. Three usual cases can be postulated:

1) High-Q mixer—$B_0 B_u^{-1} = 1$.

2) Mixer utilizing band-pass filter matching both signal and image, but rejecting other sidebands —$B_0 B_u^{-1} = 2$.

3) Broad-band mixer providing a match to signal, image, and several other sidebands—$B_0 B_u^{-1} > 2$.

To eliminate the necessity for correcting for the extra sidebands, it might seem that, for measurement purposes, a band-pass filter could be interposed between the noise generator and the mixer. If such a filter is used, however, it is necessary to provide resistive padding between it and the mixer to prevent the possibility of seriously altering the sideband terminations, thereby altering conversion loss, impedances, and noise temperature of the mixer.[10]

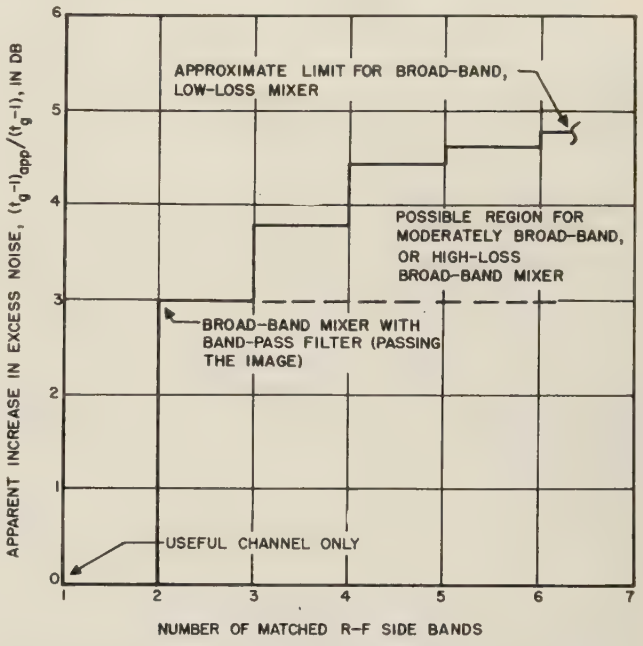

Fig. 7—Apparent increase in excess noise in a typical broad-band mixer.

Conclusion

Expressions have been given for the noise temperature of a lossy pad at an elevated temperature connected to an arbitrary number of terminations at arbitrary temperatures. The application of these expressions was shown for several receiving-system components.

It was shown that the noise temperatures of various components of a receiving system including its antenna can seriously affect noise figure and its measurement. In particular, consideration of galactic noise indicates that an optimum frequency for minimum operating noise figure lies in the region of hundreds of megacycles. Methods were given to account for the effect of the temperature of the test equipment when noise figure is to be measured and for the spurious sidebands in a superheterodyne receiver that has broad-band characteristics.

Acknowledgment

The author wishes to express his appreciation to A. J. Hendler and M. T. Lebenbaum of Airborne Instruments Laboratory, and H. I. Ewen of Ewen Knight Corp. for many stimulating discussions and suggestions which have helped to clarify some of the concepts presented here.

[10] See Strum, *loc. cit.*, for a discussion of the magnitudes of these effects.

Compact Microwave Single-Sideband Modulator Using Ferrites

J. C. CACHERIS† AND H. A. DROPKIN†

Summary—This paper describes a single-sideband modulator for shifting the frequency of an x-band signal by means of a rotating magnetic field transverse to a ferrite differential half-wave section. The device is one of the first practical applications of the double-refraction properties of ferrites.

Improvements over an earlier model include reduction in size and continuous operation without drift. An efficient and compact magnetic structure has been designed for producing the rotating magnetic field. Excessive heating of the ferrite and voltage breakdown of the coils is eliminated by a forced-air cooling system.

The modulator shifts the microwave-carrier frequency of 9375 mc by plus or minus 20 kc. With a rotating field of approximately 200 oersteds the microwave insertion loss is 1.0 db. The undesired sideband suppression is above 40 db while the carrier suppression is 23 db. For a frequency bandwidth of 500 mc, the insertion loss remains below 5 db.

WHEN A FERRITE is magnetized in a plane transverse to the direction of a propagating wave, the ferrite becomes birefringent. The principal axes are in the transverse plane and have a fixed orientation with respect to the magnetic field. By rotating a suitable transverse field about a round waveguide containing ferrite, a half-wave plate can be made to rotate in effect without any mechanical motion. One of the authors[1] has incorporated this use of a transversely magnetized ferrite in a phase shifter described by Fox[2] to obtain a shift of microwave frequency much larger than was previously possible. It is the purpose of this paper to describe a compact practical single-sideband modulator which shifts the frequency of an incident microwave signal by 20 kc.

The single-sideband modulator (Fig. 1) has an input section consisting of a transition from rectangular to round waveguide, followed by a quarter-wave plate which converts the plane polarized wave to clockwise circular polarization, which may be represented by a vector rotating clockwise f times per second.

The second section contains the transversely magnetized ferrite which acts like a half-wave plate. As the magnetic field rotates, the principal axes of the half-wave plate rotate n times per second. With respect to these rotating axes, the rotating vector representing the incident wave rotates f plus n times per second. The half-wave plate converts the clockwise wave to a counterclockwise wave. In transforming from the rotating axes of the second section to the stationary output section, another n rotations per second are introduced, so that the output has a frequency f plus $2n$.

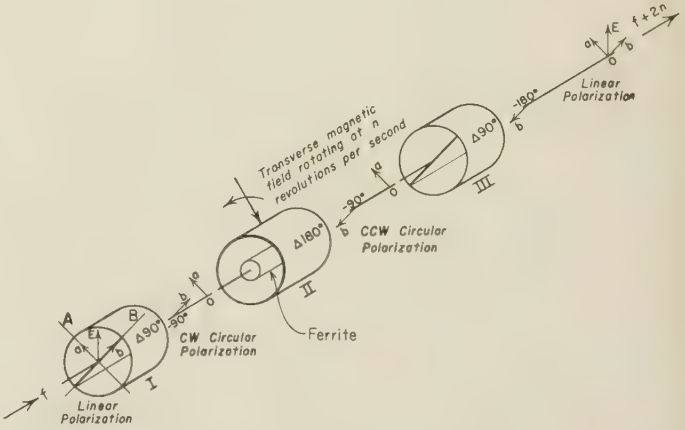

Fig. 1—Microwave single-sideband modulator.

Since the single-sideband modulator is symmetrical about a plane bisecting section II, a short circuit placed in this plane can replace the second half of the single sideband modulator. The output now appears as a reflection from the unit, with the frequency of the reflected wave shifted $2n$ cycles from the incident wave.

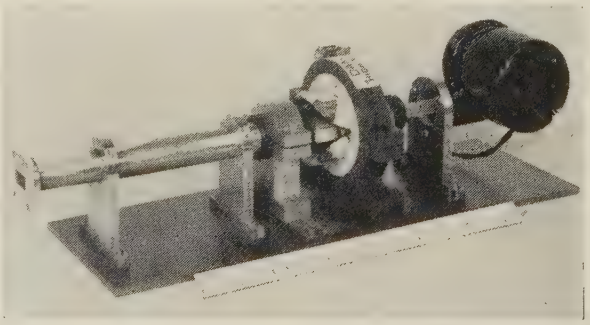

Fig. 2—Microwave single-sideband modulator (reflection type).

Fig. 2 is a photograph of a compact modulator employing the principle above to obtain a 20-kc frequency shift. A rotating magnetic field is produced by two perpendicular magnetic fields excited 90° out of phase. The two phase magnet structure is similar to those used as deflection coils for cathode ray tubes. Pancake coils are bent to fit around the waveguide. A return path is provided for the magnetic flux by an outside ferrite yoke. The short circuit is a sliding plunger which is positioned by a plastic screw. The entire magnet assembly is mounted on a rigid base plate to prevent de-

† Diamond Ordnance Fuze Lab., Washington, D.C.

[1] J. C. Cacheris, "Microwave single-sideband modulator using ferrites," PROC. IRE, vol. 42, pp. 1242–1247; August, 1954.

[2] A. G. Fox, "An adjustable waveguide phase changer," PROC. IRE, vol. 35, pp. 1489–1498; December, 1947.

formation of the circular waveguide. The magnet coils are cooled with a small blower. In addition, a small hole in the short plunger, together with vents, permits cooling air to move past the ferrite inside the waveguide.

An important feature of the single-sideband modulator is that the half-wave section may deviate appreciably from a differential phase shift of 180° without introducing appreciable loss or spurious signals. Fig. 3 shows the effect on an incident clockwise circularly polarized wave of a differential section which differs from a half-wave plate by $\theta°$. The two linearly polarized components of the input circular wave, vectors E_x and E_y, after transmission through a $180°-\theta$ section, have a relative time phase $90°-\theta°$. Each of these vectors may be resolved into time quadrature components as shown. The output vector E_{x1} and E_{y1} produce the desired counterclockwise wave of amplitude $\cos\theta/2$ and the remaining vectors E_{x2} and E_{y2} form an undesired clockwise wave. As a result, the desired power varies as $\cos^2\theta/2$ which very slowly departs from unity as the center section departs from a half-wave plate. For example, for a differential phase shift of 135° (instead of 180°) a loss of only 0.7 db is produced. For the dashed curve of Fig. 4, the differential phase shift was measured as a function of frequency, and the relative power in the counterclockwise wave calculated. The solid curve showing the measured conversion loss is the ratio of shifted frequency reflected power to the input power. This shows that the bandwidth is limited primarily by the variation of differential phase shift with frequency. The undesired circularly polarized wave produced is almost completely attenuated by the input section. Fig. 5 shows that a suppression of the undesired component of 25 db is obtained over the band. The purity of the output is made primarily dependent on the input section, and permits the ferrite half-wave plate to be uncritical.

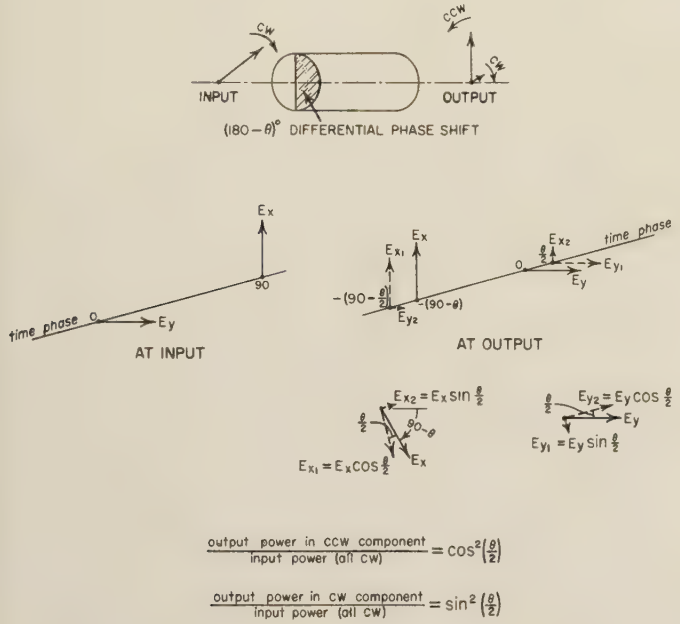

Fig. 3—Effect of imperfect half-wave plate on circularly polarized input.

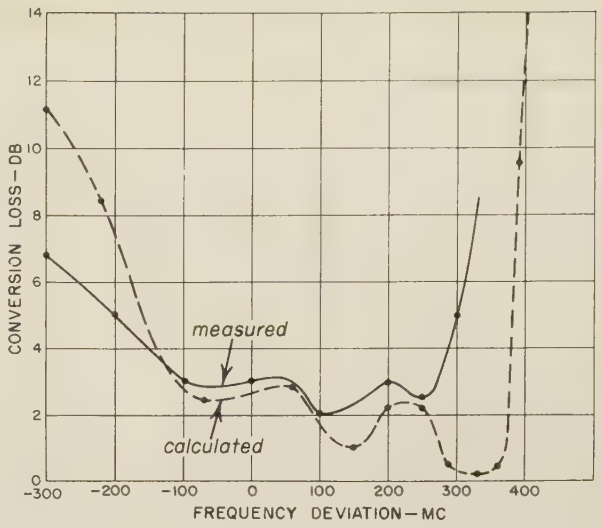

Fig. 4—Conversion loss calculated from differential phase shift compared with measured conversion loss.

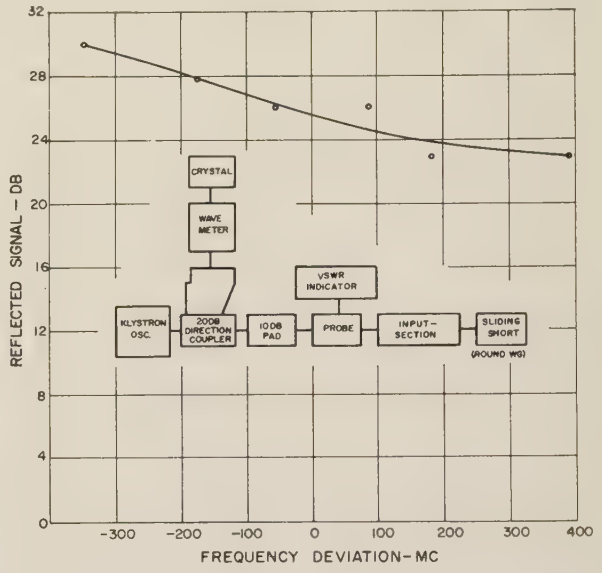

Fig. 5—Suppression of clockwise circular wave by input section.

The principal problem in the practical attainment of single-sideband modulation is to achieve the required differential phase shift with a sufficiently small applied magnetic field. A field of 230 oersteds across the $1\frac{1}{8}$-inch air gap presented by the waveguide requires 25 watts at 10 kc for each of the crossed magnetic fields. This represents the greatest power available without cumbersome power amplifiers, and also approaches the heat dissipating capacity of the coils. By using a tuned class C output stage, the two channels required for the

crossed magnetic fields, together with the oscillator, phasing network, and power supply are mounted on one 7-inch high standard rack mounting chassis.

The Polder[3] equation for an infinite plane wave propagating through lossless ferrite magnetized transversely to the direction of propagation predicts that for the two polarizations the differential phase shift per unit length is given by

$$\frac{\Delta\phi}{l} = \frac{57.3(\epsilon_r)^{1/2}\gamma^2 BM_s}{2c\omega}$$

where ϵ_r is the dielectric constant, c the velocity of light, and the gyromagnetic ratio $= 2.8 \times 10^{-6}$ sec^{-1} oersted^{-1}. At a frequency $f = \omega/2\pi$ of 10,000 mc, for a ferrite having a saturation magnetization M_s of 1700 gauss, and with a field H of 200 oersteds, this equation predicts about 2° of differential phase shift per inch. Experiments show that differential phase shifts of 180° are obtained with a field of 200 oersteds. However, the actual propagation is through a cylindrical waveguide containing a large tapered ferrite cylinder inhomogenously magnetized, filling $\frac{1}{4}$ of the waveguide cross section, followed by a short circuit. Although a theoretical analysis of this geometry is impracticable these large differential phase shifts may be qualitatively ascribed to multiple reflections and higher order modes existing in the ferrite sample. Fig. 6 shows the variation of conversion loss and audio power with field excitation. Also shown are air-gap-flux density and differential phase shift. (The differential phase shift is actually somewhat greater because of temperature difference.) At approximately 200 oersteds, indicated as the operating level, a compromise between least insertion loss and least audio power is reached.

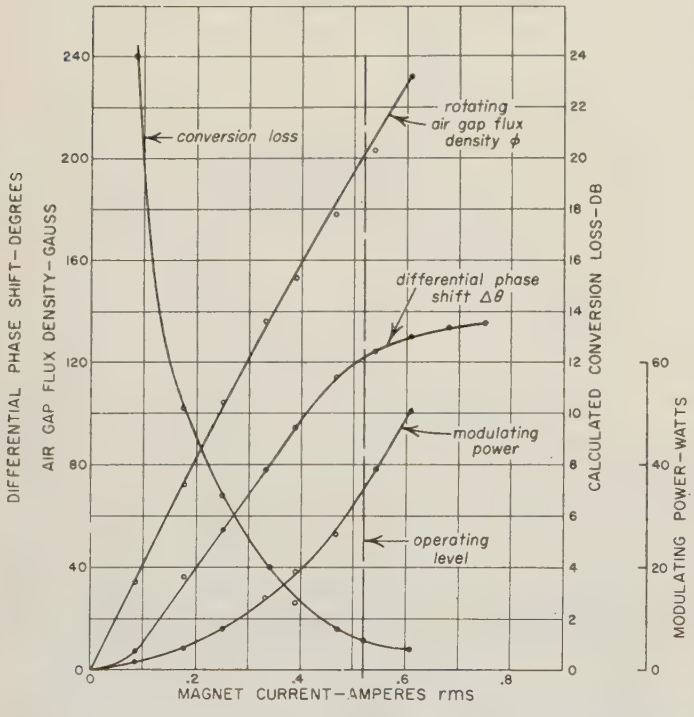

Fig. 6—Characteristic of single-sideband modulator as a function of magnet excitation.

In the absence of an adequate theory, the optimum ferrite geometry must be determined experimentally. Rather than make static differential phase measurements, the modulator itself was used to test the ferrite. In addition to increasing the speed and accuracy of measurement, this arrangement has the advantage of testing the ferrite in the environment of temperature and magnetic field distribution in which it is to be used. Fig. 7 is a block diagram of the setup. With the klystron

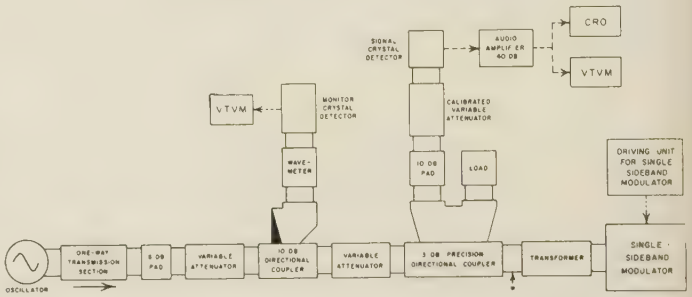

Fig. 7—Experimental arrangement for measurement of conversion loss and spurious signal suppression.

frequency and power monitored, the principal signal proceeds through a precision coupler and is reflected and shifted in frequency by the modulator. The shifted frequency signal is detected in the signal crystal arm. A calibration, effected by substitution of a short circuit at *, permits the conversion loss to be read directly from settings of the calibrated variable attenuator.

Fig. 8 shows the reduction of the bandwidth when the magnet excitation is reduced. It can be seen that the flux may be reduced 25 per cent, and consequently the power 50 per cent, if a reduced bandwidth of 350 mc is acceptable. Also, it is clear that the operation of the single-sideband modulator is in no sense critically dependent on driving current.

Variations of 1/10 inch in dimensions of the ferrite sample are sufficient to alter completely the differential phase obtainable. A number of cylinders and tapered cylinders held promise of having broadband phase shift. For several of these geometries, small dimensional variations were made to maximize the bandwidth. Essentially similar results are obtained for these various geometries. Fig. 9 shows that changes of a few thousandths of an inch in the cylinder length (t) are significant in changing the shape and the location of the conversion loss curve along the frequency axis. Despite this strong dimensional dependence, the phase properties are stable and repeatable.

[3] D. Polder, "On the theory of ferromagnetic resonance," *Phil. Mag.*, vol. 40, pp. 99–115; January, 1949.

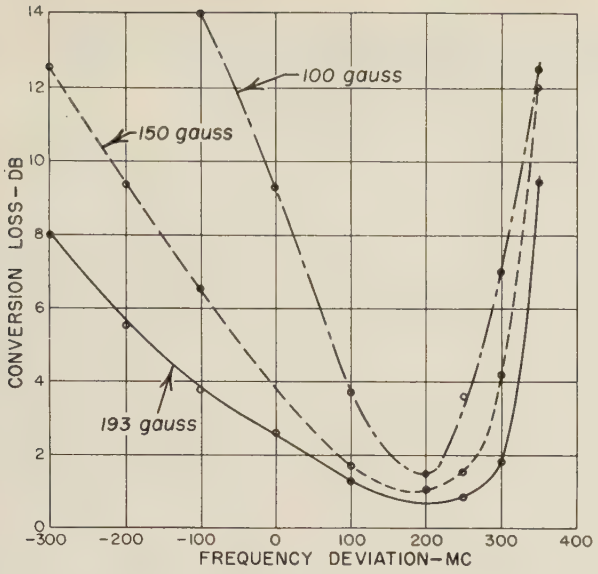

Fig. 8—Variation of conversion loss characteristic with magnetic field strength.

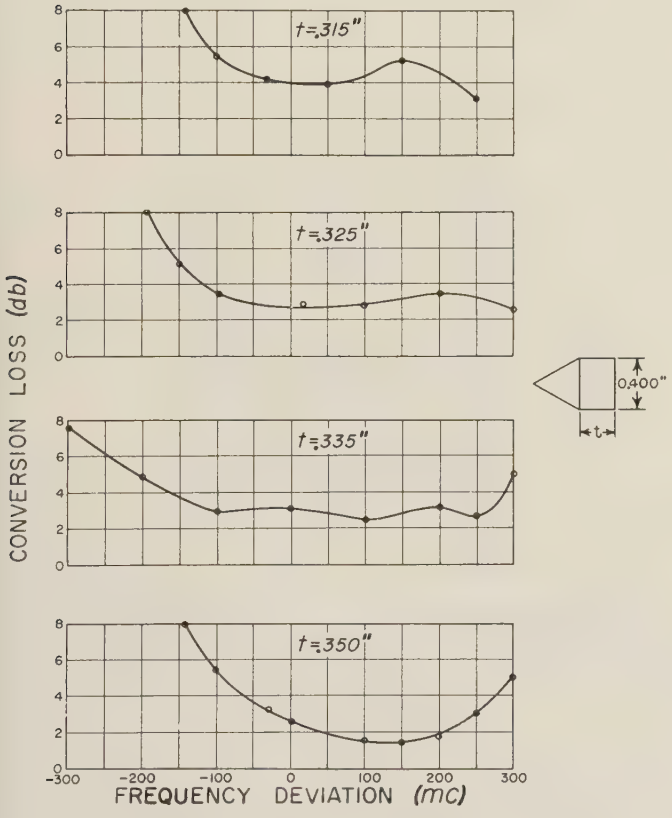

Fig. 9—Variation of conversion loss characteristic with cylinder length.

The frequency response of the reflection-type single-sideband modulator is shown in Fig. 10. The conversion loss has a minimum of about 2 db and over a 500 mc band, remains below 5 db. By adjustment of the short circuit, the minimum insertion loss can be reduced to less than 1 db, with some narrowing of the frequency response. The frequency at which the minimum loss is obtained can be shifted anywhere within the 500 mc range by the single adjustment of the short circuit plunger.

So far, the principal interest has been directed toward the conversion loss. A second important property is the suppression of undesired frequency components. The largest undesired frequency component is the unshifted signal, which is recognizable as a 20 kc envelope on the signal reflected from the modulator. The power level of the signal is determined from the relative beat amplitude, and is plotted in Fig. 10. This signal may be matched out with a transformer. Other spurious frequency components will be produced by any imperfection in the clockwise filtering action of the input section when the central section does not provide 180° phase shift. Also, it is likely that any departure from axial symmetry and any nonuniformity in the rotation of the magnetic field will produce higher order sidebands. These remain after the unshifted signal has been matched out. The power level represented by the assumption of an equivalent single frequency for these residual signals is also shown in Fig. 10.

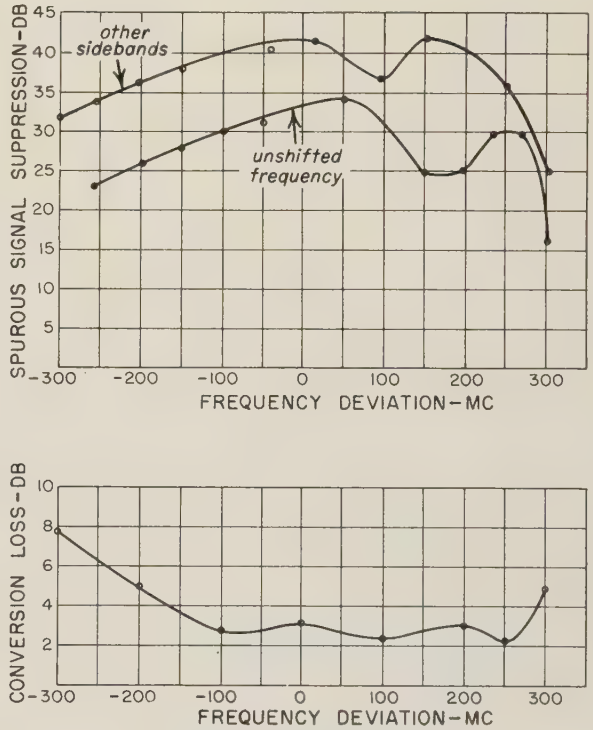

Fig. 10—Operating characteristics of compact reflection type single-sideband modulator.

The reflection-type single-sideband modulator described in this report is a compact, conservatively rated, trouble-free device. Over a 500-mc bandwidth, it has given reliable operation as an x-band 20-kc frequency shifter.

A Semi-Infinite Array of Parallel Metallic Plates of Finite Thickness for Microwave Systems*

ROBIN I. PRIMICH†

Summary—An array of parallel metallic plates of finite thickness are useful in microwave lenses. The effect of finite thickness in the idealized situation of a semi-infinite array of perfect conductivity, is treated theoretically and experimentally for normal incidence of a uniform plane wave on the plane interface separating the medium from free space. The theoretical discussion involves the approximate variational method and a procedure is given for estimating the order of magnitude of the error in the final result. It is shown that it can be advantageous to use plates of finite thickness since the reflection from the interface can be reduced from that existing for infinitely thin plates.

Introduction

TO OBTAIN a rigid structure, the practical use of a system of parallel metallic plates as a refracting medium in microwave systems, requires plates of appreciable thickness. The effect of this thickness on the reflecting and transmitting properties of the semi-infinite medium has caused much interest, but as yet no solution has been published, although Epstein[1] has given an empirical correction to the case of infinitely thin plates based on experimental evidence. An attempt was made by the author to extend the various rigorous theoretical methods to cover the case of plates of finite thickness, but these proved discouraging. Of the various approximate methods available, the variational method appears to be the most suitable as it provides a means of estimating the degree of approximation and also yields best results where the form of the trial field is known, as in the present case.

Using this method, formulas have been obtained for the complex reflection coefficients at the interface of a semi-infinite medium of parallel, perfectly conducting, metallic plates of finite thickness, for normal incidence of a uniform plane wave. An estimate of the order of accuracy is made by two methods. The polarization is such that electric vector is parallel to the plate edges. Theoretical results are confirmed by experimental results obtained in a strip transmission line at 8.0 to 11.0 cm wavelengths.

The Variational Method

The variational technique, in its form due to Schwinger[2] has been used widely in microwave problems. For the present application it is convient to obtain expressions for the complex impedance or admittance at the interface in terms of either the interface electric or magnetic field. These expressions are of such a form that they are stationary for arbitrary variations of the interface fields about their correct value. This means that if the assumed field distribution is in error to a certain order, then the desired impedance or admittance is in error to the second order, provided the original error is not too large.

The basic problem to be studied is that of the normal incidence of a uniform plane wave on the plane interface of a semi-infinite array of perfectly conducting, parallel, metallic plates of arbitrary thickness $(b-a)$ (Fig. 1). The spacing between the plates is occupied by

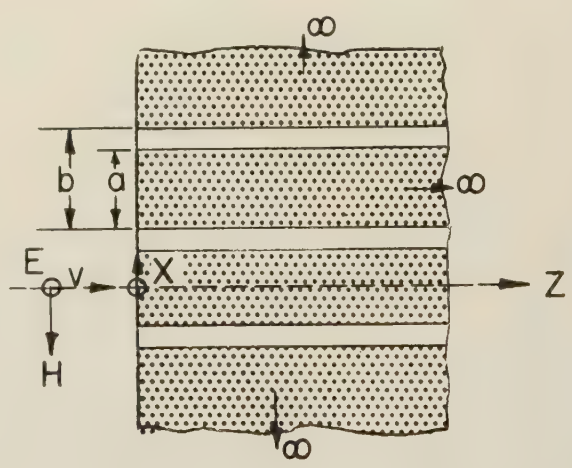

Fig. 1—A semi-infinite array of dielectric filled metal plates.

a dielectric of permittivity ϵ. The spacing a is restricted to allow the propagation of the H_{01} mode only, *i.e.*,

$$a < \left(\lambda_\epsilon = \frac{\lambda_0}{\sqrt{\epsilon}}\right) < 2a$$

λ_0 = free space wavelength.

To obtain a particular variational expression it is necessary to evaluate either the tangential electric or magnetic fields at $z=0$, over some region b, and then to integrate over this region. Consequently, it is permissible to equate fields valid for all x, or fields valid in the region b only. The latter procedure results in considerable simplification and will be used.

The field equations have been developed by Berz[3] in a related problem and are directly applicable.

* The work for this paper was performed at Imperial College, London, Eng.

† Def. Res. Board, Ottawa, Canada.

[1] D. J. Epstein, "Phase shift of microwaves in passage through parallel plate arrays," Tech. Rep. 42, Lab. for Insulation Res., M.I.T.; August, 1950.

[2] J. Schwinger, unpublished notes on waveguide discontinuities, foreword by Saxon.

[3] F. Berz, "Reflection and refraction of microwaves at a set of parallel metallic plates," *Proc. IEE*, vol. 98, pt. 3, pp. 47–55; January, 1951.

For the polarization shown the problem is two-dimensional and the only three components of the field are:

$$E_y(x, z),\ H_x(x, z) = -(j/\omega\mu)\frac{\partial E_y}{\partial z},\quad H_z(x, z) = (j/\omega\mu)\frac{\partial E_y}{\partial z}$$

and of these the continuity of E_y and H_x are only necessary to satisfy the boundary conditions at $z=0$. Furthermore, since there is no component perpendicular to the dielectric at $z=0$, it is sufficient to use $\partial E_y/\partial x$ rather than H_x.

The fields are listed below.

Plate Region: $z>0$

$$\left.\begin{aligned} E_y &= \sum_{n=1}^{\infty} B_n \cos\frac{n\pi x}{a}\exp(-j\beta_n z)\\ \frac{\partial E_y}{\partial z} &= -j\sum_{n=1}^{\infty}\beta_n B_n\cos\frac{n\pi x}{a}\exp(-j\beta_n z)\end{aligned}\right\}\ \text{with } \beta_n^2 = \epsilon\beta_0^2 - \left(\frac{n\pi}{a}\right)^2 \quad |x| \leqq \frac{a}{2}$$

and at $z=0$

$$\left.\begin{aligned} E_{y_0} &= \sum_{n=1}^{\infty} B_n\cos\frac{n\pi x}{a}\\ \left.\frac{\partial E_y}{\partial z}\right|_0 &= -j\sum_{n=1}^{\infty}\beta_n B_n\cos\frac{n\pi x}{a}\end{aligned}\right\}\ \text{with } \beta_n^2 = \epsilon\beta_0^2 - \left(\frac{n\pi}{a}\right)^2 \quad |x| \leqq \frac{a}{2}$$

by Fourier analysis

$$B_n = \frac{2}{a}\int_{-a/2}^{a/2} E_{y_0}\cos\frac{n\pi x}{a}\,dx = \frac{2}{a}\int_{ap} E_{y_0}\cos\frac{n\pi x}{a}\,dx \qquad \int_{ap} = \int_{-a/2}^{a/2}.$$

Free Space Region, $z<0$

Noting the periodicity b in the x direction, the field can be written as a Fourier Series valid for all x as follows:

$$E_y = \exp\cdot(-j\beta_0 z) + A_0\exp\cdot(j\beta_0 z) + \sum_{m=1}^{\infty} A_m\cos\frac{2m\xi\pi x}{a}\exp\cdot(j\alpha_m z)$$

$$\frac{\partial E_y}{\partial z} = -j\beta_0\exp\cdot(-j\beta_0 z) + \cdot j\beta_0 A_0\exp\cdot(j\beta_0 z) + j\sum_{m=1}^{\infty}\alpha_m A_m\cos\frac{2m\xi\pi x}{a}\exp\cdot(j\alpha_m z)$$

$$\alpha_m = \sqrt{\beta_0^2 - \left(\frac{2m\pi}{b}\right)^2},\quad \beta_0 = \frac{2\pi}{\lambda_0},\quad \xi = \frac{a}{b}$$

and at $z=0$

$$E_{y_0} = 1 + A_0 + \sum_{m=1}^{\infty} A_m\cos\frac{2m\xi\pi x}{a}$$

$$\left.\frac{\partial E_y}{\partial z}\right|_0 = -j(1-A_0)\beta_0 + j\sum_{m=1}^{\infty}\alpha_m A_m\cos\frac{2m\xi\pi x}{a}.$$

Then, by Fourier analysis,

$$1 + A_0 = \frac{1}{b}\int_{-b/2}^{b/2} E_{y_0}dx = \frac{1}{b}\int_{ap} E_{y_0}dx$$

and

$$A_m = \frac{2}{b}\int_{ap} E_{y_0}\cos\frac{2m\xi\pi x}{a}\,dx. \qquad \text{for } m \neq 0.$$

Equating the magnetic fields in the aperture

$$\left(H_{z_0} \text{ or } \left.\frac{\partial E_y}{\partial_z}\right|_0\right),$$

and substituting for A_m and B_n;

$$-j\sum_{n=1}^{\infty}\beta_n\cos\frac{n\pi x}{a}\,\frac{2}{a}\int_{ap} E_{y_0}\cos\frac{n\pi x}{a}\,dx = -j(1-A_0)\beta_0 + j\sum_{m=1}^{\infty}\alpha_m\cos\frac{2m\xi\pi x}{a}\cdot\frac{2}{b}\int_{ap} E_{y_0}\cos\frac{2m\xi\pi x}{a}\,dx. \tag{1}$$

Multiplying by E_{y_0} and integrating over the aperture ($|x| \leqq a/2$)

$$\beta_0(1-A_0)\int_{ap} E_{y_0}dx = \frac{2}{a}\sum_{n=1}^{\infty}\beta_n\int_{ap} E_{y_0}\cos\frac{n\pi x}{a}\,dx\int_{ap} E_{y_0}\cos\frac{n\pi x}{a}\,dx + \frac{2}{b}\sum_{m=1}^{\infty}\alpha_m\int_{ap} E_{y_0}\cos\frac{2m\xi\pi x}{a}\,dx\int_{ap} E_{y_0}\cos\frac{2m\xi\pi x}{a}\,dx$$

and then dividing by

$$1 + A_0 = \frac{1}{b}\int_{ap} E_{y_0} dx$$

results in

$$\beta_0 \frac{1 - A_0}{1 + A_0} = \frac{2}{\xi}\sum_{n=1}^{\infty} \beta_n \left\{ \frac{\int_{ap} E_{y_0} \cos \frac{n\pi x}{a}\, dx}{\int_{ap} E_{y_0} dx} \right\}^2 + 2\sum_{m=1}^{\infty} \alpha_m \left\{ \frac{\int_{ap} E_{y_0} \cos \frac{2m\xi\pi x}{a}\, dx}{\int_{ap} E_{y_0} dx} \right\}^2 \quad \cdots . \quad (2)$$

$$Y = \frac{1 - A_0}{1 + A_0}$$

has the dimensions of an admittance and is, in fact, the input admittance at the interface on the free space side. It is stationary with respect to arbitrary variations of E_{y_0} about its correct value. This can be seen from the following: taking the first variation of Y with respect to E_{y_0},

$$\delta\left[\beta_0 Y \left\{\int_{ap} E_{y_0} dx\right\}^2\right]$$

$$= \beta_0 \left\{\int_{ap} E_{y_0} dx\right\}^2 \delta Y + \beta_0 Y 2 \int_{ap} E_{y_0} dx \int_{ap} \delta E_{y_0} dx$$

$$= \frac{4}{\xi}\sum_{n=1}^{\infty} \beta_n \int_{ap} E_{y_0} \cos \frac{n\pi x}{a}\, dx \int_{ap} \delta E_{y_0} \cos \frac{n\pi x}{a}\, dx + 4\sum_{m=1}^{\infty} \alpha_m \int_{ap} E_{y_0} \cos \frac{2m\xi\pi x}{a} dx \int_{ap} \delta E_{y_0} \cos \frac{2m\xi\pi x}{a}\, dx.$$

Assuming that the order of summation and integration can be interchanged,

$$\beta_0 \left\{\int E_{y_0} dx\right\}^2 \delta Y$$

$$= 2\int_{ap} \delta E_{y_0} \left[\frac{2}{\xi}\sum_{n=1}^{\infty} \beta_n \cos \frac{n\pi x}{a} \int_{ap} E_{y_0} \cos \frac{n\pi x}{a}\, dx + 2\sum_{m=1}^{\infty} \alpha_m \cos \frac{2m\xi\pi x}{a} \int_{ap} E_{y_0} \cos \frac{2m\xi\pi x}{a}\, dx - \beta_0 \frac{1 - A_0}{1 + A_0} \int_{ap} E_{y_0} dx \right].$$

Using

$$1 + A_0 = \frac{1}{b}\int_{ap} E_{y_0} dx,$$

the expression in square brackets is zero by virtue of (1). Therefore $\delta Y = 0$, and Y is stationary.

Eq. (2) yields A_0, the complex reflection coefficient at the interface for free space incidence, and partially specifies the properties of the interface. To complete this specification[4] it is necessary to find B the complex reflection coefficient for plate region incidence; *i.e.*, the fields now are,

$$E_y = \cos \frac{\pi x}{a} \exp \cdot (j\beta_1 z) + B_1 \cos \frac{\pi x}{a} \exp \cdot (-j\beta_1 z) + \sum_{n=3}^{\infty} B_n \cos \frac{n\pi x}{a} \exp \cdot (-j\beta_n z) \qquad |x| \leqq \frac{a}{2},\ z < 0$$

$$E_y = A_0 \exp \cdot (j\beta_0 z) + \sum_{n=1}^{\infty} A_m \cos \frac{2m\xi\pi x}{a} \exp \cdot (j\alpha_m z) \qquad z < 0.$$

Note that B_n and A_m do not have the same values as for free space incidence, but the same symbols have been used to distinguish the plate region and free space region fields respectively.

In exactly the same way as before, one obtains, by equating the magnetic fields in the plane $z = 0$,

$$\beta_0 \frac{1 - \beta_1}{1 + B_1} = \frac{\beta_0 \xi}{2} \left\{ \frac{\int_{ap} E_{y_0} dx}{\int_{ap} E_{y_0} \cos \frac{\pi x}{a}\, dx} \right\}^2 + \sum_{n=3}^{\infty} \beta_n \left\{ \frac{\int_{ap} E_{y_0} \cos \frac{n\pi x}{a}\, dx}{\int_{ap} E_{y_0} \cos \frac{\pi x}{a}\, dx} \right\}^2 + \xi\sum_{m=1}^{\infty} \alpha_m \left\{ \frac{\int_{ap} E_{y_0} \cos \frac{2m\xi\pi x}{a}\, dx}{\int_{ap} E_{y_0} \cos \frac{\pi x}{a}\, dx} \right\}^2 \cdots . \quad (3)$$

$$Y = \frac{1 - B_1}{1 + B_1}$$

is now the input admittance at the interface for plate region incidence and it can be shown to be stationary.

[4] R. I. Primich, "A general experimental method to determine the properties of an artificial delay medium, applied to semi-infinite array of parallel metallic plates," *Proc. IEE*, vol. 102, pt. B, pp. 26–36; January, 1955.

In the absence of loss, $|B_1|_p = |A_0|_0$ since B_{1p} is now the complex reflection coefficient on the plate region side.

There are two corresponding expressions for

$$\frac{1+A_0}{1+A_0} \quad \text{and} \quad \frac{1+B_1}{1-B_1}$$

in terms of the tangential magnetic field in the aperture plane. The derivation is similar to the above except that the electric fields are now equated in the aperture, piecewise over the regions

$$|x| \leqq \frac{a}{2} \quad \text{and} \quad |x| \leqq \frac{b-a}{2}.$$

The results are

$$\frac{1}{\beta_0}\frac{1+A_0}{1-A_0} = \frac{2}{\xi}\sum_{n=1}^{\infty}\frac{1}{\beta_n}\left\{\frac{\int_{ap} F_0 \cos\frac{n\pi x}{a}\,dx}{\int_b F_0 dx}\right\}^2 + 2\sum_{m=1}^{\infty}\frac{1}{\alpha_m}\left\{\frac{\int_b F_0 \cos\frac{2m\xi\pi x}{a}\,dx}{\int_b F_0 dx}\right\}^2 \cdots \quad (4)$$

and

$$\frac{1}{\beta_1}\frac{1+B_1}{1-B_1} = \frac{\xi}{2\beta_0}\left\{\frac{\int_b F_0 dx}{\int_{ap} F_0 \cos\frac{\pi x}{a}\,dx}\right\}^2 + \sum_{n=3}^{\infty}\frac{1}{\beta_n}\left\{\frac{\int_{ap} F_0 \cos\frac{n\pi x}{a}\,dx}{\int_{ap} F_0 \cos\frac{\pi x}{a}\,dx}\right\}^2 + \xi\sum_{m=1}^{\infty}\frac{1}{\alpha_m}\left\{\frac{\int_b F_0 \cos\frac{2m\xi\pi x}{a}\,dx}{\int_b F_0 \cos\frac{\pi x}{a}\,dx}\right\}^2 \cdots \quad (5)$$

where

$$F_0 = \left.\frac{\partial E_y}{\partial z}\right|_0 \propto H_{x_0}.$$

$$\frac{1+A_0}{1-A_0} \quad \text{and} \quad \frac{1+B_1}{1-B_1}$$

now have the dimensions of an impedance Z and, in fact, are the complex input impedances at the interface for free space and plate region incidence respectively. They are stationary with respect to arbitrary variations of E_{y_0} about the correct value.

An Estimate of the Error in the Variational Solution

Use of the Complex Plane

For a given region of incidence there are a pair of corresponding expressions giving the input impedance at the interface in terms of the electric or magnetic fields in the aperture plane; *i.e.*,

$$Z_E = \left[\frac{1-A_0}{1-A_0}\right]_E \text{ from (2)}$$

$$Z_H = \left[\frac{1+A_0}{1-A_0}\right] \text{ from (4).}$$

Now for the correct fields E_{y_0} and F_0, $Z_E = Z_H$, but for any approximate field $Z_E \neq Z_H$. However, if it is assumed that it is possible to express E_{y_0} as a sum of terms which successively represent better approximations, then if $Z_E = R_E + jX_E$ is plotted in the complex plane for various degrees of approximation, a curve results which must eventually approach the correct value of Z_E, and a similar curve for $Z_H = R_H + jX_H$ must eventually intersect it at $Z_E = Z_H$. Practically, it is possible to predict the point of intersection $Z_E = Z_H$ by using a reasonable number of approximations. In the present instance, the aperture fields can be written as a series of known forms in which the addition of a single term represents a better approximation to the correct field.

An alternative approach to this problem has been used by Miles[5] who, in a study of an array of parallel metallic strips, showed that R_E, R_H and X_E, X_H are individually stationary and bounded. This means that A_0 and B_{1p} are known within wider limits that R_E and X_E or R_H and X_H and in general these limits are wider than given by the above method.

Equivalent Circuit Method

An alternative method of estimating the error is based on a suggestion of Brown's[6] and is very similar to that used by Collin,[7] but it is derived in terms of different parameters.

By using a short circuit termination in either the free space or plate regions, the input impedances and admittances become purely imaginary and one may associate with them a three-element reactive network, the values of which can be found from three short circuit positions.

[5] J. W. Miles, "On the diffraction of an electromagnetic wave through a plane screen," *J. Appl. Phys.*, vol. 20, pp. 760–771; August, 1949.

[6] J. Brown, letter in *Electronic Engrg.*; October, 1950.

[7] R. E. Collin, "Interface problems at dielectric discontinuities in waveguides," Ph.D. dissertation, Univ. of London, Eng.; 1953.

A typical variational expression will be derived, *i.e.*, for free space incidence, and in terms of the aperture electric field. (See Fig. 2.)

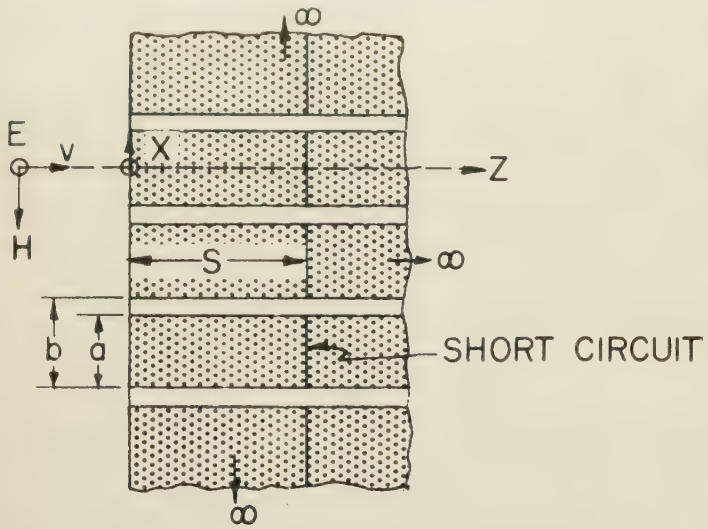

Fig. 2—A semi-infinite array of metal plates with short circuit termination.

The distance S is such that the evanescent modes excited at the interface are of negligible amplitude at the short circuit. At some plane Z in free space, again sufficiently far from the interface, the electric field will have a zero value. Let the distance of this plane from the interface be d.

If $B_1 \cos \pi x/a \exp(-j\beta_1 z)$ is the transmitted wave in the plate region, there will be a reflected wave $\exp(j\phi_p) B_1 \cos \pi x/a \exp j\beta_1 z$ due to the short circuit, where ϕ_p is the wave's phase referred to $Z=0$. At $Z=S$ the total electric field must be zero, which gives $\phi_p = \pi - 2\beta_1 S$.

The total plate region field is then

$$E_y = 2B_1 \cos\frac{\pi x}{a} \exp\left(j\frac{\phi_p}{2}\right) \cos\left(\beta_1 z + \frac{\phi_p}{2}\right) + \sum_{n=3}^{\infty} B_n \cos\frac{n\pi x}{a} \exp(-j\beta_n z)$$

$$\frac{\partial E_y}{\partial z} = -2\beta_1 B_1 \cos\frac{\pi x}{a} \cdot \exp\left(j\frac{\phi_p}{2}\right) \sin\left(\beta_1 z + \frac{\phi_p}{2}\right) - j\sum_{n=3}^{\infty} \beta_n B_n \cos\frac{n\pi x}{a} \exp(-j\beta_n z) \Bigg\} \quad |x| \leqq \frac{a}{2}$$

at $Z=0$,

$$E_{y_0} = 2B_1 \cos\frac{\pi x}{a} \cdot \exp j\frac{\phi_p}{2} \cos\frac{\phi_p}{2} + \sum_{n=3}^{\infty} B_n \cos\frac{n\pi x}{a}$$

$$\left.\frac{\partial E_y}{\partial z}\right|_0 = -2\beta_1 B_1 \cos\frac{\pi x}{a} \exp\cdot\left(j\frac{\phi p}{2}\right)$$

$$\cdot \sin\frac{\phi_p}{2} - j\sum_{n=3}^{\infty} \beta_n B_n \cos\frac{n\pi x}{a}$$

by Fourier analysis,

$$2B_1 \exp\cdot\left(j\frac{\phi_p}{2}\right) \cos\frac{\phi_p}{2} = \frac{2}{a}\int_{ap} E_{y_0} \cos\frac{\pi x}{a}\, dx$$

$$B_n = \frac{2}{a}\int_{ap} E_{y_0} \cos\frac{\pi n x}{a}\, dx.$$

The free space magnetic field is still given by

$$\left.\frac{\partial E_y}{\partial z}\right|_0 = -j\beta_0(1 - A_0) + j\frac{2}{b}\sum_{m=1}^{\infty} \alpha_m \cos\frac{2m\xi\pi x}{a}\int_{ap} E_{y_0} \cos\frac{2m\xi\pi x}{a}\, dx.$$

Equating these in the aperture ($|x| \leqq a/2$) and multiplying by E_{y_0}, then integrating over $|x| \leqq a/2$ and dividing by

$$1 + A_0 = \frac{1}{b}\int_{ap} E_y dy,$$

there results, finally

$$j\beta_0 \frac{1 - A_0}{1 + A_0} = -\frac{2\beta_1}{\xi} \tan\frac{\phi_p}{2} \left\{\frac{\int_{ap} E_{y_0} \cos\frac{\pi x}{a}\, dx}{\int_{pa} E_{y_0} dx}\right\}^2 + j\frac{2}{\xi}\sum_{n=3}^{\infty} \beta_n \left\{\frac{\int_{ap} E_{y_0} \cos\frac{n\pi x}{a}\, dx}{\int_{ap} E_{y_0} dx}\right\}^2 + j2\sum_{m=1}^{\infty} \alpha_m \left\{\frac{\int_{ap} E_{y_0} \cos\frac{2m\xi\pi x}{a}\, dx}{\int_{ap} E_{y_0}\, dx}\right\}^2$$

put

$$\frac{\alpha_m}{\beta_0} = -jQ_m; \qquad \frac{\beta_n}{\beta_0} = -jR_n$$

and

$$\frac{\beta_1}{\beta_0} = N;$$

Q_m, R_n are real and positive for $m, n \neq 1$. Under short circuit conditions $A_0 = \exp\cdot(j\phi_0)$, $\phi_0 =$ phase of the unit reflected wave referred to $z=0$. Then

$$\frac{1 - A_0}{1 + A_0} = -j \tan\frac{\phi_0}{2}$$

and so

$$\tan\frac{\phi_0}{2}=\frac{2N}{\xi}\tan\frac{\phi_p}{2}\left\{\frac{\int_{ap}E_{y_0}\cos\frac{\pi x}{a}\,dx}{\int_{ap}E_{y_0}dx}\right\}^2+\frac{2}{\xi}\sum_{n=3}^{\infty}R_n\left\{\frac{\int_{ap}E_{y_0}\cos\frac{\pi n x}{a}\,dx}{\int_{ap}E_{y_0}dx}\right\}^2+2\sum_{m=1}^{\infty}Q_m\left\{\frac{\int_{ap}E_{y_0}\cos\frac{2m\xi\pi x}{a}\,dx}{\int_{ap}E_{y_0}dx}\right\}^2\cdots. \quad (6)$$

The corresponding magnetic field expression is

$$\cot\frac{\phi_0}{2}=\frac{2}{\xi N}\cot\frac{\phi_p}{2}\left\{\frac{\int_{ap}H_{x_0}\cos\frac{\pi x}{a}\,dx}{\int_{ap}H_{x_0}dx}\right\}^2+\frac{2}{\xi}\sum_{n=3}^{\infty}\frac{1}{R_n}\left\{\frac{\int_{ap}H_{x_0}\cos\frac{n\pi x}{a}\,dx}{\int_{ap}H_{x_0}dx}\right\}^2+2\sum_{m=1}^{\infty}\frac{1}{Q_m}\left\{\frac{\int_{b}H_{x_0}\cos\frac{2m\xi\pi x}{a}\,dx}{\int_{ap}H_{x_0}dx}\right\}. \quad (7)$$

Both expressions are stationary and, for arbitrary variations about $E_{y_0}(H_{x_0})$, $\tan\phi_0/2(\cot\phi_0/2)$ is an absolute minimum (since $\tan\phi_0/2(\cot\phi_0/2)$ is real). Consequently for any trial field $\tan\phi_0/2(E_{y_0})$ is too large and $\tan\phi_0/2(H_{x_0})$ is too small. Thus for any three values of $\tan\phi_p/2$ (short circuit position) three reactances can be determined within known limits. However, only two of these reactances can be identified with known terminations in the equivalent circuit, but by setting up two similar variational expressions for plate region incidence, a further two reactances may be found and any three of the four may be chosen.

The expressions for plate region incidence are

$$N\tan\frac{\phi_p}{2}=-\frac{\xi}{2}\tan\frac{\phi_0}{2}\left\{\frac{\int_{ap}E_{y_0}dx}{\int_{ap}E_{y_0}\cos\frac{\pi x}{a}\,dx}\right\}^2+\sum_{n=3}^{\infty}R_n\left\{\frac{\int_{ap}E_{y_0}\cos\frac{n\pi x}{a}\,dx}{\int_{ap}E_{y_0}\cos\frac{\pi x}{a}\,dx}\right\}^2+\xi\sum_{m=1}^{\infty}Q_m\left\{\frac{\int_{ap}E_{y_0}\cos\frac{2m\xi\pi x}{a}\,dx}{\int_{ap}E_{y_0}\cos\frac{\pi x}{a}\,dx}\right\}^2 \quad (8)$$

$$\frac{1}{N}\cot\frac{\phi_p}{2}=-\frac{\xi}{2}\cot\frac{\phi_0}{2}\left\{\frac{\int_{b}H_{x_0}dx}{\int_{ap}H_{x_0}\cos\frac{\pi x}{a}\,dx}\right\}^2+\sum_{n=3}^{\infty}\frac{1}{R_n}\left\{\frac{\int_{ap}H_{x_0}\cos\frac{n\pi x}{a}\,dx}{\int_{ap}H_{x_0}\cos\frac{\pi x}{a}\,dx}\right\}^2+\xi\sum_{m=1}^{\infty}\frac{1}{Q_m}\left\{\frac{\int_{b}H_{x_0}\cos\frac{2m\xi\pi x}{a}\,dx}{\int_{ap}H_{x_0}\cos\frac{\pi x}{a}\,dx}\right\}^2. \quad (9)$$

Determination of the Reactances

Fig. 3 shows the form of the assumed equivalent circuit. All impedances are purely reactive and are normalized relative to Z_0.

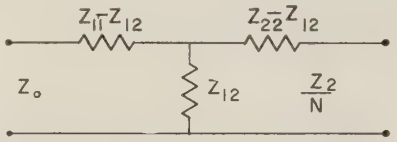

Fig. 3—Equivalent circuit of interface.

Two simple equivalent circuit terminations that can be associated with the short circuit positions in the thick plate system are the open and short circuit conditions.

Free Space Incidence

For any termination Z_R, the input impedance (Fig. 3) is

$$Z_{in}=Z_{11}-\frac{Z_{12}^2}{Z_{22}+Z_R}.$$

1) Short circuit termination, $(Z_R = 0)$

$$Z_{in} = \frac{Z_{11}Z_{22} - Z_{12}^2}{Z_{22}}$$

$$= j\frac{X_{11}X_{22} - X_{12}^2}{X_{22}} \text{ for } Z_{11} = jX_{11},\ Z_{22} = jX_{22},\ Z_{12} = jX_{12}.$$

2) Open circuit termination, $(Z_R = \infty)$

$$Z_{in} = Z_{11} = jX_{11}.$$

Now in the plate system $\tan \phi_p/2$ is the susceptance produced at $z = +0$ by the short circuit at some position s. Thus,

$$Z_R = 0 \text{ corresponds to } \tan\frac{\phi_p}{2} = \infty$$

$$Z_R = \infty \text{ corresponds to } \tan\frac{\phi_p}{2} = 0.$$

Therefore

$$\frac{1}{X_{11}} = \tan\frac{\phi_0}{2} = (6) \text{ for } \tan\frac{\phi_p}{2} = 0$$

$$\frac{X_{22}}{X_{11}X_{22} - X_{12}^2} = \tan\frac{\phi_0}{2} = (6) \text{ for } \tan\frac{\phi_p}{2} = \infty.$$

Similarly, for plate region incidence,

$$\frac{1}{X_{22}} = \tan\frac{\phi_p}{2} = (8) \text{ for } \tan\frac{\phi_0}{2} = 0$$

$$\frac{X_{11}}{X_{11}X_{22} - X_{12}^2} = \tan\frac{\phi_p}{2} = (8) \text{ for } \tan\frac{\phi_0}{2} = \infty.$$

Hence,

$$X_{11},\ X_{22},\ \frac{X_{11}X_{22} - X_{12}^2}{X_{22}}\quad \frac{X_{11}X_{22} - X_{12}^2}{X_{11}}$$

so determined will be too small, while, from the corresponding magnetic field expressions, they will be too large and thus the reactances are known within limits. Therefore, it is only necessary to find X_{11}, X_{22} together with either

$$\frac{X_{11}X_{22} - X_{12}^2}{X_{22}} \quad \text{or} \quad \frac{X_{11}X_{22} - X_{12}^2}{X_{11}}.$$

Numerical Work

Choice of a Trial Field

One of the most important factors in determining the final accuracy in the variational method is the choice of the type of trial field. For the aperture electric field in the plate region the field expansion is known, *i.e.*,

$$E_{y_0} = \sum_{n=1}^{\infty} B_n \cos\frac{n\pi x}{a} \qquad |x| \leqq a/2.$$

Using this in (2) and (3) the formulas for numerical computation (listed in the appendix) are obtained.

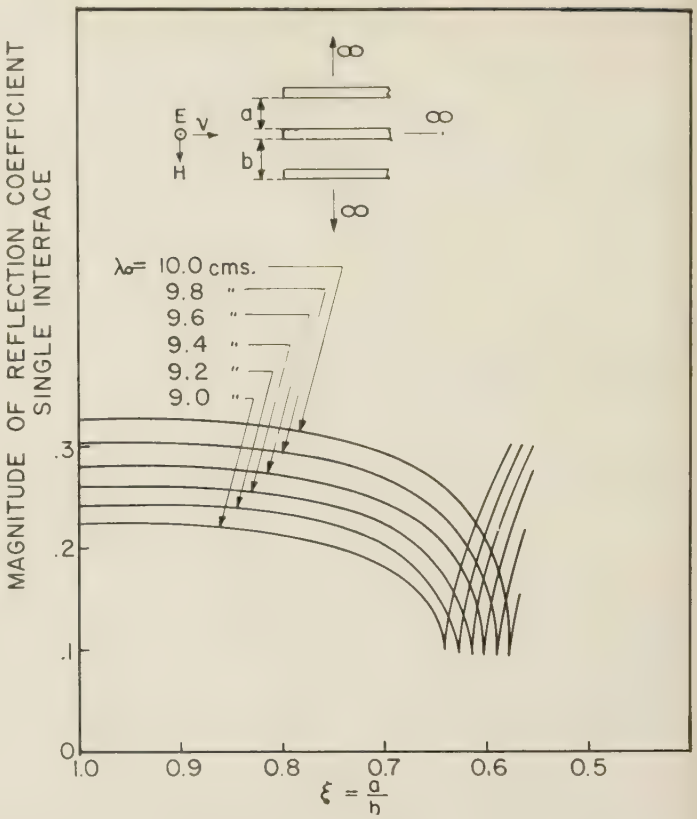

Fig. 4—Phase of reflection coefficient for single interface.

A logical choice of magnetic field is given by an expansion of the type given above for $|x| \leqq (a/2)$, and an expansion representing the current distribution over the plate edges. Apart from involving two sets of unknown coefficients, the form of the current distribution is not known, so it is far more convenient to use a more general expansion of the type already encountered for the free space region, *i.e.*,

$$H_{x_0} = 1 + \sum_{m=1}^{\infty} C_m \exp\left(\cos\frac{2m\pi x}{b}\right) \qquad |x| \leqq b/2.$$

The formulas obtained by using this in (4) and (5) are listed in the Appendix.

A maximum of four terms is used in each expansion and these are referred to as fourth approximations.

Calculations for a Typical System

The system chosen has $2a = 11.56$ cm, with no dielectric filling and a wavelength range 9.0 to 10.0 cm, or a refractive index variation of 0.5 to 0.6.

Figs. 4–6 illustrate the magnitude and phase of the complex reflection coefficients for a single interface as a function of the parameter $\xi = a/b$. The curves are thus for a fixed wavelength, constant a (and thus a constant refractive index), for increasing plate thickness.

To obtain some idea of the dispersive properties of such a system, Fig. 7 illustrates the same information as a function of wavelength for various values of ξ.

The calculations were carried out using the electric

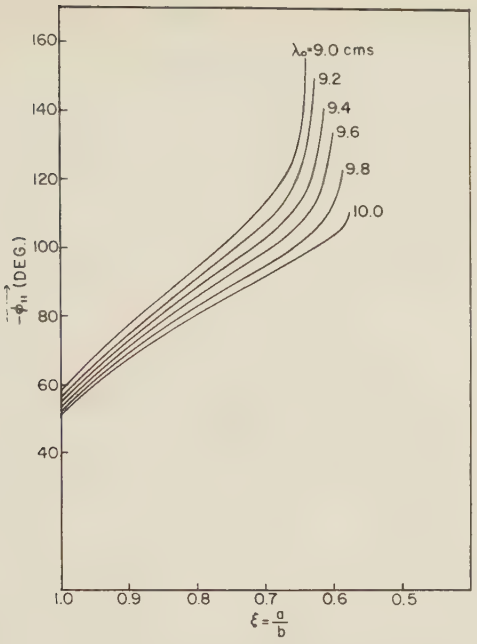

Fig. 5—Phase of reflection coefficient for single interface on free space side.

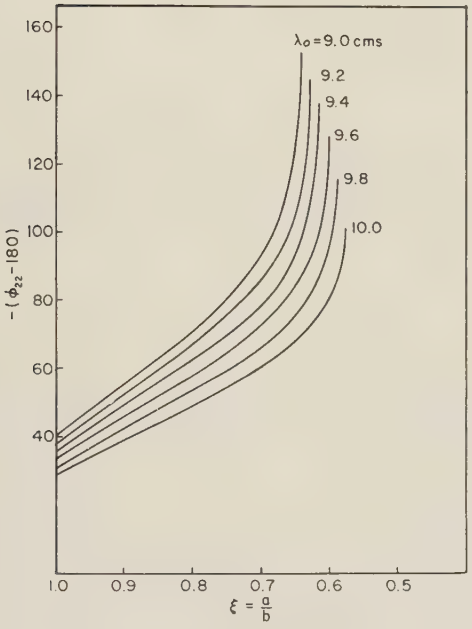

Fig. 6—Phase of reflection coefficient for plate region side.

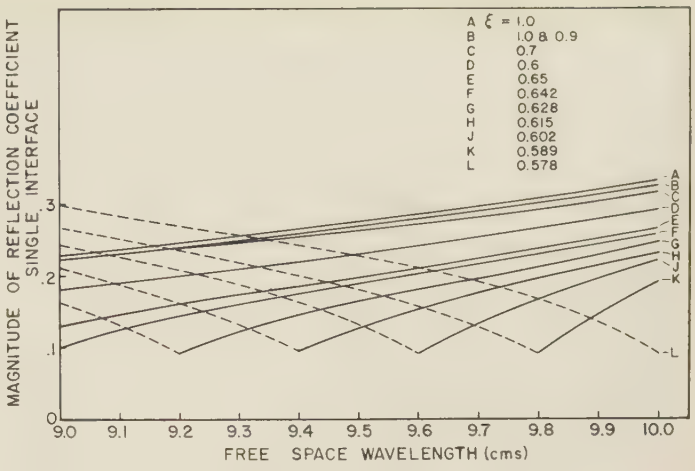

Fig. 7—Magnitude of reflection coefficient for single interface.

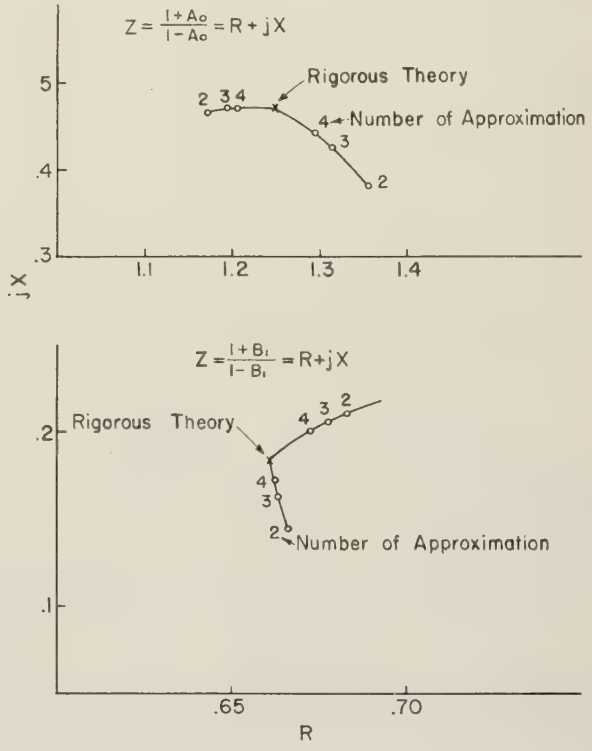

Fig. 8—Interface impedance plotted in complex plane.

field expressions with only the second approximation. An estimate of the error (see following section) shows that at $\xi = 1.0, \lambda_0 = 9$ cm, the magnitude of the reflection coefficient is 3 per cent too low and the phase is within 5 per cent.

The resonance occurs at $\lambda_0 = b$, and for $\lambda_0 < b$ higher order freely propagating modes are present in free space. Although the calculations are still valid in this region, they are incomplete to the extent that they do not include the amplitudes of these higher order waves.

The two methods for estimating the error will be illustrated for the above system at $\xi = 1.0$ and $\lambda_0 = 9.0$ cm. Under these conditions a rigorous result can be obtained from the Carlson-Heins theory[3,8] and an absolute check is possible.

The Complex Plane

The input impedances Z_E and Z_H at the interface were calculated for the second, third, and fourth approximations. These are shown in Fig. 8 for free space and plate region incidence. Since the rigorous solution is

[8] J. F. Carlson and A. E. Heins, "The reflection of an electromagnetic plane wave by an infinite set of plates," *Quart. Appl. Math.*, vol. 4, pp. 313–329; January, 1947.

known in the present instance, it is apparent that smooth curves drawn through the two sets of points intersect at the correct value. It is also apparent that straight lines drawn through the third and fourth approximations intersect very near the correct value, and in fact calculation of the reflection coefficients from this point of intersection results in an error in magnitude of less than one per cent and a phase angle within two degrees.

Reactances of the Equivalent Circuit

Using the formulas listed in the appendix the following results were obtained

			Electric Field	Magnetic Field
X_{11}	no of approx	1)	3.260	∞
		2)	3.558	5.281
		3)	3.708	4.937
		4)	3.793	4.652
$\frac{X_{11}X_{22}-X_{12}^2}{X_{22}}$		1)	0.0	0.058
		2)	0.0234	0.0429
		3)	0.0294	0.0424
		4)	0.032	0.0417
X_{22}		1)	4.021	∞
		2)	4.208	6.410
		3)	4.317	5.469
		4)	4.390	5.182

As the electric field quantities are smaller and converge more rapidly than those for the magnetic field, the geometric mean of the two was taken to give

	X_{11}	$\frac{X_{11}X_{22}-X_{12}^2}{X_{22}}$	X_{22}
Geometric mean	4.20	0.0365	4.77
Carlson-Heins theory	4.05	0.0336	4.60

Using these values the final reflection coefficients are

	A_0	B_1
Variational method	0.226/49.94°	0.226/35.43°–180°
Carlson-Heins theory	0.229/50.2°	0.229/35.9° –180°

The magnitude in error is less than 2 per cent and in phase less than one degree, so that as far as accuracy is concerned there is little to choose between the two methods of estimating the accuracy. However, the complex impedance diagram is simpler to use and gives an excellent idea of the manner of convergence.

Experimental Confirmation of the Thick Plate Theory

The equipment used has been fully described elsewhere.[4,9] It consists essentially of a strip transmission line which attempts to simulate free space conditions with uniform plane wave excitation.

Because of its finite size the line has an inherent error which results in less than −3 per cent error in magnitude of reflection coefficient and less than five degrees in phase. The line has been calibrated using an array of very thin plates.[4]

The two-interface method with a short circuit termination was used.[4] (See Fig. 9.) Full details have been

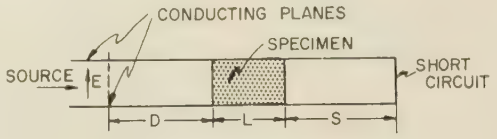

Fig. 9—Measurement of specimen in strip transmission line.

given elsewhere[4] but briefly the method consists of displacing the thick plate specimen (length L) by known amounts (S) from the short circuit and locating the corresponding positions (D) of zero field strength. From the Weissfloch curve relating D and S the complex reflection coefficient of the slab follows and by obtaining this quantity for various lengths (L), the properties of a single interface can be found.[4]

The specimen was constructed as in the previous work.[4] Waveguides were formed by wrapping 0.001 inch tin foil around machined dielectric blocks (expanded ebonite) and spacing these apart by thick plates, which consisted of machined bakelite covered with tin foil. The whole structure was wrapped in a single sheet of foil to make a rigid unit.

Experimental Results

Figs. 10–13 show the results for two cases in which the plate thickness is small, but large enough to distinguish experimentally from the case of infinitely thin plates.

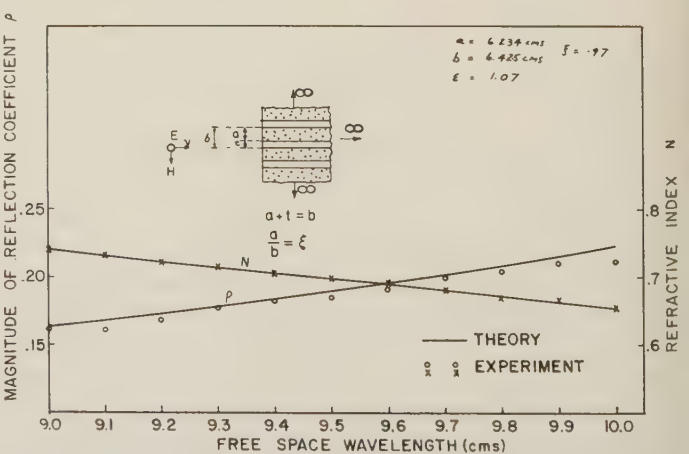

Fig. 10—Magnitude of reflection coefficient and refractive index for thick plates.[1]

[9] M. M. Z. El-Kharadly, "Investigation of certain types of artificial dielectrics," Ph.D. dissertation, Univ. of London, Eng.; 1952. Also *Proc. IEE*, vol. 102, pt. B, pp. 17–25; January, 1955.

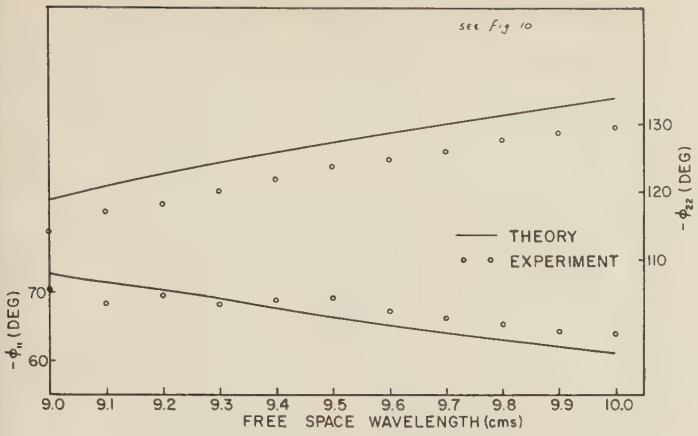

Fig. 11—Phase angles of reflection coefficient.

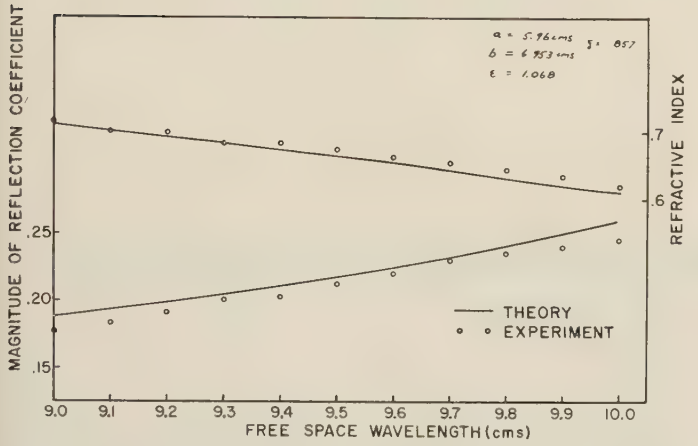

Fig. 12—Magnitude of reflection coefficient and refractive index for thick plates.[2]

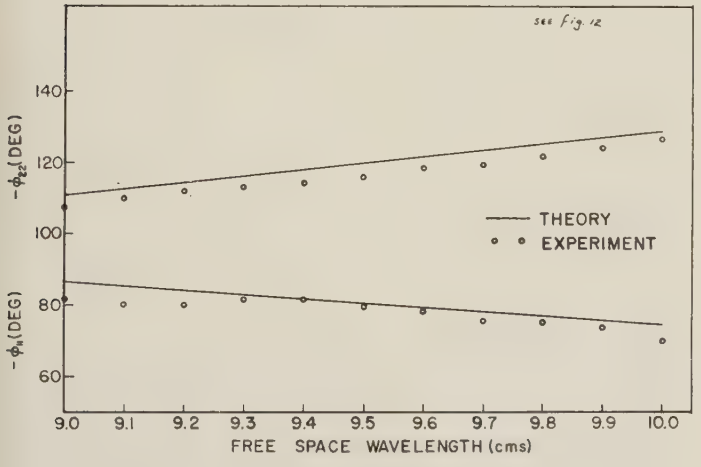

Fig. 13—Phase angles of reflection coefficient.

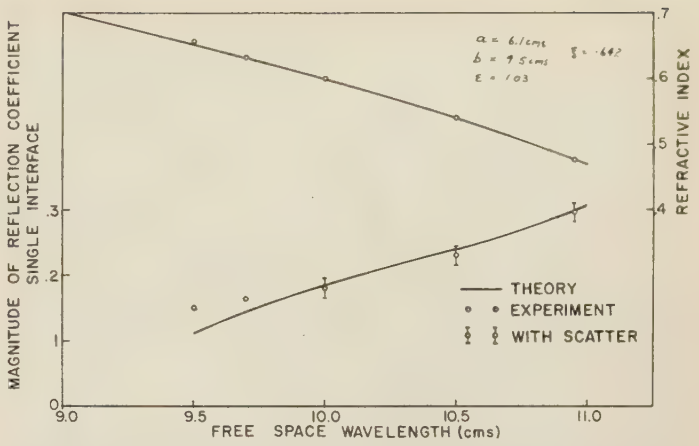

Fig. 14—Magnitude of reflection coefficient and refractive index for thick plates.[3]

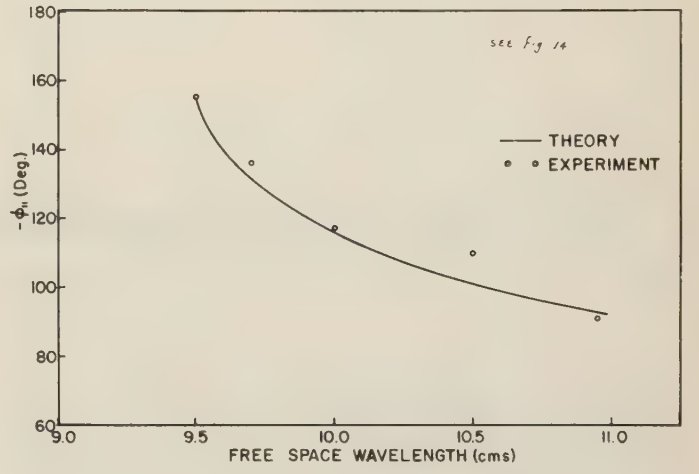

Fig. 15—Phase angle of reflection coefficient.

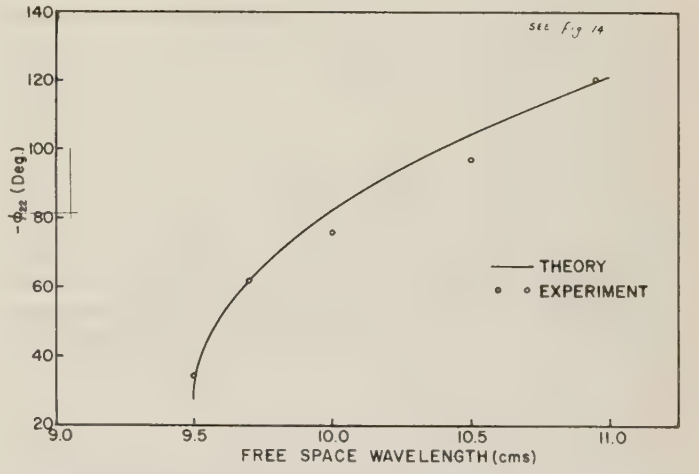

Fig. 16—Phase angle of reflection coefficient.

Figs. 14–16 show the results for a system in the region $\lambda_0 > b$. No measurements were possible for $\lambda_0 < b$ as in this case the higher order waves caused considerable interference with the main beam. In fact, this interference was observed for λ_0 larger than b, due to the finite size of the line. The field in the transmission line approximated very closely to that of the H_{01} mode[4] and from this point of view the so-called normally incident plane wave can be considered to be the sum of two uniform plane waves slightly off normal. Although this

angle is only 5 degrees it is sufficient to account for the presence of higher order propagating waves at wavelengths noticeably longer than the theoretical $\lambda_0 = b$. In a typical case the higher waves were first noticed at $\lambda_0 = 9.8$ cm compared to 9.5 cm at which point they caused considerable distortion.

The calculated curves in Figs. 7–13 were obtained from the variational expressions using the fourth approximation. An estimate of the error showed the magnitude of the reflection coefficient to be within 1 per cent and the phase within 2 degrees.

Conclusion

The experimental results given are typical of a large number taken from about ten specimens and the agreement between theory and experiment is of the same order throughout. Allowing for the inherent error of the transmission line the worst error is −5 per cent for the magnitude of reflection coefficient and within 5 degrees for the phase. Apart from the region of interference mentioned above, the thick plate theory appears to be quite satisfactory. Departures from this theory are believed to be due to the difference between the ideal and practical situations, mainly in regard to the imperfect means of plane wave excitation. Further study of the higher order propagating waves is required, although in general it is not desirable to have these higher orders present. It is worth noting that for a constant refractive index, the reflection at a single interface can actually be reduced by intentionally increasing the plate thickness, up to the point at which the first higher order wave starts to propagate.

The solution for arbitrary plane wave incidence offers no fundamental difficulty and is being extended.

The Characteristic Impedance of Trough and Slab Lines*

ROBIN M. CHISHOLM†

Summary—**A variational method is used to develop an expression for the characteristic impedance of a "trough line" consisting of a circular cylinder mounted inside and parallel to the walls of a semi-infinite rectangular trough. The "slab line" consisting of a circular cylinder between infinite, parallel plates is treated as a special case of the trough line in which the bottom of the trough is taken to be infinitely remote from the circular cylinder. The solution has not been restricted to cylinders that are mounted exactly half way between the parallel walls of the trough; a simple formula is presented for calculating the tolerances which must be placed on the "centering" of the center conductor for a given allowable error in the characteristic impedance.**

The expression for the characteristic impedance is presented as the sum of three terms. The first is a "zero order" logarithmic term, the second a "second order" correction term which vanishes as the center conductor becomes infinitely small, and the third is an "off-center" correction term which arises when the cylinder is not exactly half way between the parallel walls of the trough. The second order correction term amounts to about 0.3 ohms when the characteristic impedance is of the order of 50 ohms. A fourth order approximation using the same method changes this by about 0.001 ohm.

Introduction

DIFFICULTIES in manufacturing slotted lines for coaxial systems have led to the investigation of special types of coaxial lines for this purpose. The present work is concerned with finding the characteristic impedance of two special types of two-conductor transmission lines which can be used for standing wave measurements. The "trough line," illustrated in Fig. 1, consists of a circular cylinder mounted inside and parallel to the walls of a rectangular trough. The "slab line," consisting of a circular cylinder between infinite, parallel planes, can be considered as a special case of the trough line in which the bottom of the trough is infinitely remote from the circular cylinder. The line is excited in the TEM mode by a generator connected between the circular cylinder and the walls of the trough and propagation is along the axis of the cylinder.

The practical difficulties involved in constructing coaxial slotted lines and the application of "slab lines" to the problem have been discussed in a paper by Wholey and Eldred.[1] These authors developed a solution for the "slab line" using conformal mapping to match the outer conductor everywhere and the inner conductor at four points which was accurate to about 0.1 ohm for characteristic impedances of the order of fifty ohms. Frankel[2] treated both the "trough line" and the "slab line" using conformal mapping for the case of an infinitely thin center conductor and, although a different method is

* This work was supported in part by the Res. Council of Ontario, and by the Def. Res. Board of Canada, project number 5540–02.

† Dept. of Elect. Engrg., Univ. of Toronto, Toronto, Can.

[1] W. B. Wholey and W. N. Eldred, "A new type of slotted line section," Proc. IRE, vol. 38, pp. 244–248; March, 1950.

[2] S. Frankel, "Characteristic impedance of parallel wires in rectangular troughs," Proc. IRE, vol. 30, pp. 182–190; April, 1942.

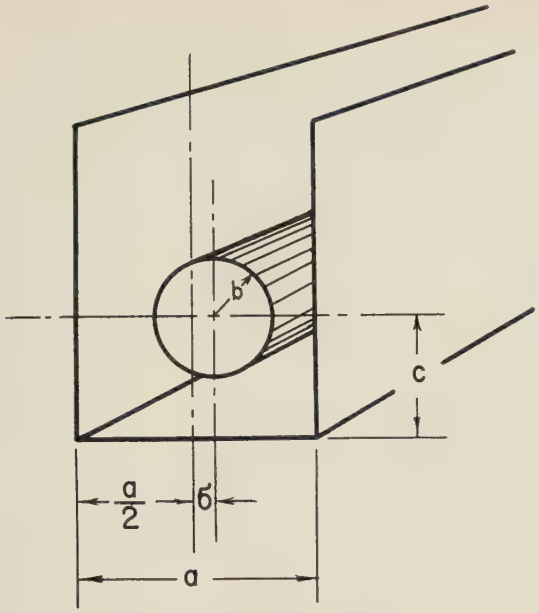

TROUGH LINE

Fig. 1—The trough line.

used, the present work yields Frankel's expressions plus a correction term which vanishes for small wires. Wheeler[3] has recently treated the "slab line" using a pair of line sources to represent his assumed field varying their displacement in order to match the boundaries.

In the present work the "trough line" is treated directly by a variational method with the "slab line" taken as a special case. The solution has not been restricted to lines in which the center conductor is placed exactly half way between the parallel walls of the trough. The final result for the characteristic impedance is presented as the sum of three terms, the first being the "zero order" term of Frankel, the second a "second order" correction term which vanishes as the center conductor becomes small, and the third an "off-center" term which is proportional to the square of the distance the center cylinder is from the center line between the parallel planes.

Formulation of the Problem

It is a well known result of wave theory that a lossless, coaxial structure of uniform cross section propagates all frequencies at the velocity of light and the electric field at any cross section at a given instant is identical in form to the electrostatic field that would occur if a static charge were placed on the center conductor. The characteristic impedance and velocity of propagation of any uniform, two conductor, lossless transmission line are given by

$$Z_0 = (L/C)^{1/2} \text{ ohms} \tag{1}$$

$$v = 1/(LC)^{1/2} \text{ meters per second} \tag{2}$$

where L is the inductance of the line in henries per meter and C is the capacitance of the line in farads per meter. The inductance L can be eliminated between (1) and (2) giving

$$Z_0 = 1/(vC); \quad v = 2.99796 \times 10^8 \text{ m/sec.} \tag{3}$$

The capacitance can then be found from the ratio of electrostatic charge on the center conductor to the voltage between conductors which would result from this charge. Let Q be the total charge per meter on the center conductor which is distributed around the periphery with a surface density $\rho(\phi)$ so that

$$Q = \int_0^{2\pi} \rho(\phi) b d(\phi) \tag{4}$$

where b is the radius of the center conductor as shown in Fig. 3.

The electrostatic field can be expressed in terms of a Green's function $G(r', \phi', r, \phi,)$ for the region. This function can be looked upon as the potential at point r, ϕ due to unit line charge at r', ϕ' [and of course subject to the boundary conditions that $G(r', \phi', r, \phi) = 0$ if r, ϕ is a point on the wall of the trough]. Using this representation the electrostatic field is given by the potential function

$$V(r, \phi) = (1/\epsilon) \int_0^{2\pi} \rho(\phi') G(b, \phi', r, \phi) b d\phi' \tag{5}$$

since the total charge in the region lies on the periphery of the cylinder where $r' = b$.

The charge distribution $\rho(\phi)$ is still unknown but is subject to the restriction that, for points on the cylinder $(r = b)$, the potential must reduce to a constant value for all ϕ. This leads to an integral equation for $\rho(\phi)$ of the form

$$V_0 = (1/\epsilon) \int_0^{2\pi} \rho(\phi') G(b, \phi', b, \phi) b d\phi' \tag{6}$$

which can be solved using a variational method (Appendix I) to give a very rapidly converging expression for the capacitance C.

The Green's Function

The function $G(r, \phi, r', \phi')$, which is interpreted as the electrostatic potential in the region due to unit line charge, must obey the same boundary conditions as the desired potential function $V(r, \phi)$. These are, namely, that it vanish on the walls of the trough and at large distances to the left of the page in Fig. 3. In addition the Green's function must be symmetric in the primed and unprimed coordinates. It is a simple matter to verify that if $G(r', \phi', r, \phi)$ in (5) obeys

[3] H. A. Wheeler, "The transmission properties of a round wire between parallel planes," Wheeler Monographs No. 19, Wheeler Laboratories Inc., Great Neck, N.Y.; 1954.

$$\nabla^2 G(r', \phi', r, \phi) = -\delta(\phi - \phi') \tag{7}$$

where ∇^2 is the Laplacian operator in two dimensions and $\delta(r-r')$ is the Dirac delta function, then V as given by (5) obeys the proper Poisson equation for the problem.

The function which obeys (7) and the proper boundary conditions can be readily found[4] and is expressible in rectangular coordinates as

$$G(x', y', x, y) = \frac{1}{2\pi}\left[\log_e \frac{1 - \exp\left(i(\pi/a)(y + y') - (\pi/a)\,|\,x - x'\,|\right)}{1 - \exp\left(i(\pi/a)(y - y') - (\pi/a)\,|\,x - x'\,|\right)}\right.$$
$$\left. - \log_e \frac{1 - \exp\left(i(\pi/a)(y + y') - (\pi/a)(x + x' - 2c)\right)}{1 - \exp\left(i(\pi/a)(y - y') - (\pi/a)(x + x' - 2c)\right)}\right] \tag{8}$$

In this formula a is the distance between the parallel plates of the trough (see Fig. 2) and c is the distance from the center of the cylinder to the bottom of the trough. For the "slab line" c becomes infinite and the second term of (8) approaches zero.

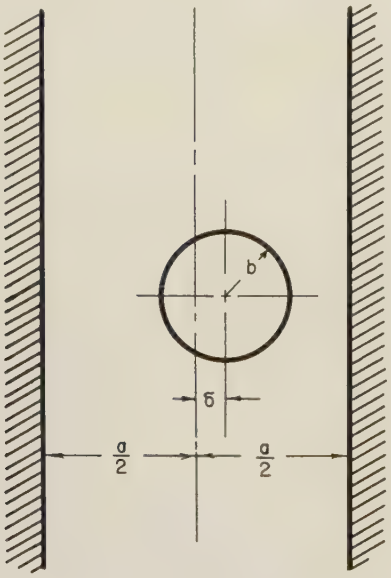

Fig. 2—The cross section of a slab line.

The Variational Expression

The variational expression for the problem is (see Appendix I)

$$\epsilon/C = \frac{\displaystyle\int_0^{2\pi}\int_0^{2\pi} \rho(\phi')G(b, \phi', b, \phi)\rho(\phi)b^2 d\phi' d\phi}{\left[\displaystyle\int_0^{2\pi} \rho(\phi) b d\phi\right]^2} \tag{9}$$

[4] This is found by assuming $G(x', y', x, y)$ to be expressible as a Fourier series in y and y' with coefficients which are functions of x and x'. The series is substituted in (9) and the resulting series expressed in closed form.

which is stationary with respect to small variations in the form of the function $\rho(\phi)$ about its correct form. As outlined in the appendix, to use this method, a trial function containing a number of arbitrary parameters is substituted for $\rho(\phi)$ in (9). The trial function used in this problem is of the form

$$\rho(\phi) = (Q/4\pi b^2)(1 + \alpha_1 \cos\phi + \alpha_2 \cos 2\phi + \cdots \alpha_n \cos n\phi + \cdots + \beta_1 \sin\phi + \beta_2 \sin 2\phi + \cdots \beta_n \sin n\phi). \tag{10}$$

The more terms taken the more accuracy can one expect. Once (10) is substituted in (9) for $\rho(\phi)$ the integrals involved can be evaluated as explicit functions (see Appendix II) of the known parameters a, b, c, and δ (see Fig. 3) and the $2n$ parameters $\alpha_1 \cdots \alpha_n$ and $\beta_1 \cdots \beta_n$. The amplitude factor $Q/4\pi b^2$ cancels out since it appears to the same power both in the numerator and in the denominator of (9).

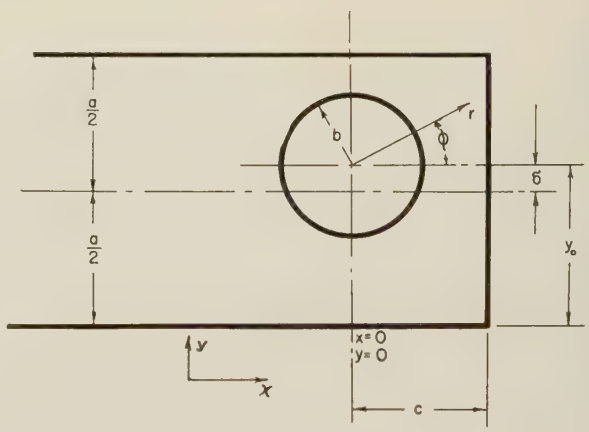

Fig. 3—The coordinates used in describing a trough line.

When the integration has been carried out (9) can be written in the form

$$\frac{\epsilon}{C} = \sum_{j,k=0}^{n} \alpha_j \alpha_k X^{j,k} + 2\sum_{j,k=0}^{n} \alpha_j \beta_k Y^{j,k} + \sum_{j,k=0}^{n} \beta_j \beta_k Z^{j,k} \tag{11}$$

where $\alpha_0 = 1$ and $\beta_0 = 0$ by definition and $X^{j,k}$, $Y^{j,k}$, and $Z^{j,k}$ are the known functions defined in Appendix II and tabulated in Table I which result from the integrations involved in (9) when the trial function of (10) is inserted for $\rho(\phi)$. These turn out to be simple functions of the parameters a, b, c, and δ, and some of the functions used to develop the "second order" approximations are tabulated in Tables I and II.

TABLE I

THE FUNCTION

$$X^{j,k} = X^{k,j} = (1/4\pi^2) \int_0^{2\pi} \int_0^{2\pi} \cos(j\phi')\, G(b, \phi', b, \phi) \cos(k\phi)\, d\phi' d\phi$$

j	k	(c/a) infinite	$(c/a)=(3/4)$	$(c/a)=(1/2)$	$(c/a)=(1/4)$
0	1	0.000	$-0.004491(b/a)^2$	$-0.02165(b/a)$	$-0.1086(b/a)$
0	2	$+0.06545(b/a)^2$	$+0.05840(b/a)^2$	$+0.03132(b/a)^2$	$-0.1206(b/a)^2$
1	1	$+0.0397887$ $-0.06545(b/a)^2$	$+0.0397887$ $-0.07250(b/a)^2$	$+0.0397887$ $-0.09958(b/a)^2$	$+0.0397887$ $-0.2515(b/a)^2$
1	2	0.000	$-0.01109(b/a)^3$	$-0.05421(b/a)^3$	$-0.3693(b/a)^3$
2	2	$+0.0198944$ $-0.1130(b/a)^4$	$+0.0198944$ $-0.1305(b/a)^4$	$+0.0198944$ $-0.2010(b/a)^4$	$+0.0198944$ $-1.092(b/a)^4$

TABLE II

SOME TYPICAL FUNCTIONS OF THE TYPE

$$Y^{j,k} = \int_0^{2\pi} \int_0^{2\pi} \cos(j\phi')\, G(b, \phi', b, \phi) \sin(k\phi)\, d\phi' d\phi \,(c/a) = (1/2)$$

j \ k	0	1	2
0	0.000	$-0.1652(2\delta/a)(b/a)$	$+0.04493(2\delta/a)(b/a)^2$
1	0.000	$+0.04493(2\delta/a)(b/a)^2$	$-0.1836(2\delta/a)(b/a)^3$
2	0.000	$+0.3009(2\delta/a)(b/a)^3$	$+0.05803(2\delta/a)(b/a)^4$

Eq. (11) can be differentiated with respect to the parameters α_j and β_j yielding $2(n+1)$ linear, homogeneous equations of the form

$$0 = \sum_{k=0}^{n} (\alpha_k X^{j,k} + \beta_k Y^{j,k}) \qquad j = 1, 2, \cdots n \tag{12a}$$

$$0 = \sum_{k=0}^{n} (\alpha_k X^{j,k} + \beta_k Z^{j,k}) \qquad j = 1, 2, 3, \cdots n. \tag{12b}$$

When the fact that $\alpha_0 = 1$ and $\beta_0 = 0$ is used these reduce to $2n$ nonhomogeneous equations which can be solved for the α_k's and β_k's by standard methods. Substitution back into (11) then yields an expression for the capacitance C.

PRACTICAL SOLUTIONS

For the results presented here n was taken to be 2 yielding four equations in four unknowns,

$$\alpha_1 X^{1,2} + \alpha_2 X^{1,2} + \beta_1 Y^{1,1} + \beta_2 Y^{1,2} = -X^{1,0} \tag{13a}$$

$$\alpha_1 X^{2,1} + \alpha_2 X^{2,2} + \beta_1 Y^{2,1} + \beta_2 Y^{2,2} = -X^{2,0} \tag{13b}$$

$$\alpha_1 Y^{1,1} + \alpha_2 Y^{2,1} + \beta_1 Z^{1,1} + \beta_2 Z^{2,1} = -Y^{0,1} \tag{13c}$$

$$\alpha_1 Y^{1,2} + \alpha_2 Y^{2,2} + \beta_1 Z^{1,2} + \beta_2 Z^{2,2} = -Y^{0,2}. \tag{13d}$$

It can be shown that all of the functions $Y^{j,k}$ and all of the coefficients β_j are proportional to (δ/a) where δ is the distance by which the cylinder is "off-center" in Fig. 2. This means that, for small values of (δ/a), the third and fourth terms in (13a) and (13b) may be neglected introducing an error in α_1 and α_2 of the order of $(\delta/\alpha)^2$. This approximation becomes exact as δ approaches zero and using it assumes that moving the cylinder "off-center" does not make an appreciable change in the amplitudes of the cosine terms in the series for the charge distribution $\rho(\phi)$.[5] The values of α_1 and α_2 found from (13a) and (13b) can then be substituted into (13c) and (13d) from which β_1 and β_2 can be found using Cramer's rule in terms of a 2×2 determinant. Since (11), which is used to find the capacitance C, is stationary with respect to variations in the parameters α_j and β_j this approximation is valid to within an error of the order of $(\delta/a)^4$.

When the cylinder is exactly centered between the parallel walls of the trough the second order approximation, given by (11) with n taken equal to 2 and using (3) for the relation between the characteristic impedance and the capacitance, is simply

$$Z_0 = {}^6Z_{fs}(X^{0,0} + 2\alpha_1 X^{0,1} + 2\alpha_2 X^{0,2} + 2\alpha_1\alpha_2 X^{1,2} + (\alpha_1)^2 X^{1,1} + (\alpha_2)^2 X^{2,2}). \tag{14}$$

where Z_0 is the characteristic impedance of the line in ohms and α_1 and α_2, using the approximations of the preceding paragraph, are given by

$$\alpha_1 = -\begin{vmatrix} X^{1,0} & X^{1,2} \\ X^{2,0} & X^{2,2} \end{vmatrix} \Big/ \begin{vmatrix} X^{1,1} & X^{1,2} \\ X^{2,1} & X^{2,2} \end{vmatrix} \tag{15a}$$

$$\alpha_2 = -\begin{vmatrix} X^{1,1} & X^{1,0} \\ X^{2,1} & X^{2,0} \end{vmatrix} \Big/ \begin{vmatrix} X^{1,1} & X^{1,2} \\ X^{2,1} & X^{2,2} \end{vmatrix}. \tag{15b}$$

[5] The function $X^{j,k}$, however, changes by order $(\delta/a)^2$ when the cylinder is moved "off-center" and this change must be taken into account because the variational expression is stationary only with respect to variations in the coefficients α_j and β_j and not with respect to changes in the integrals $X^{j,k}$, $Y^{j,k}$, and $Z^{j,k}$.

[6] Z_{fs} is the wave impedance of free space taken in the present work to be 376.735. This is based on Michelson's value (1926) for the velocity of light in free space, 2.99796×10^8 m/s. Other conditions should be adjusted accordingly from the values found from these graphs.

The function $X^{0,0}$ which is the "zero-order" term is just that found by Frankel[2] for a thin wire in a rectangular trough namely

$$X^{0,0} = \frac{1}{2\pi} \log_e \left(\frac{2a}{\pi b} \tanh \frac{\pi c}{a} \right) \tag{16}$$

while the other $X^{j,k}$'s which appear in the formula are given in Table I.

Simplified Formulas

When (15a) and (15b) are substituted into (14) an explicit formula for the characteristic impedance results. Several terms of the initial substitution cancel out and, when the expressions in Table I are used for the $X^{j,k}$'s, (14) becomes

$$Z_0 = Z_{fs} \left[(1/2\pi) \log_e \left(\frac{2a}{\pi b} \tanh \frac{\pi c}{a} \right) + \frac{N_1 R + N_2 R^2 + N_3 R^3}{1 + D_1 R + D_2 R^2 + D_3 R^3} \right] \tag{17a}$$

where $R = (b/a)^2$.

The coefficients N_j and D_j are given in Tables III and IV respectively for different values of the ratio c/a.

TABLE III

The Coefficients N_j to Be Used in (17) and (19) for the Calculation of the Second Order Correction Term

(c/a) \ j	1	2	3
1/4	−0.2966	−0.7312	+8.680
1/2	−0.01177	−0.04932	+0.3353
3/4	−0.0005068	−0.1714	+0.3220
infinite	0.000	−0.2153	0.000

TABLE IV

The Coefficients D_j to Be Used in (17) and (19) for the Calculation of the Second Order Correction Term

(c/a) \ j	1	2	3
1/4	−6.321	−54.90	+174.8
1/2	−2.503	−10.11	+ 21.58
3/4	−1.822	− 6.559	+ 11.80
infinite	0.000	− 5.682	0.000

For the "slab line" [(c/a) infinite], the numerator and denominator of the second term on the right hand side of (17a) have a common factor and the expression further simplifies to

$$Z_0 = Z_{fs} \left[(1/2\pi) \log_e \left(\frac{2a}{\pi b} \right) - \frac{0.2153 R^2}{1 - 5.682 R^2} \right] \tag{17b}$$

where, again, $R = (b/a)^2$.

Off-Center Corrections

Perhaps the most interesting result of this investigation is the formula for the change in characteristic impedance which results when the cylinder is moved slightly "off-center" from between the parallel planes.

When δ in Fig. 2 is not equal to zero the coefficients β_1 and β_2 in (13a) to (13d) do not vanish and when the series (11) for ϵ/C is terminated for $j,k = 2$, additional terms to those given in (14) result in the expression for ϵ/C all of which, to within $0(\delta/a)^4$ are proportional to $(\delta/a)^2$. In addition to these extra terms all of the $X^{j,k}$'s undergo a change of order $(\delta/a)^2$ also which must be taken into account. This change can be included with the extra terms which result when the cylinder is moved "off-center" allowing the total change in characteristic impedance, which is always less than zero, to be written in the form

$$\Delta Z_0 = -\alpha[(b/a), (c/a)] \times (\delta/a)^2. \tag{18}$$

The parameter α which depends on the ratio b/a and c/a has been calculated for a set of values of these ratios and graphs, sufficiently accurate for purposes of computation, of α vs b/a with c/a as a parameter are given in Fig. 5.

Further Calculations

Tables have been prepared of the functions $X^{j,k}$, $Y^{j,k}$, $Z^{j,k}$ and $\Delta X^{j,k}$ [the change in the value of $X^{j,k}$ when the cylinder is moved off center by an amount δ is $\Delta X^{j,k} \times (\delta/a)^2$] up as far as $j,k = 4$ enabling the calculation of a fourth order approximation. All of these functions are simple one or two term polynomials in the ratio (b/a).

A fourth order approximation has been worked out for the "slab line" in the region of fifty ohms. The difference between the second order and fourth order answers was only 0.001 ohms or one part in fifty thousand.

Conclusion

Second Order Formulas

The characteristic impedance of the trough line illustrated in Fig. 1 is given by

$$Z_0 = {}^6Z_{fs} \left[(1/2\pi) \log_e \left(\frac{2a}{\pi b} \tanh \frac{\pi c}{a} \right) + \frac{N_1 R + N_2 R^2 + N_3 R^3}{1 + D_1 R + D_2 R^2 + D_3 R^3} \right] - \alpha[(b/a), (c/a)] \times (\delta/a)^2 \text{ ohms}, \tag{19}$$

where $R = (b/a)^2$ and b is the radius of the cylinder, a is the spacing between the parallel walls of the trough, c is the distance from the center of the cylinder to the bottom of the trough and δ is the distance the center of the cylinder is displaced from the center plane between

the parallel plates. The coefficients N_j and D_j are given in Tables III and IV respectively and the coefficient $\alpha(b/a)$, (c/a) is plotted in Fig. 5 as a function of (b/a) with (c/a) as a parameter. The second term on the right hand side of (19) multiplied by $Z_{fs}=376.735$) is plotted in Fig. 4 to a logarithmic scale.

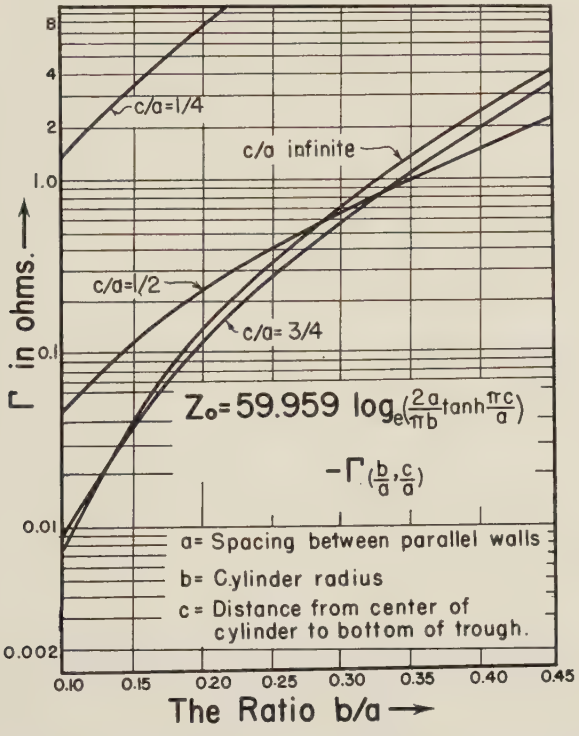

Fig. 4—The second order correction term for the trough line. Value found from this graph are to be subtracted from the zero order logarithmic term,

$$59.959\log_e\left[\left(\frac{2a}{\pi b}\right)\tanh\frac{\pi c}{a}\right].$$

For the "slab line" [$(c/a$ infinite] (19) reduces to

$$Z_0 = {}^6Z_{fs}\left[(1/2\pi)\log_e\left(\frac{2a}{\pi b}\right)-\frac{0.2153R^2}{1+5.682R^2}\right] - \alpha(b/a)\times(\delta/a)^2 \text{ ohms} \qquad (20)$$

where $R=(b/a)^2$.

As (b/a) approaches $\frac{1}{2}$ the results break down since the charge distribution $\rho(\phi)$ in the electrostatic model used for calculating ϵ/C approaches the delta function $\delta(\phi\pm(n+\frac{1}{2})\pi)$. The Fourier series for such a distribution has all of its terms of equal magnitude and cutting the series in (10) off at $n=2$ represents a very poor approximation. In practice, however, such large cylinder sizes should be avoided as the capacitance depends very critically on the nature of the surface in the region where the cylinder and the wall almost touch.

Tolerances on the Centering of the Cylinder

If Z_0 is the maximum variation in the characteristic impedance of a trough line which can be tolerated then, from (18), the maximum allowable error in the positioning of the cylinder is given by

$$\delta = a\times\left(\frac{\Delta Z_0}{\alpha}\right)^{1/2} \qquad (21)$$

where α can be found from Fig. 5 as a function of (b/a) and (c/a).

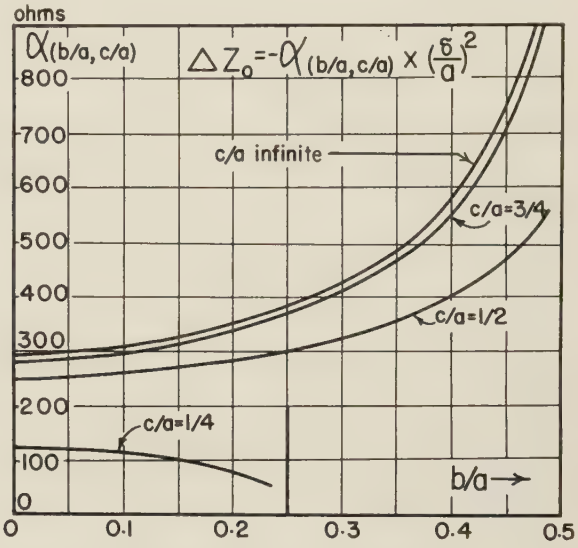

Fig. 5—The "off-center" correction coefficient. The coefficient α found from this graph, when multiplied by $(\delta/a)^2$ where a is the spacing between the parallel planes, gives the correction term to be subtracted from the regular formula for the characteristic impedance whenever the center of the cylinder is off the center line between the parallel planes by an amount δ.

Appendix I

The Variational Expression

The problem under consideration is the solution of an integral equation of the form

$$V_0 = \int_0^{2\pi}\rho(\phi')G(b,\phi',b,\phi)bd\phi'. \qquad (22)$$

Morse and Feshbach[7] treat the general problem of finding a solution to the equation

$$\mathfrak{L}(\psi) = \lambda\mathfrak{M}(\psi) \qquad (23)$$

by a variational method where ψ is the unknown function and $\mathfrak{L}$ and $\mathfrak{M}$ are differential or integral operators. If one sets

$$\psi = \rho(\phi), \qquad (24)$$

$$\mathfrak{L}(\psi) = 1/\epsilon\int_0^{2\pi}\rho(\phi')G(b,\phi',b,\phi)bd\phi' \qquad (25)$$

[7] P. M. Mores and H. Feshbach, "Methods of Theoretical Physics" McGraw-Hill Book Co., Inc., New York, N.Y., 1st ed., vol. 2, p. 1106; 1953.

which is a function of ϕ in the region $0 \leqq \phi \leqq 2\pi$,

$$\mathfrak{M}(\psi) = \int_0^{2\pi} \rho(\phi') b d\phi' \tag{26}$$

and $\lambda = 1/C$ where $C = Q/V_0$, the static capacitance, then (23) becomes

$$1/\epsilon \int_0^{2\pi} \rho(\phi') G(b, \phi', b, \phi) b d\phi' = (1/C) \int_0^{2\pi} \rho(\phi') b d\phi' = V_0 \tag{27}$$

which is the integral equation to be solved. C or $1/C$ is the quantity desired and it is shown by Morse and Feshbach[8] that

$$\delta[\lambda] = \delta\left[\frac{\int \psi \mathfrak{L}(\psi) dV}{\int \psi \mathfrak{M}(\psi) dV}\right] = 0 \tag{28}$$

with respect to arbitrary variations of ψ about its correct value. Interpreting ψ, $\mathfrak{L}$, $\mathfrak{M}$, and λ as in (24)–(26) this yields

$$\delta\left[\frac{1}{C}\right] = \delta\left[\frac{1}{\epsilon} \frac{\int_0^{2\pi} \rho(\phi) \int_0^{2\pi} G(b, \phi, b, \phi') \rho(\phi') b^2 d\phi d\phi'}{\int_0^{2\pi} \int_0^{2\pi} \rho(\phi) \rho(\phi') b^2 d\phi d\phi'}\right] = 0. \tag{29}$$

This means that (9) is stationary with respect to arbitrary variations in the form of $\rho(\phi)$ about its correct form.

To use this method a trial function is put in (9) for $\rho(\phi)$ which contains n arbitrary parameters $\alpha_1 \cdots \alpha_n$. Differentiating with respect to these parameters and equating the results to zero leads to n homogeneous, linear equations in the n unknown α's.[9]

Appendix II

Evaluating the Integrals Involved in the Variational Method

When $\rho(\phi)$ in (9) is replaced by the series of (10) and use is made of the orthogonality properties of the trigonometric functions to give $4\pi^2 b^2$ for the denominator of the right hand side of (9), ϵ/C can be expressed by the series in (11) where integrals of the following type are encountered

$$X^{j,k} = \frac{1}{4\pi^2} \int_0^{2\pi} \int_0^{2\pi} \cos(j\phi) G(b, \phi', b, \phi) \cos(k\phi') d\phi d\phi' \tag{30}$$

$$Y^{j,k} = \frac{1}{4\pi^2} \int_0^{2\pi} \int_0^{2\pi} \cos(j\phi) G(b, \phi', b, \phi) \sin(k\phi') d\phi d\phi' \tag{31}$$

$$Z^{j,k} = \frac{1}{4\pi^2} \int_0^{2\pi} \int_0^{2\pi} \sin(j\phi) G(b, \phi', b, \phi) \sin(k\phi') d\phi d\phi'. \tag{32}$$

These integrals depend on the parameters j and k and, through the Green's function $G(b, \phi', b, \phi)$, on the dimensions a, b, and c of the transmission line.

These integrals can be evaluated by removing the singularity from $G(r', \phi', r, \phi)$ at $r = r'$, $\phi = \phi'$ and using the following lemma. *If* $\nabla^2 \psi(r, \varphi) = 0$

$$\int_0^{2\pi} \psi(r, \phi) e^{in\phi} d\phi = (\pi/n!) r^{|n|} \operatorname*{Limit}_{r \to 0, \vartheta \to 0} \frac{\partial^n}{\partial r^n}\left[1 + (i/n)\frac{\partial}{\partial \phi}\right] \psi(r, \phi) \quad \text{for } n \neq 0,$$

$$= 2\pi \operatorname*{Limit}_{r \to 0, \vartheta \to 0} \psi(r, \phi) \qquad n = 0. \tag{33}$$

The differentiations involved, if carried out directly, are rather messy. However it has been found possible to express the results of this lemma in terms of a set of functions, represented by a finite power series, the coefficients of which obey a simple repetition formula.

Putting

$$\xi_0{}^n(z) = \frac{e^{inz}}{1 - e^{inz}} \tag{34}$$

and

$$(in)^k \xi_k{}^n(z) = \frac{d^k}{d_z{}^k} \xi_0{}^n(z) \tag{35}$$

it can be shown that

$$\xi_k{}^n(z) = \sum_{m=1}^{k} c_m{}^k [\xi_0{}^n(z)]^m (1 + \xi_0{}^n(z)), \tag{36}$$

where the coefficients $c_m{}^k$ obey the repetition formula

$$c_1{}^k = 1; \quad c_k{}^k = k!; \quad \text{and} \quad c_m{}^k = m(c_{m-1}{}^{k-1} + c_m{}^{k-1}).$$

For special values of the argument z, (36) is of a particularly simple form. For example, one of the functions which occurs in applying this lemma is

$$\xi_{j+k-1}{}^{(\pi/a)}(a) = \sum_{m=1}^{j+k-1} (-1)^m \frac{c_m{}^{j+k+1}}{2^{m+1}}. \tag{37}$$

It is beyond the scope of this paper to go into the details of these functions beyond pointing out, as seen from Table I, that integrals of the types under consideration, when evaluated in this way, come out as simple polynomials in the ratio (b/a).

[8] *Ibid.*, p. 1109 (9.4.8).
[9] *Ibid.*, p. 1107.

A Simplified Calibration of Two-Port Transmission Line Devices

F. L. WENTWORTH† AND D. R. BARTHEL†

Summary—During the evaluation measurements of several two-port junction devices over a wide band of frequencies the authors found that the method of shorts as described in three previous papers was too laborious to be practical. By reinterpreting and combining the ideas of earlier authors[1,2] a valuable simplification was obtained. Since this paper is based upon the previous articles, no fundamental proofs will be given except to show the necessary extensions involved.

Introduction

G. A. DESCHAMPS originally described a graphical method of measuring impedances through an unknown junction. For example, these junctions may be step or tapered transitions between two physical line sizes of the same impedance or between lines of different impedances or a combination of both. They may be baluns which convert from unbalanced lines to balanced lines or junctions which convert from coaxial to waveguide. In fact, measurements through almost any two-port junction between the measuring device (normally a slotted line) and the unknown load are possible without detailed knowledge of the junction.

The literature describes what is called a "calibration of the junction," which is a long and involved procedure in most cases. The simplest method of accomplishing the calibration is to plot on a Smith chart the measured results of a matched load and a reference short placed at the output of the junction. Its major difficulty is that matched loads are not available for most cases.

One of the methods described by Deschamps simulates a perfect matched load, regardless of the line impedance, by using a series of shorts at discrete positions along the uniform transmission line out of the unknown junction. At least four different short positions are used with the specification that they be used alternately in pairs a quarter wavelength apart. These points may be plotted on a Smith chart (Fig. 1). If straight lines are constructed between points of the pair, then the intersection of these lines is the crossover point.

The construction given by Deschamps and illustrated in Fig. 2 converts the crossover point into the iconocenter. The iconocenter is the same point that would have been found on a Smith chart had a matched load been used to terminate the junction. The difficulty with this method is that four new short positions must be made for each frequency. This becomes exceedingly difficult and time consuming when working with dielectric filled line or with line in which a movable short cannot be placed. It is also difficult to make each cut of the line under test to the exact electrical length desired.

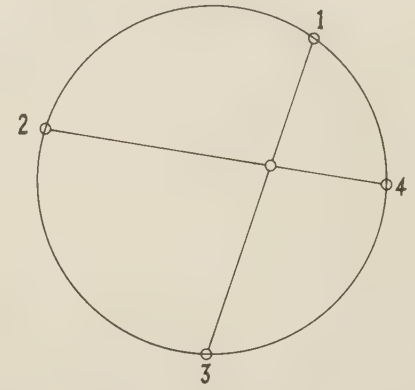

Fig. 1—Position of four shorts and location of crossover point.

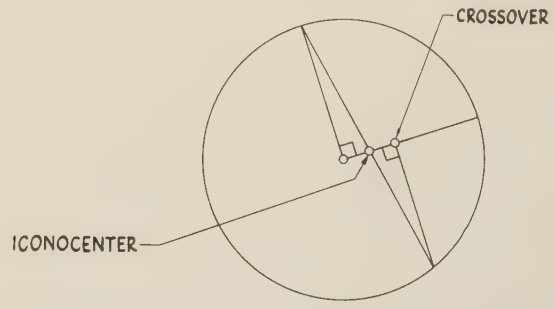

Fig. 2—Construction of iconocenter from crossover point.

The use of a matched output load locates the iconocenter, and the use of four $\lambda/8$ shorts locates the crossover point. The method described by this paper will locate the iconocenter directly where matched loads are unavailable.

In the interest of clarity, the following terms are defined, althought the definitions may not coincide with the work of other authors:

1) The test plane includes those measurements, plots, and graphs involving no transforming network. All standard impedance measurements fall into this category.
2) The transformation plane is the result of transforming all points and measurements in the test plane by the network transformation junction. Measurements performed between the generator and the two-port junction fall in the transformation plane.

† Electronics Dept., The Martin Co., Baltimore, Md.

[1] G. A. Deschamps, "A hyperbolic protractor for microwave impedance measurements and other purposes," Fed. Telecommun. Labs.; 1953, and "Determination of reflection coefficients and insertion loss of a waveguide junction," *J. Appl. Phys.*, vol. 24, pp. 1046–1050; August, 1953.

[2] J. E. Storer, L. S. Sheingold, and S. Stein, "A simple graphical analysis of a two-port waveguide junction," PROC. IRE, vol. 41, pp. 1004–1013; August, 1953.

3) The projective plane is the result of transforming all points in the transformation plane by the projective construction described by Deschamps and shown in Fig. 2.
4) The iconocenter is the center of a Smith chart after it has been transformed into the transformation plane.
5) The crossover point is the iconocenter after it has been transformed into the projective plane.
6) The elliptic angle is a construction in the projection plane drawn with straight lines from two points to a vertex which is usually the crossover point.

Simplified Graphical Construction

Analytically, the junction can be described by a transformation matrix.[2] All points measured through the junction when plotted on a Smith chart will be in the transformation plane described by this matrix. The transformation is bilinear and conformal. Therefore, circular arcs are transformed into circular arcs, and angles and sense preserved. In the transformation plane, one cannot read directly the phase angle of an unknown load. However, in the projective plane straight lines may be drawn to describe an elliptic angle, which also may not be read directly. However, Deschamps gives the relationship of the elliptic angle to the angle in the test plane. This is illustrated in Fig. 3, which also shows the center of the Smith chart in the test plane, transformation plane, and projective plane. Fig. 3 shows too that if points 1, 1′, 2, and 2′ are known, then the iconocenter is defined.

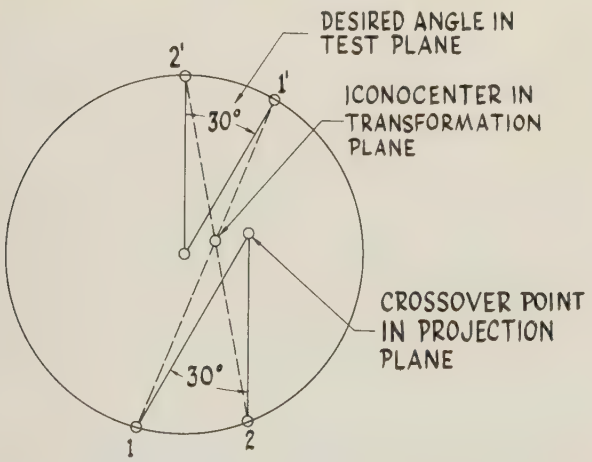

Fig. 3—Evaluation of an elliptic angle.

Fig. 4 demonstrates the measurements necessary to make the calibration. A short is placed at point 1′, and the null is read on the slotted line at point 1. The short is moved along the line an arbitrary distance (in this case, 30 degrees) to point 2′, and the null is read at point 2. The short is moved again (35 degrees this time) to point 3′, and the null read at point 3.

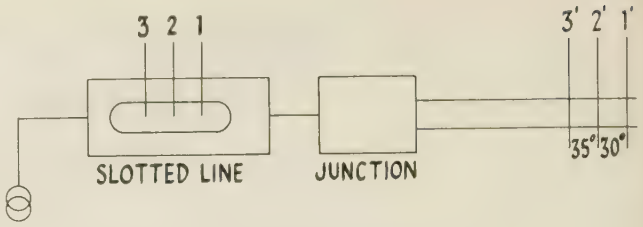

Fig. 4—Typical measurement.

Using the nulls of a reference short at the end of the slotted line, points 1, 2, and 3 are plotted on a Smith chart (Fig. 5) in the transformation plane. An arbitrary line is drawn from 1 to a point on the opposite side of the circle and the intersection is designated at point 1′. Knowing the real angle between 1′ and 2′ point 2′ is now constructed in the test plane. The intersection of 1′-1 and 2′-2 at "a" and the points 1 and 2 define a circle. It can be readily shown by similar construction that as the position of line 1′-1 is varied the point "a" describes a circle, and that the locus of the circle described by point "a" passes through points 1 and 2.

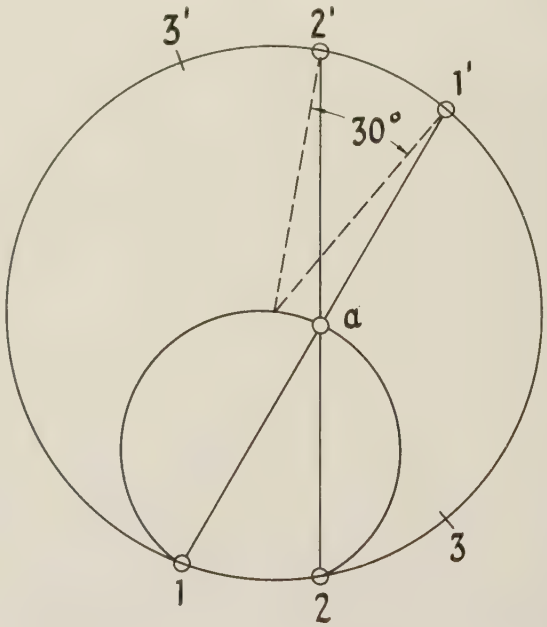

Fig. 5—Locus circle for points 1 and 2.

This circle is the locus of possible iconocenters for the junction under test. Using the points 2 and 3 and the real angle between 2′ and 3′ in a like manner, a second locus circle may be constructed (Fig. 6). Since the iconocenter must lie on both circles, then their intersection within the Smith chart locates the desired iconocenter.

It should be noted that no requirements are imposed upon the location of the shorts except that their separation be accurately known. The same three short positions may be used for calibration of the junction over a

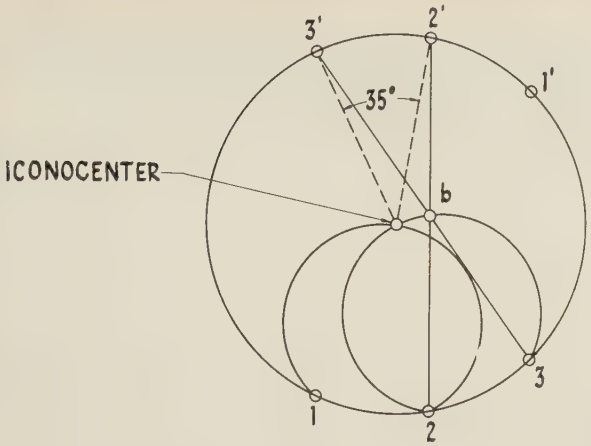

Fig. 6—Locus circle for 2 and 3. Intersection of the two circles locates the iconocenter.

wide band of frequencies and thereby provide a considerable simplification over the original calibration method.

The procedure to follow in the wide band case is to make 3 sets of impedance measurements over the frequency band, one for each short position. It is most important that the frequencies be repeated accurately in the second and third sets. However, with modern equipment this is easily accomplished.

Up to this point, the main concern was to calibrate an unknown junction for purposes of measuring impedances through this junction. However, the same method also is capable of evaluating a junction which is being designed. For instance, in designing a tapered transition, one of the requirements would be a maximum allowable reflection. In general, this test would be made simply by placing a matched load at the output and examining the reflection of the input.

For cases where a matched load is not available, the method of shorts would provide an evaluation of the junction. The iconocenter, when plotted on the Smith chart, will be a parallel combination of the equivalent reactance of the junction and the matched impedance of the output line. Since the output impedance is known, then the equivalent impedance of the junction is also known. In order to measure an impedance with a standing wave machine, one requires a reference short, where the impedance measured is said to exist. In design work one would then want to make the reference short at a point where a design correction or a matching section would be made if necessary.

Several items of accuracy that are necessary for satisfactory results are: frequency, velocity of propagation, distance between shorts, and null positions on standing wave machines. Also the transmission line used to make the shorts should be uniform, and the quality of the short circuit should be better than 50:1 vswr. If the quality of the shorts is not that good, but is fairly uniform for all three positions, then the error introduced by assuming infinite vswr is proportional to the magnification of the Γ' circle (Fig. 7). Where the quality of the short is good, but the measured vswr is not uniform, then the junction is lossy.

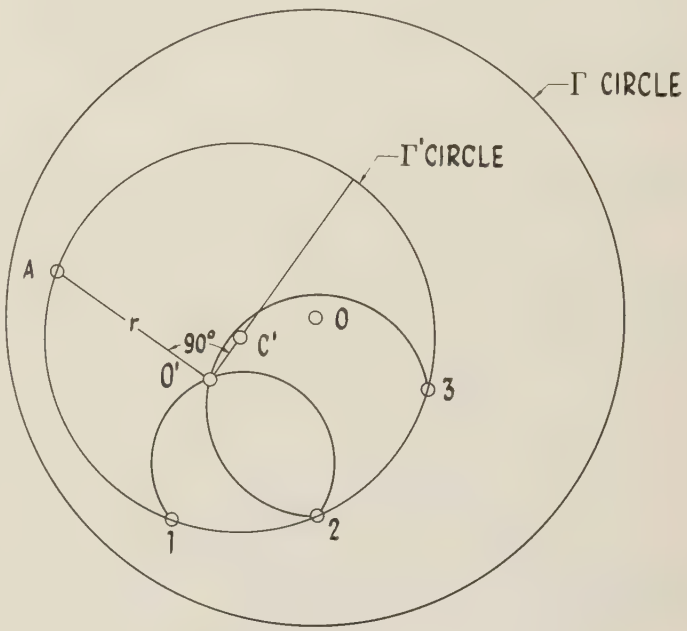

Fig. 7—Effect of a lossy junction

The procedure for lossy junctions is to plot the actual impedance measured on the Smith chart and to fit a circle to the results to form the Γ' circle. Within the Γ' circle one proceeds as before to find the iconocenter. The input reflection coefficient of the junction is $O'O$. The output reflection coefficient is $O'C'/r$. The transmission coefficient is $O'A/\sqrt{r}$ as described very nicely by Storer, Sheingold, and Stein.[2]

Impedance and Polarization-Ratio Transformations by a Graphical Method Using the Isometric Circles*

E. FOLKE BOLINDER†

Summary—The isometric circles for the direct and inverse linear fractional transformations can be used for transformations of impedances and polarization ratios. In the loxodromic case an inversion is performed in the isometric circle of the direct transformation, followed by a reflection in the symmetry line of the two circles, and a rotation around the origin of the isometric circle of the inverse transformation. In the nonloxodromic case only the first two operations have to be applied. Three illustrative examples are given: the first shows the transformation of the right half of the complex impedance plane into the unit circle (Smith Chart); the second gives a circular geometric proof of the Weissfloch transformer theorem; the third shows an example of cascading, lossless, two terminal-pair networks.

Introduction

IN THE SOLUTION of microwave transmission problems, impedance transformations are usually carried out either in the complex impedance (admittance) plane or in the complex reflection coefficient plane. If notations are introduced in accordance with Fig. 1, the input voltage and current are given in terms

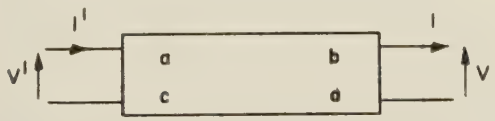

Fig. 1—An arbitrary two terminal-pair network.

of the output voltage and current by the transformation equation

$$\left.\begin{aligned} V' &= aV + bI \\ I' &= cV + dI \end{aligned}\right\}, \tag{1}$$

or in matrix notation by

$$\begin{pmatrix} V' \\ I' \end{pmatrix} = \begin{pmatrix} ab \\ cd \end{pmatrix} \begin{pmatrix} V \\ I \end{pmatrix}. \tag{2}$$

In a bilateral, two terminal-pair network the determinant of the transformation matrix is identically equal to unity:

$$ad - bc = 1. \tag{3}$$

If we let

$$\left.\begin{aligned} \frac{V'}{I'} &= Z' \\ \frac{V}{I} &= Z \end{aligned}\right\}, \tag{4}$$

we obtain

$$Z' = \frac{aZ + b}{cZ + d}, \qquad ad - bc = 1. \tag{5}$$

This is a linear fractional transformation (also called homographic or bilinear) between the impedances Z and Z'.

The properties of transformation (5) are well known.[1,2] The properties that characterize transformations and lead to their classification are usually the invariants. This transformation (5) which conformally transforms the entire complex plane into itself, is characterized by the invariance of the cross ratio, the fixed points, and the isometric circles. The first two of these have found application in the microwave field but the last one seems to have been completely neglected. In this introductory paper it will be shown that the isometric circles are useful and convenient. The method will be applied to some specific examples.

The Isometric Circles

To find the complete locus of points in the neighborhood of which lengths are unaltered in magnitude by the transformation (5), it is only necessary to study the derivative[2]

$$\frac{dZ'}{dZ} = \frac{1}{(cZ + d)^2}, \qquad ad - bc = 1. \tag{6}$$

The desired locus is clearly the circle

$$\left| cZ + d \right| = 1, \qquad c \neq 0 \tag{7}$$

which is called the isometric circle of the direct transformation. Eq. (6) shows that lengths are increased in magnitude within the circle and decreased in magnitude without the circle.

If we solve (5) for Z we get the inverse transformation

$$Z = \frac{-dZ' + b}{cZ - a}, \qquad ad - bc = 1 \tag{8}$$

which has the corresponding isometric circle

$$\left| cZ - a \right| = 1. \tag{9}$$

The isometric circle of the direct transformation, C_d, has its center at $O_d = -(d/c)$ and radius $R_c = 1/|c|$; the isometric circle of the inverse transformation has its center at $O_i = a/c$ and the same radius.

* This work was supported in part by the Army (Signal Corps), the Air Force (Office of Scientific Research, Air Research and Development Command), and the Navy (Office of Naval Research).

† Research Lab. of Electronics, M.I.T., Cambridge, Mass. Formerly at the Royal Institute of Technology, Division of Radio Engineering, Stockholm, Sweden.

[1] K. Knopp, "Elemente der Funktionentheorie," Sammlung Göschen, Band 1109, Berlin; 1949.

[2] L. R. Ford, "Automorphic Functions," 2nd ed., Chelsea Publishing Co., New York, N.Y.; 1951.

The Relationship Between the Isometric Circles and the Fixed Points of the Transformation

The points that are unchanged by transformation (5), the fixed points, are easily obtained by letting $Z'=Z$, and solving the equation

$$cZ^2 - (a - d)Z - b = 0. \tag{10}$$

The roots are

$$\zeta_1, \zeta_2 = \frac{a - d \pm \sqrt{(a + d)^2 - 4}}{2c}, \quad ad - bc = 1. \tag{11}$$

At this point, it is helpful to review the classification of different types of transformation, which can be found in works on the theory of functions.[1,2]

If $a+d$ is real and $|a+d|>2$, (11) has two real roots. A pure stretching is obtained and the transformation is called *hyperbolic*.

If $a+d$ is real and $|a+d|=2$, (11) has one root (or two coalescing roots). A pure translation is obtained and the transformation is called *parabolic*.

If $a+d$ is real and $|a+d|<2$, (11) has two complex conjugate roots. A pure rotation is obtained and the transformation is called *elliptic*.

If, finally, $a+d$ is complex, (11) has two complex roots. A combined stretching and rotation is obtained and the transformation, which can be split into a hyperbolic transformation followed by an elliptic one, or vice versa, is called *loxodromic*.

In accordance with the results of the previous section the distance between the centers of the two isometric circles is $|(a+d)/c|$, while the sum of the two radii is $2/|c|$. Therefore, if we follow the classification given above, we get the hyperbolic case if the two circles are external: the parabolic case, if they are tangent: and the elliptic case, if they intersect. (See Figs. 2–4.) In the loxodromic transformation each circle may have any relation to the other. The positions of the fixed points in relation to the isometric circles can now be obtained easily from (11). The fixed points are marked as crosses in Figs. 2, 3, and 4.

The Graphical Method

In the theory of functions (5) is usually divided in the following way:

$$Z' = \frac{a}{c} - \cfrac{\cfrac{1}{c^2}}{Z + \cfrac{d}{c}}, \qquad ad - bc = 1. \tag{12}$$

The following operations, suggested by (12), are then usually performed in the complex Z plane (see Fig. 5 on the following page):

1) a translation, $Z_1=Z+(d/c)$;
2) a complex inversion, $Z_1Z_2=1/|c|^2$;
3) a rotation around the origin through the angle $-2\phi_c$, giving Z_3;

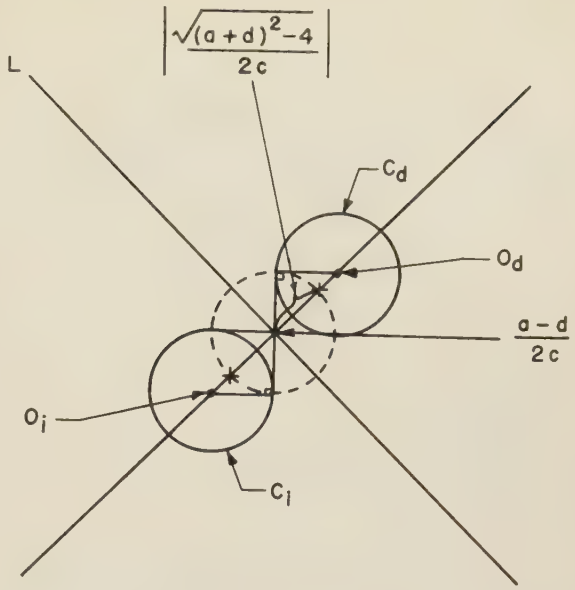

Fig. 2—The hyperbolic case.

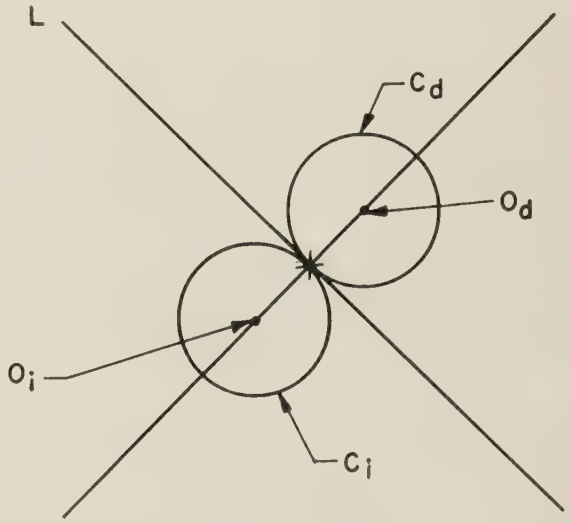

Fig. 3—The parabolic case.

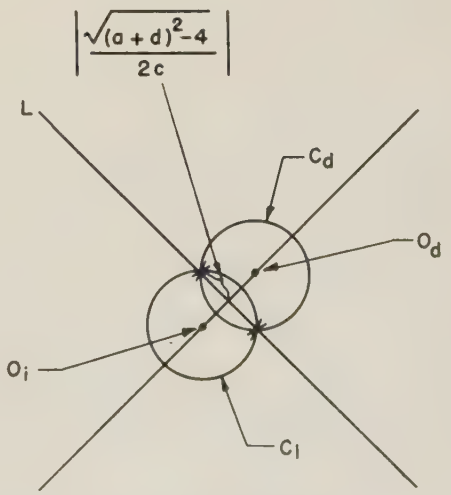

Fig. 4—The elliptic case.

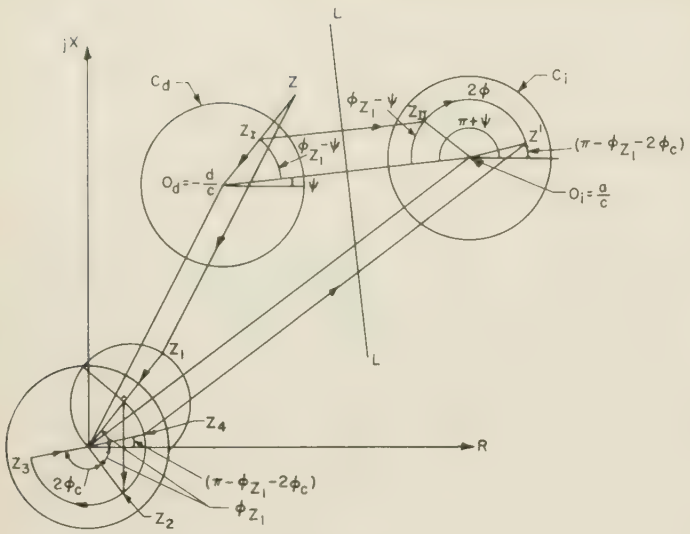

Fig. 5—Graphical interpretation of the linear fractional transformation.

4) a projection through the origin (a rotation around the origin through the angle π), giving Z_4;
5) a translation, $Z'=(a/c)+Z_4$.

If we now draw, as in Fig. 5, the two isometric circles C_d and C_i that have the same radius $R_c=1/|c|$ and the centers $O_d=-(d/c)$ and $O_i=a/c$, the transformation $Z\rightarrow Z'$ can be simplified and the following operations performed: An inversion in the isometric circle C_d of the direct transformation, giving Z_I; a reflection in the symmetry line L of the two circles, giving Z_{II}; and a rotation around the center O_i of the isometric circle of the inverse transformation through an angle -2ϕ.

From Fig. 5 it follows immediately that

$$\psi = \phi - \phi_c \tag{13}$$

or

$$\left|\frac{a+d}{c}\right| = \left|a+d-\left|\phi_c\right|\right|. \tag{14}$$

Thus in the general loxodromic case the transformation (5) can be obtained by an inversion in the isometric circle of the direct transformation, followed by a reflection in the symmetry line L, and, finally, a rotation around the center of the isometric circle of the inverse transformation through an angle -2 arg $(a+d)$. In the nonloxodromic cases, when $a+d$ is real, only the first two operations have to be applied; the same result is obtained by a reflection in L followed by an inversion in the isometric circle of the inverse transformation. This theorem was proved by Ford,[2] but he followed a different line of thought in his proof. He then used the isometric circle to study fundamental regions belonging to linear groups in the theory of automorphic functions.

In network theory graphical inversion methods have been used for symmetric networks, as for example, by König.[3] An interesting graphical interpretation of (5) was introduced by Feldtkeller[4] who bases his method on the positions of the so-called oscillation impedances (Schwingwiderstände) which are defined as the roots of the equation

$$-Z = \frac{aZ+b}{cZ+d}. \tag{15}$$

This method, however, is restricted to linear, symmetric networks ($a=d$).

Applications

Transformation of the Right Half of the Complex Impedance Plane in the Unit Circle (Smith Chart)

In order to fulfill the condition in (3), that $ad-bc=1$, the well-known formula for transforming the right half of the complex impedance plane in the unit circle, has to be written in the following way:

$$\Gamma = \frac{\dfrac{Z}{\sqrt{2}}-\dfrac{1}{\sqrt{2}}}{\dfrac{Z}{\sqrt{2}}+\dfrac{1}{\sqrt{2}}} = \frac{aZ+b}{cZ+d}; \qquad ad-bc=1. \tag{16}$$

Thus, referring to Fig. 6,

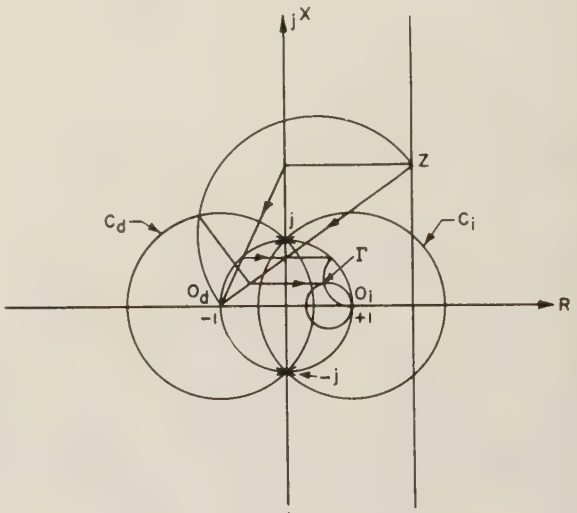

Fig. 6—Transformation of the right half of the complex impedance plane into the unit circle.

$$O_d = -\frac{d}{c} = -1$$

$$O_i = \frac{a}{c} = 1 \tag{17}$$

$$R_c = \sqrt{2}$$

$$a+d = \sqrt{2} = \text{real}.$$

The transformation is clearly nonloxodromic and elliptic, since $a+d$ is real and the isometric circles inter-

[3] H. König, "Über die Abhangigkeit des Scheinwiderstandes eines symmetrischen Vierpols von der Belastung, *Helv. Phys. Acta*, vol. 4, pp. 281–289; 1931.

[4] R. Feldtkeller, "Einführung in die Vierpoltheorie der elektrischen Nachrichtentechnik," S. Hirzel Verlag, Leipzig; 1948.

sect. The fixed points are $\pm j$. Thus Γ is simply obtained from an arbitrary Z by inverting in C_d and reflecting in L, the imaginary axis. The imaginary axis is mapped on the unit circle; the right half plane falls inside the circle. The constant $-R$ and constant $-X$ lines are transformed in two sets of orthogonal circles through the point $+1$. The diagram inside the unit circle is the familiar Smith Chart with Γ defined as the reflection coefficient. An inverse transformation $\Gamma \rightarrow Z$ is simply obtained by inverting in C_i and reflecting in L. If the different planes are stereographically mapped on a Riemann sphere, the transformation constitutes a 90°-rotation around an axis through the fixed points.

The transformation between the Z plane and the Γ plane mentioned above was recently treated by de Buhr.[5] He used the C_i circle as the inversion circle but he did not realize that this circle is one of the isometric circles; nor did he see that his graphical construction is a special case of a more general one.

A New Proof of the Weissfloch Transformer Theorem for Lossless Two Terminal-Pair Networks

Weissfloch's transformer theorem states that for a given frequency any lossless two terminal-pair network can be converted into an ideal transformer by coupling specific lengths of homogeneous transmission lines to each side of the network. The theorem was originally proved by Weissfloch[6] in the complex impedance plane. A proof in the complex reflection coefficient plane was recently given by Weissfloch[7] and by Lueg.[8] It was also proved graphically by Van Slooten,[9] who used the Cayley-Klein diagram (Van Slooten calls it "Cayley-diagram" or "C-diagram"). A new, extremely simple, proof will now be given by means of the isometric circles.

Any impedance transformation through a lossless two terminal-pair network leaves the imaginary axis invariant in the complex plane and the unit circle invariant in the complex reflection coefficient plane. All transformations of this kind that have a common fixed circle the interior of which is transformed into itself, are said to belong to a properly discontinuous group called Fuchsian.[2] The fixed circle mentioned is called the principal circle. One theorem[2] states that the isometric circles of the transformations of a Fuchsian group are orthogonal to the principal circle. In Fig. 7 the lossless network is represented by the isometric circles C_d and C_i, both cutting the principal circle perpendicularly. The network is elliptic, since the circles intersect. The fixed points are marked as crosses. If the circles are separated, the fixed points will coalesce in the tangential case and then continue along the principal circle in the external case. These are the parabolic and the hyperbolic cases. Since the ideal transformer has its fixed points at ± 1, we shall try to find a method for moving the fixed points of Fig. 7[10] to these positions.

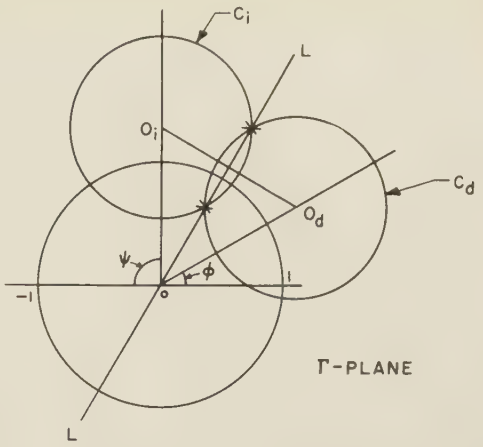

Fig. 7—The isometric circles of an arbitrary, lossless, two terminal-pair network.

A transformation by means of a lossless, homogeneous transmission line constitutes a rotation around the origin in the Γ plane. The isometric circles are straight lines through the origin. With the notations of Fig. 8

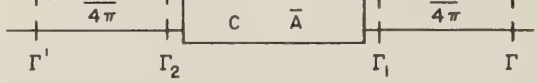

Fig. 8—An arbitrary, lossless, two terminal-pair network between two homogeneous, lossless transmission lines.

we can write

$$\Gamma_1 = e^{-i\phi} \tag{18}$$

$$\Gamma_2 = \frac{A\Gamma_1 + \bar{C}}{C\Gamma_1 + \bar{A}}, \quad |A|^2 - |C|^2 = 1 \tag{19}$$

$$\Gamma' = \Gamma_2 e^{-i\psi} \tag{20}$$

The arbitrary lossless two terminal-pair network has the centers of its isometric circles at $O_d = -(\bar{A}/C)$ and $O_i = A/C$, both having the radius $R_c = 1/|C|$. Eqs. (18) and (19) give

$$\Gamma_2 = \frac{Ae^{-i(\phi/2)}\Gamma + \bar{C}e^{+i(\phi/2)}}{Ce^{-i(\phi/2)}\Gamma + \bar{A}e^{+i(\phi/2)}} \tag{21}$$

having isometric-circle centers at $O_d' = -(\bar{A}/C)e^{i\phi}$ and $O_i' = A/C$ with radii R_c. Thus the isometric circle of the direct transformation is rotated through an angle $+\phi$, while the isometric circle of the inverse transformation is invariant.

[5] J. de Buhr, "Eine neue Methode zur Bearbeitung linearer Vierpole," *FTZ*, pp. 200–204; April, 1955.

[6] A Weissfloch, "Ein Transformationssatz über verlustlose Vierpole und seine Anwendung auf die experimentelle Untersuchung von Dezimeter—und Zentimeterwellen—Schaltungen," *Hochfr. u. Elak.*, vol. 60, pp. 67–73; September, 1942.

[7] A. Weissfloch, "Kreisgeometrische Vierpoltheorie und ihre Bedeutung für Messtechnik und Schaltungstheorie des Dezimeter— und Zentimeterwellengebietes," *Hochfr. u. Elak.*, vol. 61, pp. 100–123; 1943.

[8] H. Lueg, "Über die Transformationseigenschaften verlustloser Vierpole zwischen homogenen Leitungen und ein kreisgeometrischer Beweis des Weissfloch-schen Transformatorsatzes," *AEÜ*, vol. 7, pp. 478–484; 1953.

[9] V. Van Slooten, "Meetkundige Beschouwingen in Verband met de Theorie der Electrische Vierpolen," Thesis, Delft, 1946.

[10] Figs. 7 and 9 should be reflected, so that $\pm 1 \rightarrow \mp 1$.

Eqs. (19) and (20) give

$$\Gamma' = \frac{Ae^{-j(\psi/2)}\Gamma_1 + \overline{C}e^{-j(\psi/2)}}{Ce^{+j(\psi/2)}\Gamma_1 + \overline{A}e^{+j(\psi/2)}} \tag{22}$$

having isometric-circle centers at $O_d'' = -\overline{A}/C$ and $O_i'' = (A/C)e^{-i\psi}$ with radii R_c. Thus the isometric circle of the direct transformation is invariant, while the isometric circle of the inverse transformation is rotated through an angle $-\psi$.

The transmission lines clearly move the fixed points of Fig. 7 to the points ± 1. The lengths of the transmission lines are $\lambda\phi/4\pi$ and $\lambda\psi/4\pi$, where λ is the wavelength. Thus an ideal transformer is obtained and the Weissfloch transformer theorem is proved. If the ideal transformer is represented by

$$Z' = kZ \tag{23}$$

it can easily be proved that the connection between the radius R_c and the impedance transformation ratio k is

$$R_c = \left| \frac{2}{\sqrt{k} - \frac{1}{\sqrt{k}}} \right|. \tag{24}$$

To illustrate this proof given above, a transformation of an arbitrary reflection coefficient Γ, representing, for the sake of simplicity, a reactance, through the ideal transformer is shown in Fig. 9. Here the transformations

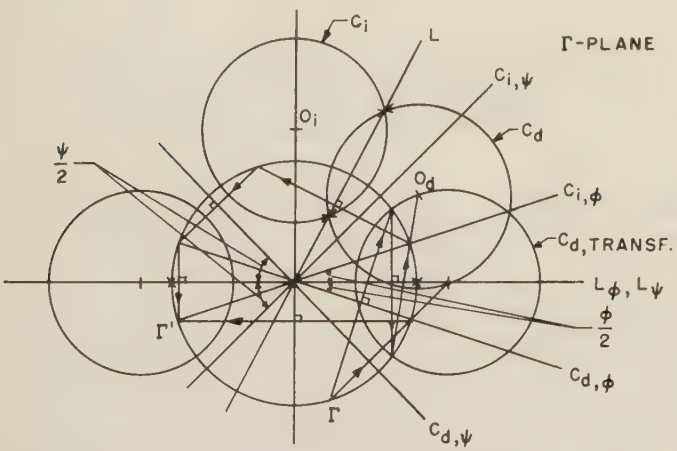

Fig. 9—A circular geometric proof of the Weissfloch transformer theorem using the isometric circles.

performed by the transmission line of length $\lambda\phi/4\pi$, the arbitrary, lossless network, and the transmission line of length $\lambda\psi/4\pi$, are shown to give the same reflection coefficient Γ' as the one obtained by a transformation through the ideal transformer.

Cascading of a Set of Equal Lossless Two Terminal-Pair Networks

In Fig. 10 an arbitrary, lossless, two terminal-pair network is represented by the isometric circles C_d and C_i in the Γ plane. An arbitrary reactance corresponding to the point Γ on the unit circle is transformed in Γ_1. If another network exactly equal to the first one is coupled in series, the new reflection coefficient Γ_2 is obtained at the input by the same operations, inverting in C_d and reflecting in L, as were performed before. For a set of equal networks the reflection coefficients Γ_1, Γ_2, Γ_3, Γ_4, $\cdots$ are obtained. It is seen in Fig. 10 that the transformations correspond to a (non-Euclidean) rotation around the fixed point, which checks with the fact that all transformations are elliptic. Similar constructions can easily be performed in the parabolic and the hyperbolic cases.

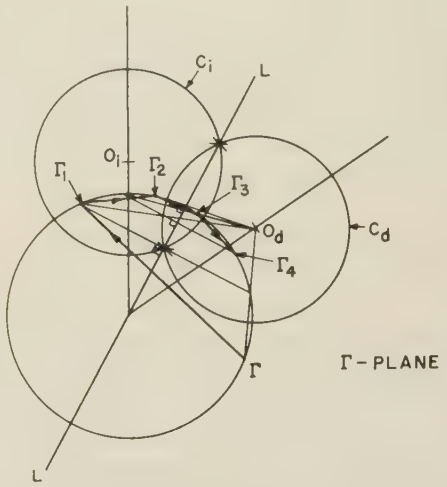

Fig. 10—Transformation through a set of equal, lossless, two terminal-pair networks.

Besides the use of the isometric circle method for impedance transformations, as shown above, the method can also be applied to transformation of polarization ratios.[11]

ACKNOWLEDGMENT

The present paper, which constitutes the first part of a study of the use of graphical methods in the microwave field, was started at the Royal Institute of Technology, Stockholm, Sweden in the summer of 1954; it was continued while the author was a guest at Instituto Nacional de la Investigaciones Cientifica, Mexico D. F., Mexico, in the winter of 1954–55; and it was completed at the Research Laboratory of Electronics, Massachusetts Institute of Technology, in the fall of 1955. The author wishes to express his gratitude to the Swedish Government Technical Research Council, Stockholm, and to Telefonaktiebolaget L. M. Ericsson, Stockholm, for grants which made possible the trips to Mexico and the United States. He also thanks the directors of the Research Laboratory of Electronics, M.I.T., for accepting him as a member of the research staff.

[11] V. H. Rumsey, G. A. Deschamps, M. L. Kales, and J. I. Bohnert, "Techniques for handling elliptically polarized waves with special reference to antennas," PROC. IRE, vol. 39, pp. 533–552; May, 1951.

A Broad-Band Dual-Mode Circular Waveguide Transducer

R. D. TOMPKINS†

Summary—This paper describes a broad-band dual-mode waveguide transducer designed to couple two orthogonal TE_{11} circular waveguide modes in separate rectangular waveguide ports. A compact, rugged, and economical junction has been developed to operate from 8600 mc to 9600 mc with a vswr of less than 1.15 at the rectangular port and a mode isolation of 50 db or greater.

Developmental models are described to indicate the evolution from theory to the final model. Some problems encountered in attaining a small physical size are discussed in detail. The new junction has application to mode multiflexing, circular waveguide ferrite devices, circular polarization, and as a circular waveguide magic-T.

THE TRANSMISSION of more than one signal in a waveguide using a common frequency is possible by utilizing the various electromagnetic symmetries or "modes" as separate information channels. One of the practical problems associated with multiplexing of this type is to extract or excite energy in one mode independent of the other propagating modes.

This has been done for single frequency operation by Ragan[1] and Kingdon[2] by taking advantage of the fact that two dominant TE_{11} modes will propagate independently if orthogonally oriented within a circular waveguide. This paper describes the development of a broad-band dual-mode waveguide transducer which was designed to couple orthogonal TE_{11} modes in 15/16-inch id circular waveguide to separate 0.4- by 0.9-inch rectangular ports over the band from 8,600 mc to 9,600 mc. The compact transducer which has been developed exhibits a high order of isolation between channels with a low input vswr over the band of frequencies considered.

Mode Transformation and Isolation

The dominant rectangular waveguide mode (TE_{10}) can be made to couple to the dominant circular waveguide mode (TE_{11}) in the manner indicated in Fig. 1(a). Ordinarily, energy introduced in the rectangular arm will split at the junction and propagate in both directions down the circular guide, but by properly locating a short circuit in the circular guide, energy will be forced to propagate in one direction. The required short circuit may take the form of a plunger completely blocking the guide, a conducting septum, or a series of thin metallic pins located parallel to the E field polarization as shown in Fig. 1(b). Thin obstacles of the septum or pin type not only produce the desired reflection of one mode, but also appear transparent to a similar mode polarized at right angles. Arranging two such transducers in tandem with a 90° angular relationship between the rectangular arms will permit independent excitation of orthogonal modes in the circular waveguide.

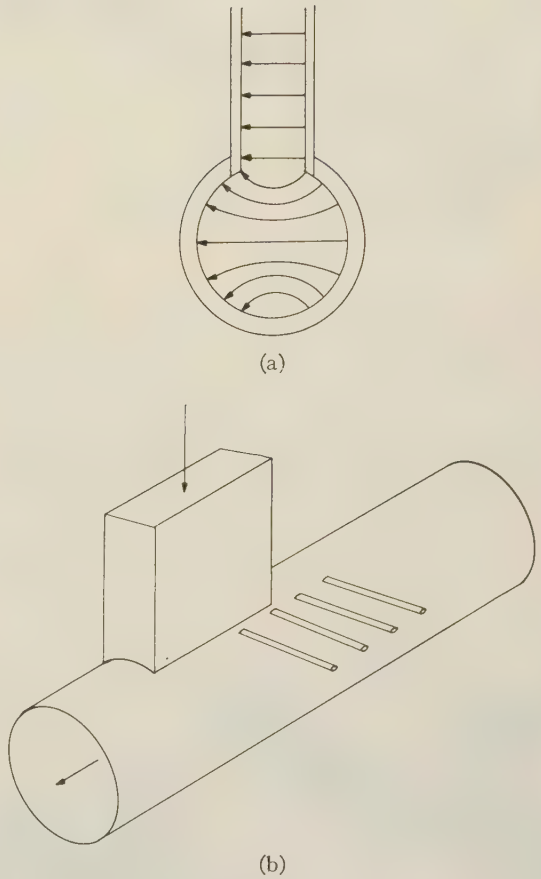

Fig. 1(a)—Transformation from the rectangular TE_{10} mode to the circular TE_{11} mode. (b) A side-arm transducer.

The isolation between the two modes, assuming mode purity, is a function of the deviation from the desired 90° angular relationship of the two rectangular arms and is given by

$$I_{db} = 20 \log \phi$$

where ϕ is a small angular deviation from 90° in radians. A plot of this function is shown in Fig. 2 where, for convenience in specifying mechanical tolerances, the angle of deviation is plotted in minutes. It can be seen from the curve that a high order of mechanical accuracy is necessary to achieve a mode isolation of 45 db or better.

† Naval Research Lab., Washington, D.C.

[1] G. L. Ragan, "Microwave Transmission Circuits," The McGraw-Hill Book Publishing Co., New York, N.Y., p. 369; 1948.

[2] B. E. Kingdon, "A circular waveguide magic-tee and its application to high power microwave transmission, *J. Brit. IRE*, vol. 13, pp. 275–287; May, 1953.

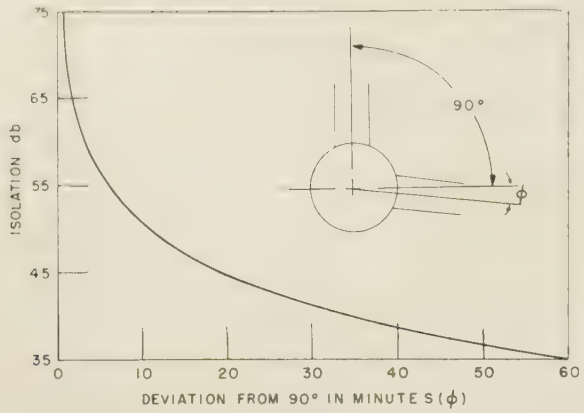

Fig. 2—Mode isolation vs the deviation from the 90° angular relationship of the rectangular arms.

Developmental Models

The two experimental models shown in Fig. 3 were built embodying the preceding principles. The major difference between these transducers is in the configuration of the rear arm (*i.e.*, the arm furthest from the circular port). Four 1/16-inch diameter pins spaced $\frac{1}{4}$ inch apart were so positioned as to provide a fairly uniform amount of reflection over the frequency band at the side arm terminal. The size and position of a matching inductive iris for this terminal was computed by the use of established broadband matching techniques.[3,4]

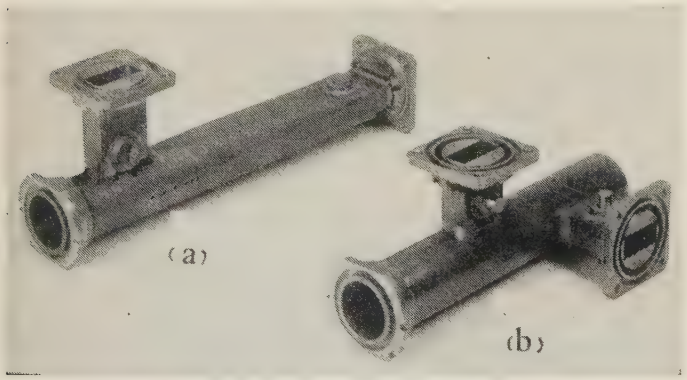

Fig. 3—(a) Two-arm transducer. (b) Tapered-arm transducer.

A further matching problem was encountered at the rear arm. The circular waveguide mode originating at this terminal will see a radiating aperture at the front arm. Although the front rectangular waveguide is beyond cutoff for this mode, some coupling will exist which will appear as undesirable reflections at the rear port. A wave filter in the form of thin vanes which are parallel to the axis of the circular guide and which provide a smooth continuation of the circular waveguide wall, was placed in the front arm to prevent distortion of this mode in the region of the front arm aperture. The effect of these vanes on the propagating mode in the front arm is negligible. Tests made on these completed models showed a mode isolation greater than 50 db and an input vswr less than 1.15 in both rectangular arms over the band.

Both of these early junctions, however, had disadvantages of being difficult to construct and physically bulky. In addition, a certain amount of structural weakness was inherent since assembly procedures dictated that the side arm be soft-soldered to the circular waveguide. The need for a more compact, rugged, and economical transducer was indicated and development proceeded along these lines.

Compact Model

Two different methods of transforming from the TE_{10} mode in rectangular guide to the TE_{11} mode in the circular guide were used for the rear ports in the previous models. Another model was built using a stepped waveguide section to perform the required mode transformation. This stepped transition is produced by means of a broad-band dielectric transformer[5] designed to permit direct connection between the end of the 15/16-inch id circular guide and a rectangular waveguide equipped with a UG-40A/U choke flange. Use of this device for one port of the two-mode transducer reduced the length of the junction to half that of the tapered-arm version.

A further reduction in size was made by eliminating the section of rectangular waveguide in the side arm and mounting a UG-40A/U choke flange directly to the circular waveguide. A coupling aperture was made by milling an opening in the circular waveguide wall. The narrow dimension of this aperture was made equal to the narrow dimension of the rectangular waveguide in order to preserve the power handling capabilities of the device. Inductive matching elements were formed from the circular waveguide wall by making the broad dimension of the aperture less than that of the rectangular guide. It was impossible to obtain acceptable broadband matching by adjusting the aperture opening solely in the broad dimension. However, by plotting admittance data for various aperture sizes, it was possible to choose an opening which provided the proper vswr and phase dispersion to allow broad-band matching by means of a supplementary iris which could be located within the flange. This matching element may be seen in the photograph of the compact model shown in Fig. 4.

Measurements were made on this model and the results were generally good. However, an undesirable mode coupling resonance was noted near 9,400 mc. At this point the isolation between rectangular ports dropped abruptly from 50 db to about 30 db. The primary cause was found to be resonant reflections between the rear arm flange and the pins due to flange misalignment. This resonance could be shifted outside the band of interest by reducing the spacing between the flange and the pins, or can be prevented entirely by the insertion of a resistance card to absorb the reflection from the pins. The latter method was used in the model

[3] R. G. Fellers and R. T. Wiedner, "Broad-band admittance matching by use of irises," Proc. IRE, vol. 35, pp. 1080–1085; October, 1947.

[4] Ragan, *op. cit.*, p. 322.

[5] I. D. Olin, "Dielectric transformers for *x*-band waveguide," *Electronics*, vol. 28, pp. 146–148; December, 1955.

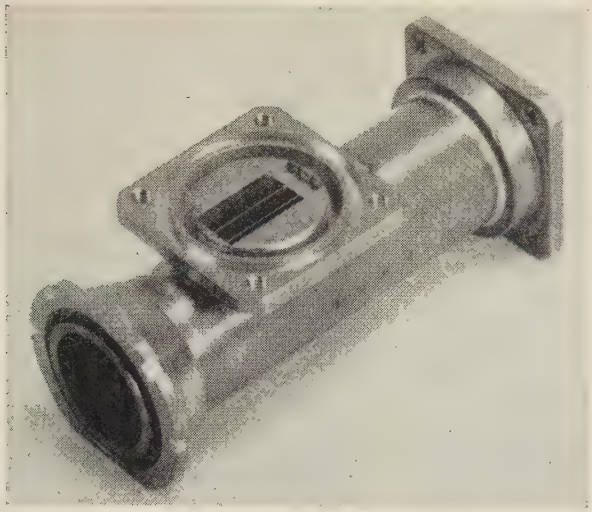

Fig. 4—Compact transducer.

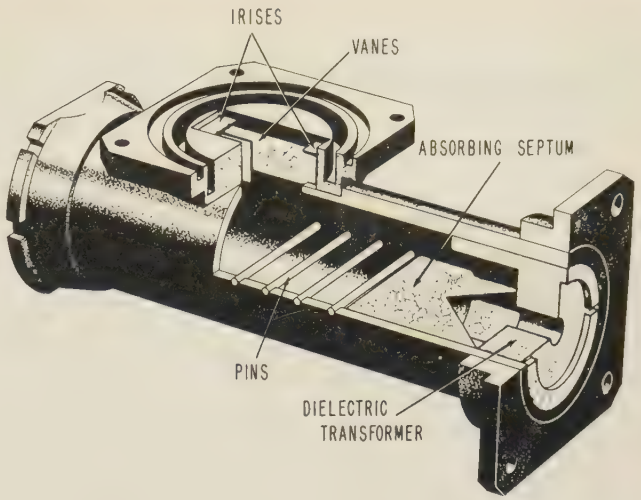

Fig. 5—Cutaway view of compact transducer.

described since development work was completed and the dimensions frozen at the time that the resonance was discovered.

With this modification the compact model now possesses electrical characteristics equal to those of the previous models. Input vswr to either rectangular arm is less than 1.15:1. Mode isolation is 50 db or greater over the band from 8,600 mc to 9,600 mc. The mechanical characteristics are far superior to the earlier versions, being of a more rugged construction and more economical to fabricate. Construction details are shown in Fig. 5. It can be seen from this view that the width of the vanes which form the wave filter was adjusted so that the matching iris would be in its proper position when seated on top of the vanes. Small slots cut in the narrow wall of the choke flange provide a convenient holding device while the vanes are being soldered. The critical dimensions which include the aperture size, the position of the pins with respect to the aperture and the position and size of the matching elements are indicated in Fig. 6.

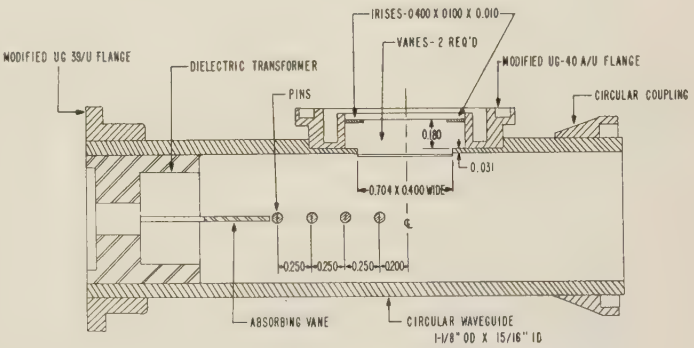

Fig. 6—Plan view of compact transducer showing critical dimensions.

Conclusion

The compact dual-mode transducer which has been developed exhibits a high order of isolation between channels with a low input vswr for the frequency range considered and provides an effective means for mode multiplexing in circular waveguide. The junction also offers utility in the design of circular waveguide ferrite devices, such as isolators, duplexers, and circulators. Kingdon has suggested several other applications for this type transducer including balanced mixers, circular or elliptical polarizers, rotary joints, a variable power splitting bridge, and a circular waveguide magic-*T*.

Acknowledgment

The author is indebted to Lt. I. D. Olin, U. S. Army, who did most of the original design and experimental work on the junction while at Naval Research Laboratory. The helpful suggestions received in discussions with P. J. Allen are greatly appreciated.

Correction

Franklin S. Coale, author of the paper "A Switch Detector Circuit," which appeared on pages 59–61 of the December, 1955 issue of Transactions on Microwave Theory and Techniques, has requested that the following information, omitted in his manuscript, be published by the editors.

The work for the paper was accomplished while Mr. Coale was a member of the Sperry Gyroscope Company under an Air Force Contract.

P. J. Sferrazza, of Sperry, developed a band-pass crystal switch at 3300 mc which gave a dynamic switching of greater than 44 db over a 10 mc bandwidth.

Correspondence

Planar Transmission Lines—II

I would like to call your attention to a certain mistake in the above paper.[1] Park's transmission line, consisting of two parallel strips between two wide plates [Fig. 1(a)], has to be changed to the line geometry indicated in Fig. 1(b) in order to maintain the results of the mentioned paper.

The mistake originates from a false interpretation of

$$jz' = \sqrt{k\rho}\ \mathrm{sn}\ (jKZ/H), \qquad (6)$$

in particular of the elliptic function sn x.

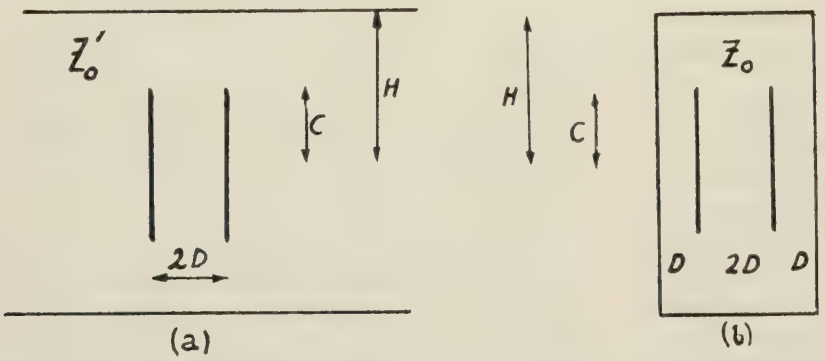

Fig. 1—(a) Open and (b) enclosed parallel plate lines.

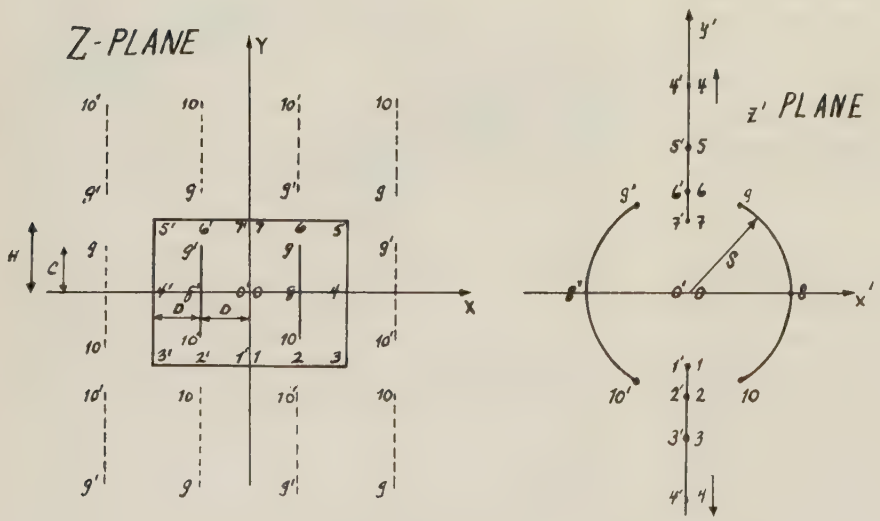

Fig. 2—Mapping of Z plane into z' plane by means of (6).

The correct mapping is shown in Fig. 2. One should note that sn x is a double periodic function. That is the reason why the two strips 9-10 and 9'-10' are actually within the rectangular box 3'-3-5-5' in contrast to the geometry given in the mentioned paper. The box is transformed into the imaginary axis of the z' plane which is a potential line of the configuration and therefore does not impair the field between the two circle electrodes 9-8-10 and 9'-8'-10'.

In order to check the validity of the statements made one can easily calculate the characteristic impedances of the open and enclosed parallel plate lines (Fig. 1) for the special case $H \to \infty$ and $C \gg D$. The impedance of the open line is found to be $Z_0' = 120\pi D/C$, and from the exact formulas of Park one has $Z_0 = 60\pi D/C$ which is half the value of Z_0' and therefore corresponds to the configuration of Fig. 1(b).

Adolf J. Giger,
Inst. for High Freq. Techn.,
Zurich, Switzerland.

[1] D. Park, Trans. IRE, vol. MTT-3, pp. 7–11; October, 1955.

Rebuttal

I should ike to thank Dr. Giger for pointing out this error—it was due to an uncritical use of somebody else's formula—and to express my regret that it should have occurred. It might be added that the problem which I have solved by inadvertence is one which arises naturally out of my first paper,[2] and (if there are no further errors) may possibly be of greater practical use than that whose solution Dr. Giger has criticized.

David Park,
University of Ceylon,
Colombo, Ceylon.

[2] David Park, "Planar transmission lines," Trans. IRE, vol. MTT-3, pp. 8–12; April, 1955.

Determination of the Parameters of Cavities Terminating Transmission Lines

The method of measuring cavity parameters outlined in the above paper[1] has been used successfully for some time by our laboratory for measuring parameters of cavities at X band having Q's as high as 150,000. For improved accuracy in these measurements, an additional refinement has been made in the method which makes all measurements independent of the law of the crystal detectors used.

The method consists simply of inserting immediately after the signal generator, in Libowitz's circuits, a precision calibrated attenuator. This attenuator is used to refer all measurements to a fixed power level in the crystal. For example, in measuring loaded Q the 3 db point on the observed cavity absorption dip is determined by changing the attenuator 3 db. VSWR measurements of coupling parameters are taken in db from the attenuator and converted to other desired parameters by the scales on a Smith Chart. Such measurements are simplified further by use of a dc coupled oscilloscope.

Maurice W. St. Clair,
Instrument-Division,
Varian Associates,
Palo Alto, Calif.

[1] R. A. Libowitz, Trans. IRE, vol. MTT-4, pp. 51–53; January, 1956.

A Low VSWR Matching Technique

A variation on the method described by Feller and Weidner[1] for obtaining low standing wave ratios over a frequency band has

[1] R. G. Fellers and R. T. Weidner, "Broad-band waveguide admittance matching by use of irises," Proc. IRE, vol. 35, pp. 1080–1085; October, 1947.

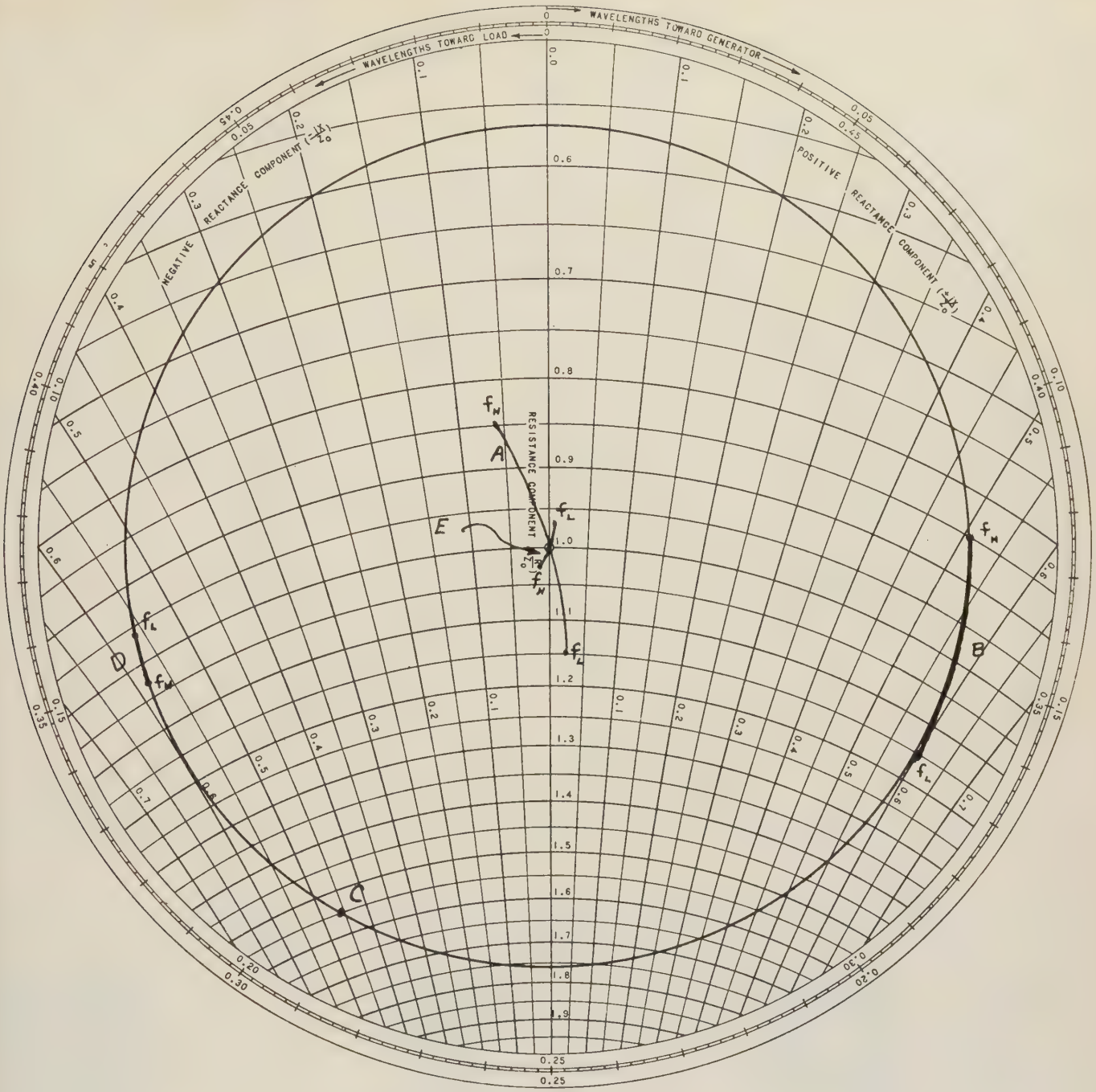

Fig. 1

proven to be very useful in the design of low vswr microwave components. If curve A in Fig. 1 represents the input admittance of the device to be matched, the method described by Feller proceeds as follows:

1) Insert a value of susceptance which causes the curve to lie along a constant vswr circle (curve B).
2) Move toward the generator until the frequency sensitivity of the line length causes the curve to reduce to a point (point C).
3) Move to the nearest intersection with the $g=1$ circle (curve D).
4) Insert a value of susceptance which transforms the admittance plot to the center of the chart; *i.e.*, a matched condition (curve E).

Although this method insures that the admittance plot is on a constant vswr circle, it does not guarantee that the plot will lie along a constant phase line *at the point where the final susceptance is to be inserted*. In order to satisfy both conditions, a method will be described which although involving some trial and error leads to the desired result in about two attempts. Given the admittance plot A in Fig. 2, the method is as follows:

1) Insert a value of susceptance which produces a phase spread θ equal to the phase sensitivity of a 3/4λ length of line (curve B). That is,

$$\theta = \frac{3/4\lambda_{g0}}{\lambda_{gH}} - \frac{3/4\lambda_{g0}}{\lambda_{gL}} = 3/4\left(\frac{\lambda_{g0}}{\lambda_{gH}} - \frac{\lambda_{g0}}{\lambda_{gL}}\right) \quad (1)$$

where λ_{gL}, λ_{g0}, and λ_{gH} are the guide wavelengths at the low, center and high ends of of the frequency band respectively.

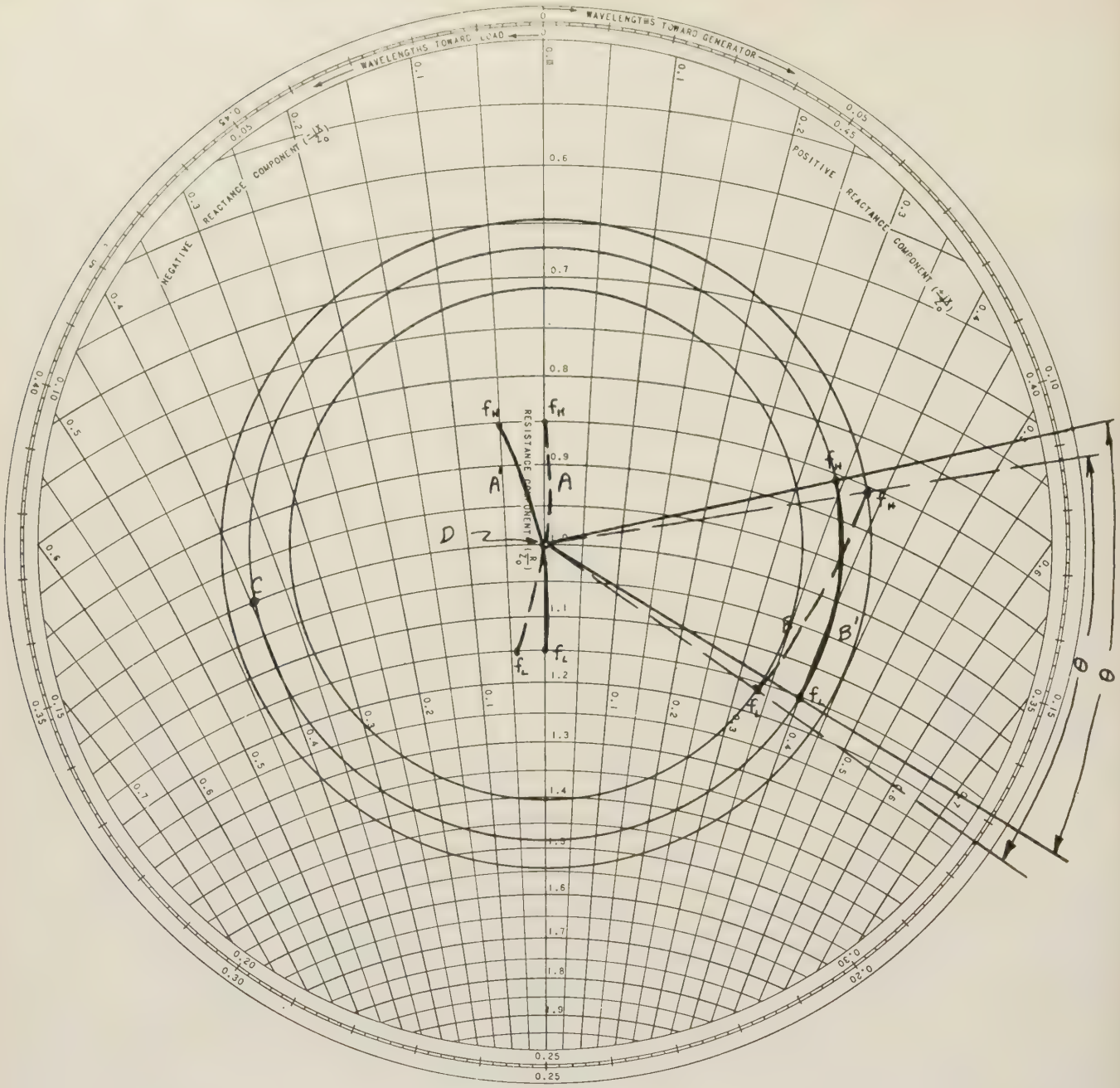

Fig. 2

2) Since curve B is not a constant vswr circle, change the original curve A in order to have the admittance plot lie on a constant vswr circle and yet maintain a phase spread given by (1). This can be done by inserting the first susceptance at a point along the transmission line corresponding to the admittance curve A' instead of a point corresponding to the curve A. Introduction of the susceptance at this point now yields the admittance curve B' which is on a constant vswr circle and has a phase sensitivity equal to that of a $3/4\lambda$ length of line.

3) Now move approximately $3/4\lambda$ toward the generator which reduces the admittance plot to the point C.[2]

4) Insert a second susceptance, identical to the first, which transforms the admittance plot to the center of the Smith Chart; *i.e.*, a matched condition (point D).

In the above discussion no mention has been made of the frequency sensitivity of the irises. However, it can easily be shown by use of the Smith Chart that since the two susceptances are equal in both amplitude and sign, their frequency sensitivities will cancel each other. Therefore in using the above method, the frequency sensitivity of the susceptances can be neglected.

This method has been used in matching components with admittance plots not as well behaved as those shown in Figs. 1 and 2. Standing wave ratios of less than 1.03 across a 6 per cent frequency band have been obtained.

[2] A $3/4\lambda$ line length is chosen in preference to a $\lambda/4$ line length in order to avoid the possibility of higher order mode interaction between the susceptances. In addition, the size of the irises required is reduced by this choice.

Peter A. Rizzi,
Raytheon Mfg. Co.,
Missile Systems Div.,
Bedford, Mass.

Microwave Equipment for College Laboratories

I should like to take advantage of this correspondence column to discuss briefly a problem which we at Clarkson College may have in common with many other private colleges.

We believe that our undergraduate curriculum should include a course in microwaves and that this course to be effective must include some laboratory work. The problem is that it is very difficult to equip a microwave laboratory on the sort of budget existing in a small college. Commercial equipment is, in general, much too expensive and is really much higher quality than is required for simple student laboratory work. We have been able to meet our needs in part by constructing our own waveguide components and in part through the generosity of several concerns which have given us used or rejected equipment or made it available to us at very low cost. We have been given a variety of microwave tubes plus some oscillators and a number of waveguide and coaxial components which make it possible for us to operate our laboratory.

In the interest of furthering study in the microwave field, would it not be possible for more companies in the field to make available for educational purposes used or rejected equipment?

ROBERT J. REICH,
Asst. Prof. Elect. Engrg.,
Clarkson College of Tech.,
Potsdam, N.Y.

Russian Edition of "Principles and Applications of Waveguide Transmission," by George C. Southworth

(The attention of the Editor was called recently to the Editorial Preface to the Russian edition of the above book. The preface is reprinted below in the belief that the commentary will be of interest to many readers.—The Editor.)

This book was written by the well-known American specialist in the uhf field who was one of the pioneers of waveguide techniques. As the author mentions in his preface, the book does not pretend to encompass fully the subject; however, in addition to a description of the fundamentals of the theory of waveguide transmission it contains extensive material devoted to the design and operation of various waveguide components and assemblies and also of electron apparatus applied in conjunction with waveguide apparatus. A part of this material was published earlier in periodicals but is being published now for the first time in book form.

It is necessary to point out the well-known "one sidedness" of the material. The book reflects mainly the results obtained by Bell Telephone Laboratories. The extensive bibliography of the author omits many important papers of Soviet specialists and also specialists from other countries. However, no attempt has been made to introduce into the book additional material since it would cause a considerable increase in volume and it would affect the general style of the book. The reader anticipates from the Soviet scientists in the near future new manuals on uhf techniques which will give a full and objective generalization of the main achievements of the Soviet and non-Soviet engineering in this field.

The book was published in 1950 and, therefore, naturally it either does not deal at all, or deals only very superficially, with achievements obtained during recent years (new types of transmission lines, problems of application of ferrites, triodes, new types of electron equipment for amplification and generation of uhf energy, etc.). In spite of these mentioned drawbacks, the book is written in a simple and clear style and encompasses a wide range of problems and will be of great help to many engineers and physicists and also to students who are interested in uhf techniques.

Contributors

Donald R. Barthel (S'48–A'50) was born in Milledgeville, Ill., on December 2, 1923. He was graduated from the University of Illinois in 1948, receiving the degree of Bachelor of Science in electrical engineering. Since 1948, Mr. Barthel has been a member of the engineering staff of The Glenn L. Martin Company, located in Baltimore, Md. In this position, Mr. Barthel has been engaged in antenna and microwave component developments for aircraft and guided missiles.

D. R. BARTHEL

❖

E. Folke Bolinder (A'50–M'55) was born at Uppsala, Sweden, August 11, 1922. He received the civilingenjör degree in electrical engineering at the Royal Institute of Technology, Stockholm, in 1945. After a year of military service as a special engineer in the Swedish Air Force, where he worked on uhf antennas and circuits, he worked during 1946–1951 on different microwave and pulse technique projects for the Swedish defense, combining the work with graduate studies at the Royal Institute of Technology. In 1951 he became a Fellow of the American-Scandinavian Foundation under whose auspices he worked (during 1952–1953) in transient synthesis as research assistant at the Research Laboratory of Electronics, M.I.T. He received the degree of Licenciate of Technology at the Royal Institute of Technology, Stockholm, in 1954. During the winter of 1954–55 he was a guest at Instituto Nacional de la Investigacion Cientifica, Mexico City. Since the summer of 1955 he has been a research staff member of the Research Laboratory of Electronics, M.I.T., working with geometrical methods in the microwave field.

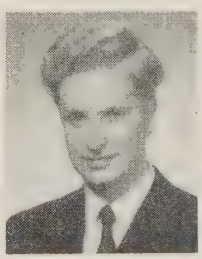

E. F. BOLINDER

Duncan M. Bowie was born on March 12, 1923, in Tulsa, Okla. He first entered the University of Tulsa, College of Engineering, in 1940, and received the B.S. degree in geophysical engineering there in 1948. During this interval he served eighteen months in master layout work with Douglas Aircraft Co. and two years as electrical technician with the U.S. Army Air Corps. From 1949 to 1951 he worked as seismic computer with Geophysical Service, Inc., Dallas, Texas.

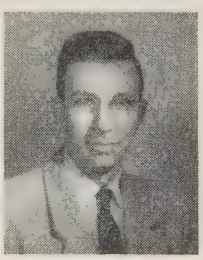

D. M. BOWIE

From 1951 to 1954 he served as teaching fellow at the University of Utah, and there conducted research in nuclear physical measurements. He received the M.S. degree in Physics in 1954, and in that year joined the staff of Melpar, Inc., at Falls Church, Va., where he has worked principally with artificial dielectric materials and microwave measurement techniques. He is a member of Sigma Pi Sigma and Sigma Xi.

John C. Cacheris (SM'56) was born on May 18, 1916, in Chicago, Ill. He graduated from the Capitol Radio Engineering Institute in 1941, received the B.S. degree in electrical engineering from Carnegie Institute of Technology in 1946, and the M.S. degree from Maryland University in 1953.

J. C. Cacheris

From 1941 to 1946 Mr. Cacheris was employed as a radio engineer in the Test Department of the Radio Division of the Westinghouse Electric Corporation, Baltimore, Md. From 1946 until 1949, as an electronic scientist with the Naval Ordnance Laboratory in White Oak, Md. he designed circuits and instruments for ultra high and microwave frequency ranges.

He joined the staff of the Ordnance Development Division of the National Bureau of Standards, Washington, D.C., in 1949, where he engaged in microwave antenna and diffraction studies, and in investigations of the microwave properties of ferrites. He is continuing the latter investigations at the Diamond Ordnance Fuze Laboratories, Department of the Army, to which the functions and staff of the Ordnance Development Division were transferred on September 27, 1953. Mr. Cacheris is chief of the Ferrite Research Section of the Supporting Research Laboratory.

Mr. Cacheris is a member of the American Physical Society and Eta Kappa Nu, and is a registered professional engineer in the District of Columbia.

❖

Robin M. Chisholm (S'52–A'54) was born in London, Can., in January, 1930. He attended Queen's University in Kingston, Ontario, where he received the B.Sc. degree in engineering physics in 1952. Since then he has been a full-time graduate student at the University of Toronto, where he received the M.A.Sc. degree in 1954 and where, at present, he is working towards a Ph.D. degree in electromagnetic theory.

R. M. Chisholm

Since graduation he has worked summers for the National Research Council of Canada at Ottawa, Ontario, in radar development work.

He is a member of the Association of Professional Engineers for the Province of Ontario.

❖

Herbert Dropkin (A'50) was born in Brooklyn, N.Y., on July 29, 1929. He received his B.E.E. degree from the Cooper Union School of Engineering in 1950, and is now attending the Maryland University Graduate School, in College Park.

H. Dropkin

In 1950, Mr. Dropkin was employed by the Ordnance Development Division of the National Bueau of Standards as an electronic scientist in the Electromechanical Devices Section.

In 1951 he transferred to what has subsequently become the Supporting Research Laboratory of the Diamond Ordnance Fuze Laboratories. There, he was first engaged in the development of cw altimeters. He is presently in the Ferrite Research Section studying microwave properties and applications of ferrites.

❖

E. T. Jaynes (SM'54) was born in Waterloo, Iowa, on July 5, 1922. He attended Cornell College and Iowa State University, receiving the B.A. degree in physics from the latter in 1942. He studied in the graduate school of the University of California in Berkeley and at Princeton University from which he received the M.A. degree in 1948 and the Ph.D. degree in theoretical physics in 1950.

E. T. Jaynes

From 1942 to 1946 he was engaged in microwave research and development as a project engineer at the Sperry Gyroscope Co., in Garden City, N. Y., and in the combined research group of the Naval Research Laboratory.

Since 1950, he has been on the faculty of Stanford University, and at present holds the titles of associate professor in the microwave laboratory and lecturer in physics.

❖

Kenneth S. Kelleher was born on December 25, 1922, in Richmond, Va. He received the Bachelor of Arts degree in Mathematics from the University of North Carolina in 1943 and the Master of Arts degree in Mathematics from the University of Maryland in 1948.

K. S. Kelleher

From 1943 to 1953 he was engaged in the design and development of antennas at the Naval Research Laboratory. In 1953, he left his position as head of the Microwave Optics Section at the Naval Research Laboratory to accept his present position as head of the Antenna Section at Melpar, Inc.

Robin I. Primich (S'48–A'50–M'55) was born in Johannesburg, South Africa, on June 17, 1927. He received the B.S. degree in electrical engineering from the University of the Witwatersrand in 1949.

R. I. Primich

From 1950 to 1954 he studied at Imperial College, London, Eng., on a scholarship from the Witwatersrand University and with financial assistance from the Department of Scientific and Industrial Research, England.

In 1954 he was awarded the diploma of Imperial College and the Ph.D. degree from the University of London. Since the beginning of 1955, he has been with the Radio Physics Laboratory, Defence Research Board, Ottawa, Can., engaged in microwave work.

❖

Peter D. Strum (A'45–SM'55) was born in Brunswick County, Va., on April 25, 1922. He received the B.E.E. degree with honors from North Carolina State College in 1945 and the M.S. degree in electrical engineering from Stanford University in 1947.

P. D. Strum

Mr. Strum was an instructor at North Carolina State College in 1944 and 1945, following the completion of his undergraduate studies.

In 1947 he joined the engineering staff of Airborne Instruments Laboratory in Mineola, N.Y., where he participated in receiver research and the development of receivers, beacons, automatic direction finders, and test equipment. In 1952, he was appointed assistant supervising engineer of the newly-formed Applied Electronics Section of the Laboratory.

In May, 1955, Mr. Strum joined the staff of National Company, Malden, Mass., as chief engineer of the Receiver Department, concerned with the development of communication receivers.

Since October, 1955, he has been with Ewen Knight Corp., Needham, Mass., as director of the Radio Astronomy Engineering Division, concerned with the development of radio astronomy receivers.

Mr. Strum is a member of Sigma Xi, Tau Beta Pi, and Eta Kappa Nu.

❖

R. D. Tompkins was born on July 27, 1926 in Paterson, N.J. After serving as an electronics technician in the Navy during World War II, he attended Case Institute of Technology where he received the B.S. degree in electrical engineering in 1950.

From 1950 to 1952 Mr. Tompkins was employed by the Radar Division of the Naval Research Laboratory. In 1952 he left the Naval Research Laboratory to accept a position as electrical engineer for the Bethlehem Chile Iron Mines Company in El Tofo, Chile. Returning to the United States in 1954, he rejoined the staff of the Naval Research Laboratory, where he is working currently on microwave systems and techniques for the Tracking Branch of the Radar Division.

R. D. Tompkins

He is a member of Eta Kappa Nu.

❖

For a photo and biography of P. H. Vartanian, see p. 63 of Transactions of the IRE, Vol. MTT-4, No. 1; January, 1956.

❖

James R. Wait (SM'56) was born in Ottawa, Can., in January, 1924. He attended McGill University for a brief period before enlisting in the Canadian Army in 1942. By the end of the war he was in charge of a radar maintenance group at Kingston, Ontario.

He received the B.A.S. and M.A.S. degrees in engineering physics from the University of Toronto in 1948 and 1949 respectively. At this time he was employed as a junior research engineer at the Hydro Electric Power Commission of Ontario, where he assisted in the development of an infra-red bolometer. Returning to further graduate work to the University of Toronto, he obtained a Ph.D. degree in electromagnetic theory in 1951.

J. R. Wait

From 1949 to 1952 Dr. Wait was associated with Newmont Exploration Limited of Jerome, Ariz., where he conducted theoretical and experimental research in electrical prospecting. From 1952 to 1955 he was a section leader in the Defence Research Telecommunications Establishment in Ottawa where he was mainly concerned with theoretical problems in radiation. He has been associated briefly with McGill University during 1954 and Colorado University in 1955 where he taught graduate extension courses in electrical engineering. At present he is a consulting theoretical physicist to the Radio Propagation Engineering Division of the National Bureau of Standards in Boulder, Colo.

Dr. Wait is a member of RESA and the Canadian Association of Physicists and an associate member of the Society of Exploration Geophysicists.

❖

Frederick L. Wentworth (S'54–A'55) was born in Cumberland, Md. on July 30, 1924. He attended classes in McCoy College of the Johns Hopkins University, Baltimore, Md., from 1947 to 1955, when he was awarded the Bachelor of Science degree in electrical engineering.

F. L. Wentworth

In 1952 he joined the Radiation Laboratory of The Johns Hopkins University as a research assistant, working with problems of the proximity fuse.

In 1954 he was employed by The Glenn L. Martin Company, Baltimore, Md. as an engineer in the radio frequency section.

Tables of Constants for Rectangular Waveguides (In Decimal Frequencies)

Sperry Gyroscope Company
Division of Sperry Rand Corporation
Great Neck, N. Y.

Foreword

The Professional Group on Microwave Theory and Techniques is especially pleased to be able to publish "Tables of Constants for Rectangular Waveguides."

We are deeply indebted to the Microwave Electronics Division of the Sperry Gyroscope Company for providing us with these invaluable tables for publication.

The tables should be of great value to every microwave engineer and in fact will undoubtedly become fully as indispensable as his slide rule.

We would especially like to thank Hugh E. Webber, Chief Engineer of the Microwave Electronics Division of the Sperry Gyroscope Company, for his part in making these tables available. We would also like to thank Dr. Kiyo Tomiyasu for suggesting their publication.

Tables of Constants for Rectangular Waveguides (In Decimal Frequencies)*

Introduction

IN FREE SPACE, the frequency f, wavelength λ, and phase velocity c, of an electromagnetic wave are related by the equation $f\lambda = c$. The phase velocity in free space is a constant but the phase velocity of an electromagnetic wave in a uniform waveguide with air dielectric is greater than that in free space and is a function of frequency. Hence, the waveguide wavelength λ_g is greater than λ and the ratio λ_g/λ is frequency dependent. This set of tables has been compiled to provide conveniently waveguide wavelengths and other useful waveguide data as a function of frequency.

These tables have been calculated for the dominant mode (TE_{10}) propagation in eleven different sizes of rectangular waveguides which cover the frequency range from 1000 to 42,000 mc. As a function of frequency, the following are tabulated:

1) λ (cm) = free space wavelength in centimeters.
2) λ_g (cm) = waveguide wavelength in centimeters.
3) λ_g (*in*) = waveguide wavelength in inches.
4) λ_g/λ (dimensionless).
5) λ/λ_g (dimensionless).
6) $1/\lambda_g$ in inches^{-1}.

The ratio λ_g/λ is useful in scaling between waveguides as well as in determining the operating ranges of waveguides. This ratio ranges from about 2 to 1.15. The TE_{20} mode can propagate when $\lambda_g/\lambda = 1.154700$. The ratio λ/λ_g is useful in the design of certain antennas as it is equal to the index of refraction. The quantity $1/\lambda_g$ is an important factor in the equivalent circuits of some waveguide discontinuities.

Discussion of Tables

The dominant mode waveguide wavelengths have been calculated using the formula[1]

$$\lambda_g = \frac{\lambda}{\sqrt{1-\left(\frac{\lambda}{2a}\right)^2}} = \frac{1}{\sqrt{\left(\frac{f}{c}\right)^2-\left(\frac{1}{2a}\right)^2}}$$

where

λ = free space wavelength,
f = frequency (cps),
c = velocity of propagation in free space,
a = inside wide dimension of rectangular waveguide.

All calculations are based on the following conditions:

1) Vacuo (zero loss) dielectric (*i.e.*, $\epsilon_r = \mu_r = 1.00000000$).
2) Infinitely conducting waveguide walls.
3) Unslotted waveguide transmission line.
4) Perfect rectangular internal cross section.
5) Parallel and plane waveguide walls.
6) Zero waveguide dimensional tolerances.
7) Zero frequency error (to eight decimals).
8) One inch = 2.54000000 centimeters.
9) Free space phase velocity = $2.99776000 \times 10^{10}$ cm per second.

The effect due to finite conductivity is to reduce very slightly the waveguide wavelength while a slotted waveguide will increase it by a small amount.[2] The effect due to an increase in the wide a dimension of the waveguide is to shorten the wavelength, which is independent of the narrow b dimension. The effect of dielectric loss is considered by Moreno.[3]

The waveguide wavelengths were computed to seven significant figures but are tabulated with only four digits to the right of the decimal point believing that this would be completely adequate for all practical purposes. The numbers were rounded off in accordance with the general practice of increasing the last desired digit to the next higher value only if the following digit is between 5 and 9 inclusive. The actual accuracy of the computations as a function of the tolerances of the parameters is described in the Appendix following the tables.

Since the relationship between waveguide wavelength and frequency is an analytical function, the first and all higher order derivatives are also analytical. Thus for equal frequency increments the wavelength differences must behave as a continuous monotonic function. This fact was used to check the calculations by taking first and second differences.

For most applications a linear interpolation to determine the values of the constants at points between those listed in the tables should be adequate. For greater accuracy a Taylor's series expansion can be used as described in the Appendix.

It is hoped that there will not be any errors in these tables; however, if any are discovered and reported, the subsequent printings of these tables will be corrected. For reference purposes, all original calculations will be kept on file.

* Copies of these tables are available on request from the Microwave Electronics Div., Sperry Gyroscope Co., Div. of Sperry Rand Corp., Great Neck, N.Y.

[1] T. Moreno, "Microwave Transmission Design Data," McGraw-Hill Book Co., Inc., New York, N.Y.; 1948.

[2] C. G. Montgomery, "Technique of Microwave Measurements," vol. 11, M.I.T. Radiation Lab. Series, McGraw-Hill Book Co., Inc., New York, N.Y., Ch. 8; 1947.

[3] Moreno, *op. cit.*, p. 139.

TABLE I

Outside Dimensions = 6.660″×3.410″
Wall Thickness = 0.080″

Inside Dimensions a = 6.500″ = 16.510 cm
b = 3.250″ = 8.255 cm
a/b = 2.000

Cutoff Wavelength = 13.000″ = 33.020 cm
Cutoff Frequency = 907.862 mc

F (mc)	λ (cm)	λ_g (cm)	λ_g (in)	λ_g/λ	λ/λ_g	$1/\lambda_g$ (in)
1000	29.9776	71.4996	28.1495	2.3851	0.41927	0.03553
1020	29.3898	64.4737	25.3833	2.1937	0.45584	0.03940
1040	28.8246	59.0886	23.2632	2.0499	0.48782	0.04299
1060	28.2808	54.7874	21.5698	1.9373	0.51619	0.04636
1080	27.7570	51.2466	20.1758	1.8463	0.54164	0.04956
1100	27.2524	48.2640	19.0016	1.7710	0.56465	0.05263
1120	26.7657	45.7055	17.9943	1.7076	0.58561	0.05557
1140	26.2961	43.4784	17.1175	1.6534	0.60481	0.05842
1160	25.8428	41.5161	16.3449	1.6065	0.62248	0.06118
1180	25.4047	39.7696	15.6573	1.5654	0.63880	0.06387
1200	24.9813	38.2016	15.0400	1.5292	0.65393	0.06649
1210	24.7749	37.4753	14.7541	1.5126	0.66110	0.06778
1220	24.5718	36.7834	14.4817	1.4970	0.66801	0.06905
1230	24.3720	36.1232	14.2217	1.4822	0.67469	0.07032
1240	24.1755	35.4923	13.9734	1.4681	0.68115	0.07156
1250	23.9821	34.8887	13.7357	1.4548	0.68739	0.07280
1260	23.7917	34.3103	13.5080	1.4421	0.69343	0.07403
1270	23.6044	33.7555	13.2896	1.4301	0.69928	0.07525
1280	23.4200	33.2227	13.0798	1.4186	0.70494	0.07645
1290	23.2385	32.7104	12.8781	1.4076	0.71043	0.07765
1300	23.0597	32.2175	12.6840	1.3971	0.71575	0.07884
1310	22.8837	31.7426	12.4971	1.3871	0.72091	0.08002
1320	22.7103	31.2847	12.3168	1.3776	0.72592	0.08119
1330	22.5395	30.8427	12.1428	1.3684	0.73079	0.08235
1340	22.3713	30.4159	11.9748	1.3596	0.73551	0.08351
1350	22.2056	30.0033	11.8123	1.3512	0.74011	0.08466
1360	22.0424	29.6042	11.6552	1.3431	0.74457	0.08580
1370	21.8815	29.2178	11.5031	1.3353	0.74891	0.08693
1380	21.7229	28.8435	11.3557	1.3278	0.75313	0.08806
1390	21.5666	28.4806	11.2128	1.3206	0.75724	0.08918
1400	21.4126	28.1286	11.0743	1.3137	0.76124	0.09030
1420	21.1110	27.4552	10.8091	1.3005	0.76892	0.09251
1440	20.8178	26.8194	10.5588	1.2883	0.77622	0.09471
1460	20.5326	26.2177	10.3219	1.2769	0.78316	0.09688
1480	20.2551	25.6473	10.0974	1.2662	0.78976	0.09904
1500	19.9851	25.1055	9.8841	1.2562	0.79604	0.1012
1520	19.7221	24.5901	9.6811	1.2468	0.80203	0.1033
1540	19.4660	24.0989	9.4878	1.2380	0.80775	0.1054
1560	19.2164	23.6302	9.3032	1.2297	0.81322	0.1075
1580	18.9732	23.1822	9.1268	1.2218	0.81844	0.1096
1600	18.7360	22.7535	8.9581	1.2144	0.82343	0.1116
1620	18.5047	22.3428	8.7964	1.2074	0.82822	0.1137
1640	18.2790	21.9489	8.6413	1.2008	0.83280	0.1157
1660	18.0588	21.5706	8.4924	1.1945	0.83719	0.1178
1680	17.8438	21.2070	8.3492	1.1885	0.84141	0.1198
1700	17.6339	20.8571	8.2115	1.1828	0.84546	0.1218
1720	17.4288	20.5201	8.0788	1.1774	0.84935	0.1238
1740	17.2285	20.1954	7.9509	1.1722	0.85309	0.1258
1760	17.0327	19.8820	7.8276	1.1673	0.85669	0.1278
1780	16.8413	19.5795	7.7084	1.1626	0.86015	0.1297
1800	16.6542	19.2871	7.5934	1.1581	0.86349	0.1317
1820	16.4712	19.0045	7.4821	1.1538	0.86670	0.1337
1840	16.2922	18.7309	7.3744	1.1497	0.86980	0.1356
1860	16.1170	18.4661	7.2701	1.1458	0.87279	0.1376
1880	15.9455	18.2095	7.1691	1.1420	0.87567	0.1395

TABLE II

Outside Dimensions = 4.460″×2.310″
Wall Thickness = 0.080″

Inside Dimensions a = 4.300″ = 10.922 cm
b = 2.150″ = 5.461 cm
a/b = 2.000

Cutoff Wavelength = 8.600″ = 21.844 cm
Cutoff Frequency = 1372.35 mc

F (mc)	λ (cm)	λ_g (cm)	λ_g (in)	λ_g/λ	λ/λ_g	$1/\lambda_g$ (in)
1500	19.9851	49.5070	19.4910	2.4772	0.40368	0.05131
1520	19.7221	45.8726	18.0601	2.3260	0.42993	0.05537
1540	19.4660	42.9015	16.8904	2.2039	0.45374	0.05921
1560	19.2164	40.4123	15.9104	2.1030	0.47551	0.06285
1580	18.9732	38.2866	15.0735	2.0179	0.49556	0.06634
1600	18.7360	36.4429	14.3476	1.9451	0.51412	0.06970
1620	18.5047	34.8234	13.7100	1.8819	0.53139	0.07294
1640	18.2790	33.3857	13.1440	1.8265	0.54751	0.07608
1660	18.0588	32.0978	12.6369	1.7774	0.56262	0.07913
1680	17.8438	30.9351	12.1792	1.7337	0.57682	0.08211
1700	17.6339	29.8783	11.7631	1.6944	0.59019	0.08501
1720	17.4288	28.9122	11.3828	1.6589	0.60282	0.08785
1740	17.2285	28.0243	11.0332	1.6266	0.61477	0.09064
1760	17.0327	27.2045	10.7105	1.5972	0.62610	0.09337
1780	16.8413	16.4445	10.4112	1.5702	0.63686	0.09605
1800	16.6542	25.7372	10.1328	1.5454	0.64709	0.09869
1820	16.4712	25.0768	9.8728	1.5225	0.65683	0.1013
1840	16.2922	24.4582	9.6292	1.5012	0.66612	0.1039
1860	16.1170	23.8772	9.4005	1.4815	0.67500	0.1064
1880	15.9455	23.3301	9.1851	1.4631	0.68348	0.1089
1900	15.7777	22.8136	8.9817	1.4459	0.69159	0.1113
1920	15.6133	22.3250	8.7894	1.4299	0.69936	0.1138
1940	15.4524	21.8619	8.6071	1.4148	0.70682	0.1162
1960	15.2947	21.4221	8.4339	1.4006	0.71397	0.1186
1980	15.1402	21.0037	8.2692	1.3873	0.72084	0.1209
2000	14.9888	20.6050	8.1122	1.3747	0.72744	0.1233
2020	14.8404	20.2244	7.9624	1.3628	0.73379	0.1256
2040	14.6949	19.8607	7.8192	1.3515	0.73990	0.1279
2060	14.5522	19.5127	7.6822	1.3409	0.74578	0.1302
2080	14.4123	19.1792	7.5509	1.3308	0.75146	0.1324
2100	14.2750	18.8592	7.4249	1.3211	0.75693	0.1347
2120	14.1404	18.5519	7.3039	1.3120	0.76221	0.1369
2140	14.0082	18.2564	7.1876	1.3033	0.76730	0.1391
2160	13.8785	17.9721	7.0756	1.2950	0.77223	0.1413
2180	13.7512	17.6981	6.9678	1.2870	0.77699	0.1435
2200	13.6262	17.4340	6.8638	1.2794	0.78159	0.1457
2220	13.5034	17.1790	6.7634	1.2722	0.78604	0.1479
2240	13.3829	16.9328	6.6665	1.2653	0.79035	0.1500
2260	13.2644	16.6948	6.5728	1.2586	0.79452	0.1521
2280	13.1481	16.4646	6.4821	1.2522	0.79857	0.1543
2300	13.0337	16.2417	6.3944	1.2461	0.80248	0.1564
2320	12.9214	16.0259	6.3094	1.2403	0.80628	0.1585
2340	12.8109	15.8166	6.2270	1.2346	0.80997	0.1606
2360	12.7024	15.6136	6.1471	1.2292	0.81354	0.1627
2380	12.5956	15.4167	6.0696	1.2240	0.81701	0.1648
2400	12.4907	15.2254	5.9942	1.2189	0.82038	0.1668
2420	12.3874	15.0395	5.9211	1.2141	0.82366	0.1689
2440	12.2859	14.8589	5.8500	1.2094	0.82684	0.1709
2460	12.1860	14.6832	5.7808	1.2049	0.82993	0.1730
2480	12.0877	14.5122	5.7135	1.2006	0.83294	0.1750
2500	11.9910	14.3457	5.6479	1.1964	0.83586	0.1771
2520	11.8959	14.1836	5.5841	1.1923	0.83871	0.1791
2540	11.8022	14.0256	5.5219	1.1884	0.84148	0.1811
2560	11.7100	13.8716	5.4613	1.1846	0.84417	0.1831
2580	11.6192	13.7214	5.4021	1.1809	0.84680	0.1851
2600	11.5298	13.5749	5.3444	1.1774	0.84935	0.1871

TABLE II (*continued*)

F (mc)	λ (cm)	λ_g (cm)	λ_g (in)	λ_g/λ	λ/λ_g	$1/\lambda_g$ (in)
2620	11.4418	13.4319	5.2881	1.1739	0.85184	0.1891
2640	11.3552	13.2922	5.2332	1.1706	0.85427	0.1911
2660	11.2698	13.1558	5.1795	1.1674	0.85664	0.1931
2680	11.1857	13.0226	5.1270	1.1642	0.85894	0.1950
2700	11.1028	12.8924	5.0757	1.1612	0.86119	0.1970
2720	11.0212	12.7650	5.0256	1.1582	0.86339	0.1990
2740	10.9407	12.6405	4.9766	1.1554	0.86553	0.2009
2760	10.8614	12.5187	4.9286	1.1526	0.86762	0.2029
2780	10.7833	12.3995	4.8817	1.1499	0.86966	0.2048
2800	10.7063	12.2827	4.8357	1.1472	0.87165	0.2068

TABLE III

Outside Dimensions = 3.560″ × 1.860″
Wall Thickness = 0.080″

Inside Dimensions a = 3.400″ = 8.636 cm
b = 1.700″ = 4.318 cm
a/b = 2.000

Cutoff Wavelength = 6.800″ = 17.272 cm
Cutoff Frequency = 1735.62 mc

F (mc)	λ (cm)	λ_g (cm)	λ_g (in)	λ_g/λ	λ/λ_g	$1/\lambda_g$ (in)
1950	15.3731	33.7247	13.2774	2.1937	0.45584	0.07532
1975	15.1785	31.8074	12.5226	2.0956	0.47720	0.07986
2000	14.9888	30.1648	11.8759	2.0125	0.49690	0.08420
2025	14.8038	28.7364	11.3135	1.9412	0.51516	0.08839
2050	14.6232	27.4789	10.8185	1.8791	0.53216	0.09243
2075	14.4470	26.3606	10.3782	1.8246	0.54805	0.09636
2100	14.2750	25.3572	9.9831	1.7763	0.56296	0.1002
2125	14.1071	24.4501	9.6260	1.7332	0.57698	0.1039
2150	13.9431	23.6247	9.3011	1.6944	0.59019	0.1075
2175	13.7828	22.8693	9.0037	1.6593	0.60268	0.1111
2200	13.6262	22.1745	8.7301	1.6273	0.61450	0.1146
2225	13.4731	21.5324	8.4773	1.5982	0.62571	0.1180
2250	13.3234	20.9366	8.2428	1.5714	0.63637	0.1213
2275	13.1770	20.3818	8.0243	1.5468	0.64651	0.1246
2300	13.0337	19.8635	7.8203	1.5240	0.65617	0.1279
2325	12.8936	19.3777	7.6290	1.5029	0.66538	0.1311
2350	12.7564	18.9212	7.4493	1.4833	0.67419	0.1342
2375	12.6221	18.4911	7.2800	1.4650	0.68261	0.1374
2400	12.4907	18.0850	7.1201	1.4479	0.69067	0.1405
2425	12.3619	17.7006	6.9687	1.4319	0.69839	0.1435
2450	12.2358	17.3361	6.8252	1.4168	0.70580	0.1465
2475	12.1122	16.9899	6.6889	1.4027	0.71291	0.1495
2500	11.9910	16.6603	6.5592	1.3894	0.71974	0.1525
2525	11.8723	16.3462	6.4355	1.3768	0.72630	0.1554
2550	11.7559	16.0463	6.3175	1.3650	0.73262	0.1583
2575	11.6418	15.7597	6.2046	1.3537	0.73871	0.1612
2600	11.5298	15.4853	6.0966	1.3431	0.74457	0.1640
2625	11.4200	15.2222	5.9930	1.3329	0.75022	0.1669
2650	11.3123	14.9699	5.8936	1.3233	0.75567	0.1697
2675	11.2066	14.7274	5.7982	1.3142	0.76093	0.1725
2700	11.1028	14.4942	5.7064	1.3055	0.76602	0.1752
2725	11.0010	14.2698	5.6180	1.2971	0.77093	0.1780
2750	10.9009	14.0535	5.5329	1.2892	0.77567	0.1807
2775	10.8027	13.8449	5.4508	1.2816	0.78027	0.1835
2800	10.7063	13.6436	5.3715	1.2744	0.78471	0.1862
2825	10.6115	13.4492	5.2949	1.2674	0.78901	0.1889
2850	10.5185	13.2611	5.2209	1.2608	0.79318	0.1915
2875	10.4270	13.0792	5.1493	1.2544	0.79722	0.1942
2900	10.3371	12.9031	5.0800	1.2482	0.80113	0.1969
2925	10.2488	12.7325	5.0128	1.2424	0.80493	0.1995

TABLE III (*continued*)

F (mc)	λ (cm)	λ_g (cm)	λ_g (in)	λ_g/λ	λ/λ_g	$1/\lambda_g$ (in)
2950	10.1619	12.5671	4.9477	1.2367	0.80861	0.2021
2975	10.0765	12.4067	4.8845	1.2313	0.81218	0.2047
3000	9.9925	12.2509	4.8232	1.2260	0.81565	0.2073
3025	9.9100	12.0997	4.7637	1.2210	0.81902	0.2099
3050	9.8287	11.9527	4.7058	1.2161	0.82230	0.2125
3075	9.7488	11.8098	4.6495	1.2114	0.82548	0.2151
3100	9.6702	11.6709	4.5948	1.2069	0.82858	0.2176
3125	9.5928	11.5356	4.5416	1.2025	0.83158	0.2202
3150	9.5167	11.4039	4.4897	1.1983	0.83451	0.2227
3175	9.4418	11.2756	4.4392	1.1942	0.83736	0.2253
3200	9.3680	11.1506	4.3900	1.1903	0.84013	0.2278
3225	9.2954	11.0287	4.3420	1.1865	0.84283	0.2303
3250	9.2239	10.9099	4.2952	1.1828	0.84546	0.2328
3275	9.1535	10.7939	4.2496	1.1792	0.84802	0.2353
3300	9.0841	10.6807	4.2050	1.1758	0.85052	0.2378
3325	9.0158	10.5701	4.1615	1.1724	0.85295	0.2403
3350	8.9485	10.4622	4.1190	1.1692	0.85532	0.2428
3375	8.8823	10.3567	4.0774	1.1660	0.85764	0.2453
3400	8.8169	10.2535	4.0368	1.1629	0.85989	0.2477
3425	8.7526	10.1527	3.9971	1.1600	0.86209	0.2502
3450	8.6892	10.0541	3.9583	1.1571	0.86424	0.2526
3475	8.6266	9.9576	3.9203	1.1543	0.86634	0.2551
3500	8.5650	9.8632	3.8831	1.1516	0.86838	0.2575
3525	8.5043	9.7707	3.8467	1.1489	0.87038	0.2600

TABLE IV

Outside Dimensions = 3.000″ × 1.500″
Wall Thickness = 0.080″

Inside Dimensions a = 2.840″ = 7.214 cm
b = 1.340″ = 3.404 cm
a/b = 2.1194

Cutoff Wavelength = 5.680″ = 14.427 cm
Cutoff Frequency = 2077.85 mc

F (mc)	λ (cm)	λ_g (cm)	λ_g (in)	λ_g/λ	λ/λ_g	$1/\lambda_g$ (in)
2350	12.7564	27.3086	10.7514	2.1408	0.46712	0.09301
2375	12.6221	26.0611	10.2603	2.0647	0.48433	0.09746
2400	12.4907	24.9595	9.8266	1.9983	0.50044	0.1018
2425	12.3619	23.9771	9.4398	1.9396	0.51557	0.1059
2450	12.2358	23.0937	9.0920	1.8874	0.52983	0.1100
2475	12.1122	22.2936	8.7770	1.8406	0.54330	0.1139
2500	11.9910	21.5642	8.4899	1.7984	0.55606	0.1189
2525	11.8723	20.8958	8.2267	1.7600	0.56817	0.1216
2550	11.7559	20.2800	7.9843	1.7251	0.57968	0.1252
2575	11.6418	19.7104	7.7600	1.6931	0.59064	0.1289
2600	11.5298	19.1813	7.5517	1.6636	0.60110	0.1324
2625	11.4200	18.6881	7.3575	1.6364	0.61109	0.1359
2650	11.3123	18.2268	7.1759	1.6112	0.62066	0.1394
2675	11.2066	17.7942	7.0056	1.5878	0.62979	0.1427
2700	11.1028	17.3874	6.8454	1.5660	0.63856	0.1461
2725	11.0010	17.0038	6.6944	1.5457	0.64697	0.1494
2750	10.9009	16.6413	6.5517	1.5266	0.65505	0.1526
2775	10.8027	16.2981	6.4166	1.5087	0.66282	0.1558
2800	10.7063	15.9724	6.2883	1.4919	0.67030	0.1590
2825	10.6115	15.6628	6.1665	1.4760	0.67750	0.1622
2850	10.5185	15.3680	6.0504	1.4611	0.68444	0.1653
2875	10.4270	15.0869	5.9397	1.4469	0.69113	0.1684
2900	10.3371	14.8184	5.8340	1.4335	0.69759	0.1714
2925	10.2488	14.5616	5.7329	1.4208	0.70382	0.1744
2950	10.1619	14.3156	5.6361	1.4088	0.70985	0.1774
2975	10.0765	14.0798	5.5432	1.3973	0.71567	0.1804
3000	9.9925	13.8534	5.4541	1.3864	0.72131	0.1833
3025	9.9100	13.6358	5.3684	1.3760	0.72676	0.1863

TABLE IV (*continued*)

F (mc)	λ (cm)	λ_g (cm)	λ_g (in)	λ_g/λ	λ/λ_g	$1/\lambda_g$ (in)
3050	9.8287	13.4265	5.2860	1.3660	0.73204	0.1892
3075	9.7488	13.2249	5.2067	1.3566	0.73715	0.1921
3100	9.6702	13.0306	5.1302	1.3475	0.74211	0.1949
3125	9.5928	12.8432	5.0564	1.3388	0.74692	0.1978
3150	9.5167	12.6622	4.9851	1.3305	0.75159	0.2006
3175	9.4418	12.4873	4.9162	1.3226	0.75611	0.2034
3200	9.3680	12.3181	4.8496	1.3149	0.76051	0.2062
3225	9.2954	12.1544	4.7852	1.3076	0.76478	0.2090
3250	9.2239	11.9958	4.7228	1.3005	0.76892	0.2117
3275	9.1535	11.8421	4.6623	1.2937	0.77296	0.2145
3300	9.0841	11.6931	4.6036	1.2872	0.77688	0.2172
3325	9.0158	11.5485	4.5467	1.2809	0.78069	0.2199
3350	8.9485	11.4081	4.4914	1.2749	0.78440	0.2226
3375	8.8823	11.2717	4.4377	1.2690	0.78801	0.2253
3400	8.8169	11.1391	4.3855	1.2634	0.79153	0.2280
3425	8.7526	11.0102	4.3347	1.2579	0.79495	0.2307
3450	8.6892	10.8847	4.2853	1.2527	0.79829	0.2334
3475	8.6266	10.7626	4.2372	1.2476	0.80154	0.2360
3500	8.5650	10.6437	4.1904	1.2427	0.80471	0.2386
3525	8.5043	10.5278	4.1448	1.2379	0.80780	0.2413
3550	8.4444	10.4148	4.1003	1.2333	0.81081	0.2439
3575	8.3853	10.3046	4.0569	1.2289	0.81375	0.2465
3600	8.3271	10.1971	4.0146	1.2246	0.81662	0.2491
3625	8.2697	10.0922	3.9733	1.2204	0.81941	0.2517
3650	8.2130	9.9897	3.9330	1.2163	0.82215	0.2543
3675	8.1572	9.8897	3.8936	1.2124	0.82482	0.2568
3700	8.1021	9.7919	3.8551	1.2086	0.82742	0.2594
3725	8.0477	9.6964	3.8175	1.2049	0.82997	0.2620
3750	7.9940	9.6030	3.7807	1.2013	0.83245	0.2645
3775	7.9411	9.5116	3.7447	1.1978	0.83489	0.2670
3800	7.8888	9.4222	3.7095	1.1944	0.83726	0.2696
3825	7.8373	9.3347	3.6751	1.1911	0.83959	0.2721
3850	7.7864	9.2491	3.6414	1.1879	0.84186	0.2746
3875	7.7362	9.1652	3.6084	1.1847	0.84408	0.2771
3900	7.6866	9.0831	3.5760	1.1817	0.84625	0.2796
3925	7.6376	9.0026	3.5443	1.1787	0.84838	0.2821
3950	7.5893	8.9237	3.5133	1.1758	0.85046	0.2846
3975	7.5415	8.8464	3.4828	1.1730	0.85250	0.2871
4000	7.4944	8.7706	3.4530	1.1703	0.85449	0.2896
4025	7.4479	8.6962	3.4237	1.1676	0.85645	0.2921
4050	7.4019	8.6233	3.3950	1.1650	0.85836	0.2946
4075	7.3565	8.5517	3.3668	1.1625	0.86023	0.2970
4100	7.3116	8.4815	3.3392	1.1600	0.86207	0.2995
4125	7.2673	8.4125	3.3120	1.1576	0.86387	0.3019
4150	7.2235	8.3448	3.2854	1.1552	0.86563	0.3044
4175	7.1803	8.2783	3.2592	1.1529	0.86736	0.3068

TABLE V

Outside Dimensions = 2.000″ × 1.000″
Wall Thickness = 0.064″

Inside Dimensions a = 1.872″ = 4.755 cm
b = 0.872″ = 2.215 cm
a/b = 2.1468

Cutoff Wavelength = 3.744″ = 9.510 cm
Cutoff Frequency = 3152.22 mc

F (mc)	λ (cm)	λ_g (cm)	λ_g (in)	λ_g/λ	λ/λ_g	$1/\lambda_g$ (in)
3600	8.3271	17.2416	6.7880	2.0705	0.48297	0.1473
3650	8.2130	16.2924	6.4143	1.9837	0.50410	0.1559
3700	8.1021	15.4741	6.0922	1.9099	0.52359	0.1641
3750	7.9940	14.7590	5.8106	1.8463	0.54164	0.1721

TABLE V (*continued*)

F (mc)	λ (cm)	λ_g (cm)	λ_g (in)	λ_g/λ	λ/λ_g	$1/\lambda_g$ (in)
3800	7.8888	14.1268	5.5618	1.7907	0.55843	0.1798
3850	7.7864	13.5626	5.3396	1.7418	0.57411	0.1873
3900	7.6866	13.0547	5.1397	1.6984	0.58880	0.1946
3950	7.5893	12.5944	4.9584	1.6595	0.60259	0.2017
4000	7.4944	12.1745	4.7931	1.6245	0.61558	0.2086
4050	7.4019	11.7895	4.6415	1.5928	0.62784	0.2154
4100	7.3116	11.4347	4.5018	1.5639	0.63943	0.2221
4150	7.2235	11.1062	4.3725	1.5375	0.65040	0.2287
4200	7.1375	10.8011	4.2524	1.5133	0.66081	0.2352
4250	7.0536	10.5165	4.1404	1.4910	0.67071	0.2415
4300	6.9715	10.2503	4.0356	1.4703	0.68013	0.2478
4350	6.8914	10.0006	3.9372	1.4512	0.68910	0.2540
4400	6.8131	9.7657	3.8448	1.4334	0.69766	0.2601
4450	6.7365	9.5441	3.7575	1.4168	0.70583	0.2661
4500	6.6617	9.3348	3.6751	1.4013	0.71364	0.2721
4550	6.5885	9.1365	3.5970	1.3867	0.72112	0.2780
4600	6.5169	8.9483	3.5230	1.3731	0.72828	0.2839
4650	6.4468	8.7695	3.4525	1.3603	0.73514	0.2896
4700	6.3782	8.5991	3.3855	1.3482	0.74173	0.2954
4750	6.3111	8.4367	3.3215	1.3368	0.74805	0.3011
4800	6.2453	8.2815	3.2605	1.3260	0.75413	0.3067
4850	6.1809	8.1332	3.2020	1.3158	0.75997	0.3123
4900	6.1179	7.9910	3.1461	1.3062	0.76559	0.3179
4950	6.0561	7.8548	3.0924	1.2970	0.77101	0.3234
5000	5.9955	7.7240	3.0409	1.2883	0.77622	0.3288
5050	5.9362	7.5983	2.9914	1.2800	0.78125	0.3343
5100	5.8780	7.4774	2.9438	1.2721	0.78610	0.3397
5125	5.8493	7.4186	2.9207	1.2683	0.78846	0.3424
5150	5.8209	7.3609	2.8980	1.2646	0.79078	0.3451
5175	5.7928	7.3043	2.8757	1.2609	0.79306	0.3477
5200	5.7649	7.2487	2.8538	1.2574	0.79530	0.3504
5225	5.7373	7.1941	2.8323	1.2539	0.79751	0.3531
5250	5.7100	7.1405	2.8112	1.2505	0.79967	0.3557
5275	5.6830	7.0877	2.7905	1.2472	0.80180	0.3584
5300	5.6562	7.0359	2.7701	1.2439	0.80389	0.3610
5325	5.6296	6.9850	2.7500	1.2408	0.80595	0.3636
5350	5.6033	6.9350	2.7303	1.2377	0.80798	0.3663
5375	5.5772	6.8875	2.7109	1.2346	0.80997	0.3689
5400	5.5514	6.8373	2.6919	1.2316	0.81193	0.3715
5425	5.5258	6.7897	2.6731	1.2287	0.81385	0.3741
5450	5.5005	6.7428	2.6547	1.2259	0.81575	0.3767
5475	5.4754	6.6967	2.6365	1.2231	0.81762	0.3793
5500	5.4505	6.6513	2.6186	1.2203	0.81945	0.3819
5525	5.4258	6.6067	2.6011	1.2176	0.82126	0.3845
5550	5.4014	6.5627	2.5837	1.2150	0.82304	0.3870
5575	5.3771	6.5194	2.5667	1.2124	0.82479	0.3896
5600	5.3531	6.4767	2.5499	1.2099	0.82652	0.3922
5625	5.3294	6.4347	2.5334	1.2074	0.82822	0.3947
5650	5.3058	6.3933	2.5171	1.2050	0.82989	0.3973
5675	5.2824	6.3526	2.5010	1.2026	0.83154	0.3998
5700	5.2592	6.3124	2.4852	1.2003	0.83316	0.4024
5725	5.2363	6.2728	2.4696	1.1980	0.83476	0.4049
5750	5.2135	6.2338	2.4542	1.1957	0.83633	0.4075
5775	5.1909	6.1953	2.4391	1.1935	0.83788	0.4100
5800	5.1686	6.1574	2.4242	1.1913	0.83941	0.4125
5825	5.1464	6.1200	2.4094	1.1892	0.84092	0.4150
5850	5.1244	6.0831	2.3949	1.1871	0.84240	0.4176
5875	5.1026	6.0467	2.3806	1.1850	0.84386	0.4201
5900	5.0809	6.0108	2.3665	1.1830	0.84530	0.4226
5925	5.0595	5.9754	2.3525	1.1810	0.84672	0.4251
5950	5.0383	5.9405	2.3388	1.1791	0.84812	0.4276
5975	5.0172	5.9048	2.3247	1.1769	0.84968	0.4302
6000	4.9963	5.8720	2.3118	1.1753	0.85087	0.4326
6050	4.9550	5.8053	2.2855	1.1716	0.85353	0.4375

TABLE V (*continued*)

F (mc)	λ (cm)	λ_g (cm)	λ_g (in)	λ_g/λ	λ/λ_g	$1/\lambda_g$ (in)
6100	4.9144	5.7402	2.2599	1.1681	0.85612	0.4425
6150	4.8744	5.6769	2.2350	1.1646	0.85865	0.4474
6200	4.8351	5.6150	2.2106	1.1613	0.86110	0.4524
6250	4.7964	5.5547	2.1869	1.1581	0.86349	0.4573
6300	4.7583	5.4958	2.1637	1.1550	0.86582	0.4622
6350	4.7209	5.4383	2.1411	1.1520	0.86808	0.4671
6400	4.6840	5.3822	2.1190	1.1491	0.87028	0.4719

TABLE VI

Outside Dimensions = 1.500″ × 0.750″
Wall Thickness = 0.064″

Inside Dimensions a = 1.372″ = 3.485 cm
b = 0.622″ = 1.580 cm
a/b = 2.2058

Cutoff Wavelength = 2.744″ = 6.970 cm
Cutoff Frequency = 4300.95 mc

F (mc)	λ (cm)	λ_g (cm)	λ_g (in)	λ_g/λ	λ/λ_g	$1/\lambda_g$ (in)
4900	6.1179	12.7700	5.0275	2.0873	0.47908	0.1989
4950	6.0561	12.2350	4.8169	2.0203	0.49498	0.2076
5000	5.9955	11.7575	4.6289	1.9610	0.50993	0.2160
5050	5.9362	11.3278	4.4598	1.9083	0.52403	0.2242
5100	5.8780	10.9384	4.3065	1.8609	0.53737	0.2322
5150	5.8209	10.5833	4.1666	1.8182	0.55001	0.2400
5200	5.7649	10.2576	4.0384	1.7793	0.56201	0.2476
5250	5.7100	9.9576	3.9203	1.7439	0.57343	0.2551
5300	5.6562	9.6799	3.8110	1.7114	0.58432	0.2624
5350	5.6033	9.4218	3.7094	1.6815	0.59471	0.2696
5400	5.5514	9.1813	3.6147	1.6539	0.60465	0.2767
5450	5.5005	8.9562	3.5261	1.6283	0.61415	0.2836
5500	5.4505	8.7451	3.4429	1.6045	0.62326	0.2905
5550	5.4014	8.5465	3.3647	1.5823	0.63200	0.2972
5600	5.3531	8.3592	3.2910	1.5615	0.64039	0.3039
5650	5.3058	8.1821	3.2213	1.5421	0.64846	0.3104
5700	5.2592	8.0145	3.1553	1.5239	0.65622	0.3169
5750	5.2135	7.8554	3.0927	1.5067	0.66368	0.3233
5800	5.1686	7.7041	3.0331	1.4906	0.67088	0.3297
5850	5.1244	7.5601	2.9764	1.4753	0.66782	0.3360
5900	5.0809	7.4227	2.9223	1.4609	0.68452	0.3422
5950	5.0383	7.2914	2.8706	1.4472	0.69099	0.3484
6000	4.9963	7.1659	2.8212	1.4342	0.69723	0.3545
6050	4.9550	7.0456	2.7739	1.4219	0.70327	0.3605
6100	4.9144	6.9303	2.7285	1.4102	0.70911	0.3665
6150	4.8744	6.8196	2.6849	1.3991	0.71477	0.3725
6200	4.8351	6.7131	2.6430	1.3884	0.72024	0.3784
6250	4.7964	6.6107	2.6027	1.3783	0.72555	0.3842
6300	4.7583	6.5121	2.5638	1.3686	0.73069	0.3900
6350	4.7209	6.4171	2.5264	1.3593	0.73568	0.3958
6400	4.6840	6.3253	2.4903	1.3504	0.74051	0.4016
6450	4.6477	6.2368	2.4554	1.3419	0.74521	0.4073
6500	4.6119	6.1512	2.4217	1.3338	0.74977	0.4120
6550	4.5767	6.0684	2.3891	1.3250	0.75419	0.4186
6600	4.5421	5.9882	2.3576	1.3184	0.75850	0.4242
6650	4.5079	5.9106	2.3270	1.3112	0.76268	0.4297
6700	4.4743	5.8354	2.2974	1.3042	0.76675	0.4353
6750	4.4411	5.7624	2.2687	1.2975	0.77070	0.4408
6800	4.4085	5.6916	2.2408	1.2911	0.77455	0.4463
6850	4.3763	5.6229	2.2137	1.2849	0.77830	0.4517
6900	4.3446	5.5561	2.1874	1.2789	0.78195	0.4572
6950	4.3133	5.4912	2.1619	1.2731	0.78550	0.4626

TABLE VI (*continued*)

F (mc)	λ (cm)	λ_g (cm)	λ_g (in)	λ_g/λ	λ/λ_g	$1/\lambda_g$ (in)
7000	4.2825	5.4280	2.1370	1.2675	0.78896	0.4679
7050	4.2521	5.3666	2.1128	1.2621	0.79234	0.4733
7100	4.2222	5.3067	2.0893	1.2569	0.79563	0.4786
7150	4.1927	5.2485	2.0663	1.2518	0.79884	0.4840
7200	4.1636	5.1917	2.0440	1.2469	0.80197	0.4892
7250	4.1348	5.1363	2.0222	1.2422	0.80502	0.4945
7300	4.1065	5.0824	2.0009	1.2376	0.80800	0.4998
7350	4.0786	5.0297	1.9802	1.2332	0.81090	0.5050
7400	4.0510	4.9783	1.9599	1.2289	0.81374	0.5102
7450	4.0238	4.9281	1.9402	1.2247	0.81651	0.5154
7500	3.9970	4.8790	1.9209	1.2207	0.81922	0.5206
7550	3.9705	4.8311	1.9020	1.2167	0.82187	0.5258
7600	3.9444	4.7843	1.8836	1.2129	0.82445	0.5309
7650	3.9186	4.7385	1.8655	1.2092	0.82698	0.5360
7700	3.8932	4.6937	1.8479	1.2056	0.82945	0.5412
7750	3.8681	4.6499	1.8307	1.2021	0.83187	0.5463
7800	3.8433	4.6070	1.8138	1.1987	0.83423	0.5513
7850	3.8188	4.5650	1.7972	1.1954	0.83654	0.5564
7900	3.7946	4.5239	1.7811	1.1922	0.83880	0.5615
7950	3.7708	4.4836	1.7652	1.1890	0.84101	0.5665
8000	3.7472	4.4441	1.7497	1.1860	0.84318	0.5715
8050	3.7239	4.4055	1.7344	1.1830	0.84530	0.5766
8100	3.7009	4.3675	1.7195	1.1801	0.84737	0.5816
8150	3.6782	4.3304	1.7049	1.1773	0.84941	0.5866
8200	3.6558	4.2939	1.6905	1.1745	0.85140	0.5915
8250	3.6336	4.2581	1.6764	1.1719	0.85335	0.5965
8300	3.6118	4.2230	1.6626	1.1692	0.85526	0.6015
8350	3.5901	4.1885	1.6490	1.1667	0.85713	0.6064
8400	3.5688	4.1547	1.6357	1.1642	0.85897	0.6114
8450	3.5476	4.1215	1.6226	1.1618	0.86077	0.6163
8500	3.5268	4.0889	1.6098	1.1594	0.86253	0.6212
8550	3.5062	4.0568	1.5972	1.1571	0.86426	0.6261
8600	3.4858	4.0254	1.5848	1.1548	0.86595	0.6310
8650	3.4656	3.9944	1.5726	1.1526	0.86762	0.6359

TABLE VII

Outside Dimensions = 1.250″ × 0.625″
Wall Thickness = 0.064″

Inside Dimensions a = 1.122″ = 2.850 cm
b = 0.497″ = 1.262 cm
a/b = 2.2575

Cutoff Wavelength = 2.244″ = 5.700 cm
Cutoff Frequency = 5259.23 mc

F (mc)	λ (cm)	λ_g (cm)	λ_g (in)	λ_g/λ	λ/λ_g	$1/\lambda_g$ (in)
6000	4.9963	10.3813	4.0871	2.0778	0.48128	0.2447
6050	4.9550	10.0254	3.9470	2.0233	0.49424	0.2534
6100	4.9144	9.7012	3.8194	1.9741	0.50657	0.2618
6150	4.8744	9.4043	3.7025	1.9293	0.51832	0.2701
6200	4.8351	9.1310	3.5949	1.8885	0.52953	0.2782
6250	4.7964	8.8782	3.4953	1.8510	0.54025	0.2861
6300	4.7583	8.6435	3.4030	1.8165	0.55051	0.2939
6350	4.7209	8.4248	3.3169	1.7846	0.56035	0.3015
6400	4.6840	8.2204	3.2364	1.7550	0.56980	0.3090
6450	4.6477	8.0288	3.1609	1.7275	0.57888	0.3164
6500	4.6119	7.8486	3.0900	1.7018	0.58762	0.3236
6550	4.5767	7.6787	3.0231	1.6778	0.59603	0.3308
6600	4.5421	7.5183	2.9599	1.6553	0.60414	0.3378
6650	4.5079	7.3664	2.9001	1.6341	0.61196	0.3448
6700	4.4743	7.2222	2.8434	1.6142	0.61951	0.3517
6750	4.4411	7.0853	2.7895	1.5954	0.62681	0.3585

TABLE VII (*continued*)

F (mc)	λ (cm)	λ_g (cm)	λ_g (in)	λ_g/λ	λ/λ_g	$1/\lambda_g$ (in)
6800	4.4085	6.9549	2.7381	1.5776	0.63387	0.3652
6850	4.3763	6.8306	2.6892	1.5608	0.64069	0.3719
6900	4.3446	6.7118	2.6425	1.5449	0.64730	0.3784
6950	4.3133	6.5983	2.5977	1.5297	0.65370	0.3850
7000	4.2825	6.4895	2.5549	1.5154	0.65991	0.3914
7050	4.2521	6.3853	2.5138	1.5017	0.66593	0.3978
7100	4.2222	6.2852	2.4745	1.4886	0.67177	0.4041
7150	4.1927	6.1890	2.4366	1.4762	0.67744	0.4104
7200	4.1636	6.0965	2.4002	1.4643	0.68294	0.4166
7250	4.1348	6.0074	2.3651	1.4529	0.68829	0.4228
7300	4.1065	5.9215	2.3313	1.4420	0.69349	0.4289
7350	4.0786	5.8387	2.2987	1.4316	0.69854	0.4350
7400	4.0510	5.7587	2.2672	1.4215	0.70346	0.4411
7450	4.0238	5.6814	2.2368	1.4119	0.70825	0.4471
7500	3.9970	5.6066	2.2073	1.4027	0.71291	0.4530
7550	3.9075	5.5343	2.1788	1.3938	0.71745	0.4590
7600	3.9444	5.4642	2.1512	1.3853	0.72187	0.4649
7650	3.9186	5.3962	2.1245	1.3771	0.72618	0.4707
7700	3.8932	5.3304	2.0986	1.3692	0.73038	0.4765
7750	3.8681	5.2664	2.0734	1.3615	0.73448	0.4823
7800	3.8433	5.2044	2.0490	1.3542	0.73847	0.4881
7850	3.8188	5.1441	2.0252	1.3470	0.74237	0.4938
7900	3.7946	5.0854	2.0021	1.3402	0.74618	0.4995
7950	3.7708	5.0284	1.9797	1.3335	0.74989	0.5051
8000	3.7472	4.9729	1.9578	1.3271	0.75352	0.5108
8050	3.7239	4.9189	1.9366	1.3209	0.75706	0.5164
8100	3.7009	4.8663	1.9159	1.3149	0.76052	0.5220
8150	3.6782	4.8150	1.8957	1.3091	0.76391	0.5275
8200	3.6558	4.7650	1.8760	1.3034	0.76721	0.5331
8250	3.6336	4.7163	1.8568	1.2980	0.77045	0.5386
8300	3.6118	4.6687	1.8381	1.2926	0.77361	0.5441
8350	3.5901	4.6223	1.8198	1.2875	0.77670	0.5495
8400	3.5688	4.5769	1.8019	1.2825	0.77973	0.5550
8450	3.5476	4.5327	1.7845	1.2777	0.78269	0.5604
8500	3.5268	4.4894	1.7675	1.2729	0.78558	0.5658
8550	3.5062	4.4471	1.7508	1.2684	0.78842	0.5712
8600	3.4858	4.4057	1.7345	1.2639	0.79120	0.5765
8650	3.4656	4.3652	1.7186	1.2596	0.79392	0.5819
8700	3.4457	4.3256	1.7030	1.2554	0.79658	0.5872
8750	3.4260	4.2868	1.6877	1.2513	0.79919	0.5925
8800	3.4065	4.2489	1.6728	1.2473	0.80175	0.5978
8850	3.3873	4.2117	1.6582	1.2434	0.80426	0.6031
8900	3.3683	4.1753	1.6438	1.2396	0.80671	0.6083
8950	3.3495	4.1396	1.6298	1.2359	0.80912	0.6136
9000	3.3308	4.1046	1.6160	1.2323	0.81148	0.6188
9050	3.3124	4.0704	1.6025	1.2288	0.81380	0.6240
9100	3.2942	4.0367	1.5893	1.2254	0.81607	0.6292
9150	3.2762	4.0037	1.5763	1.2221	0.81829	0.6344
9200	3.2584	3.9714	1.5635	1.2188	0.82048	0.6396
9250	3.2408	3.9396	1.5510	1.2156	0.82262	0.6447
9300	3.2234	3.9084	1.5388	1.2125	0.82473	0.6499
9350	3.2062	3.8778	1.5267	1.2095	0.82679	0.6550
9400	3.1891	3.8478	1.5149	1.2065	0.82882	0.6601
9450	3.1722	3.8182	1.5032	1.2036	0.83081	0.6652
9500	3.1555	3.7892	1.4918	1.2008	0.83277	0.6703
9550	3.1390	3.7607	1.4806	1.1981	0.83469	0.6754
9600	3.1227	3.7327	1.4696	1.1954	0.83657	0.6805
9650	3.1065	3.7051	1.4587	1.1927	9.83843	0.6855
9700	3.0905	3.6781	1.4481	1.1901	0.84024	0.6906
9750	3.0746	3.6514	1.4376	1.1876	0.84203	0.6956
9800	3.0589	3.6252	1.4273	1.1851	0.84379	0.7006
9850	3.0434	3.5995	1.4171	1.1827	0.84552	0.7057
9900	3.0280	3.5741	1.4071	1.1803	0.84721	0.7107
9950	3.0128	3.5492	1.3973	1.1780	0.84888	0.7157

TABLE VII (*continued*)

F (mc)	λ (cm)	λ_g cm	λ_g (in)	λ_g/λ	λ/λ_g	$1/\lambda_g$ (in)
10000	2.9978	3.5246	1.3876	1.1758	0.85052	0.7206
10050	2.9828	3.5004	1.3781	1.1735	0.85213	0.7256
10100	2.9681	3.4766	1.3688	1.1714	0.85372	0.7306
10150	2.9535	3.4532	1.3595	1.1692	0.85528	0.7355
10200	2.9390	3.4301	1.3504	1.1671	0.85681	0.7405
10250	2.9246	3.4074	1.3415	1.1651	0.85832	0.7454
10300	2.9104	3.3850	1.3327	1.1631	0.85980	0.7504
10350	2.8964	3.3629	1.3240	1.1611	0.86127	0.7553
10400	2.8825	3.3412	1.3154	1.1592	0.86270	0.7602
10450	2.8687	3.3198	1.3070	1.1573	0.86412	0.7651
10500	2.8550	3.2987	1.2987	1.1554	0.86551	0.7700
10550	2.8415	3.2778	1.2905	1.1536	0.86688	0.7749
10600	2.8281	3.2573	1.2824	1.1518	0.86822	0.7798
10650	2.8148	3.2371	1.2744	1.1500	0.86955	0.7847

TABLE VIII

Outside Dimensions = 1.000″ × 0.500″
Wall Thickness = 0.050″

Inside Dimensions a = 0.900″ = 2.286 cm
b = 0.400″ = 1.016 cm
a/b = 2.250

Cutoff Wavelength = 1.800″ = 4.572 cm
Cutoff Frequency = 6556.78 mc

F (mc)	λ (cm)	λ_g (cm)	λ_g (in)	λ_g/λ	λ/λ_g	$1/\lambda_g$ (in)
7500	3.9970	8.2328	3.2413	2.0597	0.48550	0.3085
7600	3.9444	7.8006	3.0711	1.9776	0.50566	0.3256
7700	3.8932	7.4254	2.9234	1.9073	0.52431	0.3421
7800	3.8433	7.0957	2.7936	1.8463	0.54164	0.3580
7900	3.7946	6.8028	2.6783	1.7927	0.55780	0.3734
8000	3.7472	6.5403	2.5749	1.7454	0.57294	0.3884
8100	3.7009	6.3032	2.4816	1.7031	0.58715	0.4030
8200	3.6558	6.0878	2.3967	1.6652	0.60052	0.4172
8300	3.6118	5.8906	2.3191	1.6309	0.61314	0.4312
8350	3.5901	5.7981	2.2827	1.6150	0.61919	0.4381
8400	3.5688	5.7094	2.2478	1.5998	0.62507	0.4449
8450	3.5476	5.6241	2.2142	1.5853	0.63079	0.4516
8500	3.5268	5.5420	2.1819	1.5714	0.63637	0.4583
8550	3.5062	5.4630	2.1508	1.5581	0.64180	0.4649
8600	3.4858	5.3869	2.1208	1.5454	0.64709	0.4715
8650	3.4656	5.3134	2.0919	1.5332	0.65224	0.4780
8700	3.4457	5.2425	2.0640	1.5214	0.65727	0.4845
8750	3.4260	5.1738	2.0369	1.5102	0.66218	0.4909
8800	3.4065	5.1075	2.0108	1.4993	0.66696	0.4973
8850	3.3873	5.0433	1.9856	1.4889	0.67164	0.5036
8900	3.3683	4.9812	1.9611	1.4789	0.67620	0.5099
8950	3.3495	4.9209	1.9374	1.4692	0.68066	0.5162
9000	3.3308	4.8625	1.9144	1.4598	0.68501	0.5224
9050	3.3124	4.8057	1.8920	1.4508	0.68927	0.5285
9100	3.2942	4.7507	1.8703	1.4421	0.69343	0.5347
9150	3.2762	4.6971	1.8493	1.4337	0.69750	0.5408
9200	3.2584	4.6451	1.8288	1.4256	0.70148	0.5468
9250	3.2408	4.5945	1.8089	1.4177	0.70537	0.5528
9300	3.2234	4.5453	1.7895	1.4101	0.70918	0.5588
9350	3.2062	4.4973	1.7706	1.4027	0.71291	0.5648
9400	3.1891	4.4506	1.7522	1.3956	0.71656	0.5707
9450	3.1722	4.4051	1.7343	1.3886	0.72013	0.5766

TABLE VIII (*continued*)

F (mc)	λ (cm)	λ_g (cm)	λ_g (in)	λ_g/λ	λ/λ_g	$1/\lambda_g$ (in)
9500	3.1555	4.3607	1.7168	1.3819	0.72363	0.5825
9550	3.1390	4.3174	1.6998	1.3754	0.72706	0.5883
9600	3.1227	4.2752	1.6831	1.3691	0.73042	0.5941
9650	3.1065	4.2339	1.6669	1.3629	0.73371	0.5999
9700	3.0905	4.1937	1.6510	1.3570	0.73694	0.6057
9750	3.0746	4.1543	1.6356	1.3512	0.74011	0.6114
9800	3.0589	4.1159	1.6204	1.3455	0.74321	0.6171
9900	3.0280	4.0415	1.5911	1.3347	0.74924	0.6285
10000	2.9978	3.9703	1.5631	1.3244	0.75504	0.6397
10100	2.9681	3.9021	1.5363	1.3147	0.76063	0.6509
10200	2.9390	3.8367	1.5105	1.3055	0.76602	0.6620
10300	2.9104	3.7739	1.4858	1.2967	0.77121	0.6730
10400	2.8825	3.7135	1.4620	1.2883	0.77622	0.6840
10500	2.8550	3.6553	1.4391	1.2803	0.78106	0.6949
10600	2.8281	3.5993	1.4170	1.2727	0.78573	0.7057
10700	2.8016	3.5453	1.3958	1.2654	0.79025	0.7164
10800	2.7757	3.4931	1.3752	1.2585	0.79462	0.7271
10900	2.7502	3.4428	1.3554	1.2518	0.79884	0.7378
11000	2.7252	3.3941	1.3363	1.2454	0.80293	0.7484
11100	2.7007	3.3470	1.3177	1.2393	0.80689	0.7589
11200	2.6766	3.3015	1.2998	1.2335	0.81073	0.7694
11300	2.6529	3.2573	1.2824	1.2278	0.81444	0.7798
11400	2.6296	3.2145	1.2656	1.2224	0.81804	0.7902
11500	2.6067	3.1730	1.2492	1.2172	0.82154	0.8005
11600	2.5843	3.1327	1.2334	1.2122	0.82493	0.8108
11700	2.5622	3.0936	1.2180	1.2074	0.82822	0.8210
11800	2.5405	3.0556	1.2030	1.2028	0.83141	0.8313
11900	2.5191	3.0187	1.1885	1.1983	0.83451	0.8414
12000	2.4981	2.9828	1.1743	1.1940	0.83753	0.8516
12100	2.4775	2.9478	1.1606	1.1898	0.84045	0.8617
12200	2.4572	2.9138	1.1472	1.1858	0.84330	0.8717
12300	2.4372	2.8806	1.1341	1.1819	0.84607	0.8818
12400	2.4175	2.8483	1.1214	1.1782	0.84876	0.8918
12500	2.3982	2.8168	1.1090	1.1746	0.85138	0.9017
12600	2.3792	2.7861	1.0969	1.1710	0.85394	0.9117
12700	2.3604	2.7562	1.0851	1.1677	0.85642	0.9216
12800	2.3420	2.7269	1.0736	1.1644	0.85884	0.9314
12900	2.3238	2.6984	1.0624	1.1612	0.86119	0.9413
13000	2.3060	2.6705	1.0514	1.1581	0.86349	0.9511
13100	2.2884	2.6433	1.0407	1.1551	0.86573	0.9609
13200	2.2710	2.6167	1.0302	1.1522	0.86791	0.9707

TABLE IX

Outside Dimensions = 0.702″ × 0.391″
Wall Thickness = 0.040″

Inside Dimensions a = 0.622″ = 1.580 cm
b = 0.311″ = 0.790 cm
a/b = 2.000

Cutoff Wavelength = 1.244″ = 3.160 cm
Cutoff Frequency = 9486.58 mc

F (mc)	λ (cm)	λ_g (cm)	λ_g (in)	λ_g/λ	λ/λ_g	$1/\lambda_g$ (in)
11000	2.7252	5.3847	2.1200	1.9759	0.50611	0.4717
11100	2.7007	5.2024	2.0482	1.9263	0.51912	0.4882
11200	2.6766	5.0361	1.9827	1.8815	0.53148	0.5044
11300	2.6529	4.8834	1.9226	1.8408	0.54325	0.5201
11400	2.6296	4.7426	1.8672	1.8036	0.55446	0.5356
11500	2.6067	4.6123	1.8159	1.7694	0.56517	0.5507
11600	2.5843	4.4911	1.7682	1.7379	0.57542	0.5656
11700	2.5622	4.3781	1.7237	1.7087	0.58523	0.5802

TABLE IX (*continued*)

F (mc)	λ (cm)	λ_g (cm)	λ_g (in)	λ_g/λ	λ/λ_g	$1/\lambda_g$ (in)
11800	2.5405	4.2724	1.6820	1.6817	0.59463	0.5945
11900	2.5191	4.1731	1.6429	1.6566	0.60366	0.6087
12000	2.4981	4.0797	1.6062	1.6331	0.61234	0.6226
12100	2.4775	3.9916	1.5715	1.6111	0.62068	0.6363
12200	2.4572	3.9083	1.5387	1.5906	0.62871	0.6499
12300	2.4372	3.8294	1.5076	1.5712	0.63645	0.6633
12400	2.4175	3.7544	1.4781	1.5530	0.64392	0.6765
12500	2.3982	3.6832	1.4501	1.5358	0.65112	0.6896
12600	2.3792	3.6153	1.4234	1.5196	0.65808	0.7026
12700	2.3604	3.5506	1.3979	1.5042	0.66480	0.7154
12800	2.3420	3.4888	1.3735	1.4897	0.67130	0.7281
12900	2.3238	3.4296	1.3502	1.4758	0.67759	0.7406
13000	2.3060	3.3729	1.3279	1.4627	0.68368	0.7531
13100	2.2884	3.3185	1.3065	1.4502	0.68958	0.7654
13200	2.2710	3.2663	1.2859	1.4382	0.69529	0.7776
13300	2.2540	3.2161	1.2662	1.4269	0.70084	0.7898
13400	2.2371	3.1678	1.2472	1.4160	0.70621	0.8018
13500	2.2206	3.1213	1.2288	1.4056	0.71143	0.8138
13600	2.2042	3.0764	1.2112	1.3957	0.71650	0.8256
13700	2.1881	3.0331	1.1941	1.3862	0.72142	0.8374
13800	2.1723	2.9913	1.1777	1.3770	0.72621	0.8491
13900	2.1567	2.9509	1.1618	1.3683	0.73086	0.8608
14000	2.1413	2.9118	1.1464	1.3598	0.73538	0.8723
14100	2.1261	2.8739	1.1315	1.3518	0.73978	0.8838
14200	2.1111	2.8373	1.1170	1.3440	0.74406	0.8952
14300	2.0963	2.8017	1.1030	1.3365	0.74823	0.9066
14400	2.0818	2.7673	1.0895	1.3293	0.75229	0.9179
14500	2.0674	2.7338	1.0763	1.3223	0.75624	0.9291
14600	2.0533	2.7013	1.0635	1.3156	0.76010	0.9403
14700	2.0393	2.6697	1.0511	1.3091	0.76386	0.9514
14800	2.0255	2.6390	1.0390	1.3029	0.76752	0.9625
14900	2.0119	2.6092	1.0272	1.2969	0.77109	0.9735
15000	1.9985	2.5801	1.0158	1.2910	0.77458	0.9845
15100	1.9853	2.5518	1.0047	1.2854	0.77798	0.9954
15200	1.9722	2.5243	0.9938	1.2799	0.78130	1.006
15300	1.9593	2.4974	0.9832	1.2746	0.78454	1.017
15400	1.9466	2.4712	0.9729	1.2695	0.78771	1.028
15500	1.9340	2.4457	0.9629	1.2645	0.79080	1.039
15600	1.9216	2.4208	0.9531	1.2597	0.79382	1.049
15700	1.9094	2.3964	0.9435	1.2551	0.79677	1.060
15800	1.8973	2.3727	0.9341	1.2505	0.79966	1.071
15900	1.8854	2.3494	0.9250	1.2461	0.80248	1.081
16000	1.8736	2.3268	0.9160	1.2419	0.80524	1.092
16100	1.8620	2.3046	0.9073	1.2377	0.80794	1.102
16200	1.8505	2.2829	0.8988	1.2337	0.81058	1.113
16300	1.8391	2.2617	0.8904	1.2298	0.81316	1.123
16400	1.8279	2.2409	0.8823	1.2260	0.81569	1.133
16500	1.8168	2.2206	0.8743	1.2222	0.81817	1.144
16600	1.8059	2.2007	0.8664	1.2186	0.82059	1.154
16700	1.7951	2.1812	0.8587	1.2151	0.82296	1.164
16800	1.7844	2.1621	0.8512	1.2117	0.82529	1.175
16900	1.7738	2.1434	0.8439	1.2084	0.82756	1.185
17000	1.7634	2.1251	0.8367	1.2051	0.82979	1.195
17100	1.7531	2.1071	0.8296	1.2020	0.83198	1.205
17200	1.7429	2.0895	0.8226	1.1989	0.83412	1.216
17300	1.7328	2.0722	0.8158	1.1959	0.83622	1.226
17400	1.7229	2.0552	0.8091	1.1929	0.83828	1.236
17500	1.7130	2.0386	0.8026	1.1901	0.84030	1.246
17600	1.7033	2.0222	0.7962	1.1873	0.84228	1.256
17700	1.6937	2.0062	0.7898	1.1845	0.84422	1.266
17800	1.6841	1.9904	0.7836	1.1819	0.84612	1.276
17900	1.6747	1.9749	0.7775	1.1793	0.84799	1.286
18000	1.6654	1.9597	0.7715	1.1767	0.84982	1.296
18100	1.6562	1.9448	0.7657	1.1742	0.85162	1.306

TABLE IX (*continued*)

F (mc)	λ (cm)	λ_g (cm)	λ_g (in)	λ_g/λ	λ/λ_g	$1/\lambda_g$ (in)
18200	1.6471	1.9301	0.7599	1.1718	0.85339	1.316
18300	1.6381	1.9157	0.7542	1.1694	0.85512	1.326
18400	1.6292	1.9015	0.7486	1.1671	0.85682	1.336
18500	1.6204	1.8875	0.7431	1.1648	0.85850	1.346
18600	1.6117	1.8738	0.7377	1.1626	0.86014	1.356
18700	1.6031	1.8603	0.7324	1.1604	0.86175	1.365
18800	1.5946	1.8470	0.7272	1.1583	0.86333	1.375
18900	1.5861	1.8339	0.7220	1.1562	0.86489	1.385
19000	1.5778	1.8210	0.7169	1.1542	0.86641	1.395
19100	1.5695	1.8084	0.7120	1.1522	0.86792	1.405
19200	1.5613	1.7959	0.7070	1.1502	0.86939	1.414

TABLE X

Outside Dimensions $=0.500'' \times 0.250''$
Wall Thickness $=0.040''$

Inside Dimensions $a=0.420''=1.067$ cm
$b=0.170''=0.432$ cm
$a/b=2.471$

Cutoff Wavelength $=0.840''=2.134$ cm
Cutoff Frequency $=14{,}047.6$ mc

F (mc)	λ (cm)	λ_g (cm)	λ_g (in)	λ_g/λ	λ/λ_g	$1/\lambda_g$ (in)
16000	1.8736	3.9164	1.5419	2.0903	0.47840	0.6486
16200	1.8505	3.7174	1.4635	2.0089	0.49779	0.6833
16400	1.8279	3.5440	1.3953	1.9388	0.51578	0.7167
16600	1.8059	3.3910	1.3350	1.8778	0.53255	0.7490
16800	1.7844	3.2548	1.2814	1.8240	0.54824	0.7804
17000	1.7634	3.1324	1.2332	1.7763	0.56296	0.8109
17200	1.7429	3.0216	1.1896	1.7337	0.57682	0.8406
17400	1.7229	2.9206	1.1499	1.6952	0.58989	0.8697
17600	1.7033	2.8282	1.1135	1.6605	0.60225	0.8981
17800	1.6841	2.7431	1.0800	1.6288	0.61396	0.9260
18000	1.6654	2.6644	1.0490	1.5998	0.62506	0.9533
18200	1.6471	2.5913	1.0202	1.5732	0.63563	0.9802
18400	1.6292	2.5232	0.9934	1.5487	0.64569	1.007
18600	1.6117	2.4596	0.9683	1.5261	0.65528	1.033
18800	1.5946	2.3999	0.9448	1.5051	0.66443	1.058
19000	1.5778	2.3438	0.9227	1.4855	0.67317	1.084
19200	1.5613	2.2909	0.9019	1.4673	0.68154	1.109
19400	1.5452	2.2409	0.8823	1.4502	0.68955	1.133
19600	1.5295	2.1936	0.8636	1.4343	0.69723	1.158
19800	1.5140	2.1488	0.8460	1.4193	0.70460	1.182
20000	1.4989	2.1061	0.8292	1.4051	0.71167	1.206
20200	1.4840	2.0656	0.8132	1.3918	0.71847	1.230
20400	1.4695	2.0269	0.7980	1.3793	0.72501	1.253
20600	1.4552	1.9899	0.7834	1.3674	0.73131	1.276
20800	1.4412	1.9546	0.7695	1.3562	0.73737	1.300
21000	1.4275	1.9207	0.7562	1.3455	0.74321	1.322
21200	1.4140	1.8883	0.7434	1.3354	0.74884	1.345
21400	1.4008	1.8572	0.7312	1.3258	0.75428	1.368
21600	1.3879	1.8273	0.7194	1.3166	0.75953	1.390
21800	1.3751	1.7985	0.7081	1.3079	0.76460	1.412
22000	1.3626	1.7708	0.6972	1.2996	0.76950	1.434
22200	1.3503	1.7441	0.6866	1.2916	0.77424	1.456
22400	1.3383	1.7183	0.6765	1.2840	0.77882	1.478
22600	1.3264	1.6935	0.6667	1.2767	0.78326	1.500
22800	1.3148	1.6695	0.6573	1.2698	0.78756	1.521
23000	1.3034	1.6463	0.6481	1.2631	0.79172	1.543

TABLE X (*continued*)

F (mc)	λ (cm)	λ_g (cm)	λ_g (in)	λ_g/λ	λ/λ_g	$1/\lambda_g$ (in)
23200	1.2921	1.6238	0.6393	1.2567	0.79576	1.564
23400	1.2811	1.6020	0.6307	1.2505	0.79967	1.585
23600	1.2702	1.5809	0.6224	1.2446	0.80347	1.607
23800	1.2596	1.5605	0.6144	1.2389	0.80715	1.628
24000	1.2491	1.5407	0.6066	1.2335	0.81073	1.649
24200	1.2387	1.5214	0.5990	1.2282	0.81420	1.669
24400	1.2286	1.5027	0.5916	1.2231	0.81757	1.690
24600	1.2186	1.4846	0.5845	1.2183	0.82085	1.711
24800	1.2088	1.4669	0.5775	1.2135	0.82403	1.732
25000	1.1991	1.4497	0.5708	1.2090	0.82713	1.752
25200	1.1896	1.4330	0.5642	1.2046	0.83014	1.773
25400	1.1802	1.4167	0.5578	1.2004	0.83308	1.793
25600	1.1710	1.4008	0.5515	1.1963	0.83593	1.813
25800	1.1619	1.3854	0.5454	1.1923	0.83871	1.833
26000	1.1530	1.3703	0.5395	1.1885	0.84141	1.854
26200	1.1442	1.3556	0.5337	1.1848	0.84405	1.874
26400	1.1355	1.3412	0.5280	1.1812	0.84661	1.894
26600	1.1270	1.3272	0.5225	1.1777	0.84912	1.914
26800	1.1186	1.3136	0.5171	1.1743	0.85156	1.934
27000	1.1103	1.3002	0.5119	1.1711	0.85394	1.954
27200	1.1021	1.2871	0.5067	1.1679	0.85626	1.973
27400	1.0941	1.2744	0.5017	1.1648	0.85812	1.993
27600	1.0861	1.2619	0.4968	1.1618	0.86073	2.013
27800	1.0783	1.2497	0.4920	1.1589	0.86288	2.033
28000	1.0706	1.2377	0.4873	1.1561	0.86499	2.052
28200	1.0630	1.2260	0.4827	1.1534	0.86704	2.072

TABLE XI

Outside Dimensions $=0.360'' \times 0.220''$
Wall Thickness $=0.040''$

Inside Dimensions $a=0.280''=0.711$ cm
$b=0.140''=0.356$ cm
$a/b=2.000$

Cutoff Wavelength $=0.560''=1.422$ cm
Cutoff Frequency $=21{,}075.4$ mc

F (mc)	λ (cm)	λ_g (cm)	λ_g (in)	λ_g/λ	λ/λ_g	$1/\lambda_g$ (in)
24000	1.2491	2.6109	1.0279	2.0903	0.47840	0.9728
24250	1.2362	2.4991	0.9839	2.0216	0.49466	1.016
24500	1.2236	2.3995	0.9447	1.9611	0.50992	1.059
24750	1.2112	2.3101	0.9095	1.9073	0.52431	1.100
25000	1.1991	2.2293	0.8777	1.8591	0.53789	1.139
25250	1.1872	2.1557	0.8487	1.8157	0.55075	1.178
25500	1.1756	2.0882	0.8221	1.7763	0.56296	1.216
25750	1.1642	2.0262	0.7977	1.7405	0.57456	1.254
26000	1.1530	1.9689	0.7751	1.7076	0.58561	1.290
26250	1.1420	1.9156	0.7542	1.6774	0.59615	1.326
26500	1.1312	1.8660	0.7347	1.6496	0.60622	1.361
26750	1.1207	1.8197	0.7164	1.6238	0.61585	1.396
27000	1.1103	1.7763	0.6993	1.5998	0.62507	1.430
27250	1.1001	1.7354	0.6832	1.5775	0.63391	1.464
27500	1.0901	1.6969	0.6681	1.5567	0.64239	1.497
27750	1.0803	1.6606	0.6538	1.5372	0.65054	1.530
28000	1.0706	1.6262	0.6402	1.5189	0.65837	1.562
28250	1.0612	1.5935	0.6274	1.5017	0.66591	1.594
28500	1.0518	1.5625	0.6152	1.4855	0.67317	1.626
28750	1.0427	1.5330	0.6035	1.4702	0.68017	1.657

TABLE XI (*continued*)

F (mc)	λ (cm)	λ_g (cm)	λ_g (in)	λ_g/λ	λ/λ_g	$1/\lambda_g$ (in)
29000	1.0337	1.5049	0.5925	1.4558	0.68692	1.688
29250	1.0249	1.4780	0.5819	1.4421	0.69343	1.719
29500	1.0162	1.4523	0.5718	1.4292	0.69972	1.749
29750	1.0077	1.4277	0.5621	1.4168	0.70580	1.779
30000	0.9993	1.4041	0.5528	1.4051	0.71167	1.809
30250	0.9910	1.3815	0.5439	1.3940	0.71736	1.839
30500	0.9829	1.3597	0.5353	1.3834	0.72286	1.868
30750	0.9749	1.3388	0.5271	1.3733	0.72819	1.897
31000	0.9670	1.3186	0.5191	1.3636	0.73335	1.926
31250	0.9593	1.2992	0.5115	1.3544	0.73836	1.955
31500	0.9517	1.2805	0.5041	1.3455	0.74321	1.984
31750	0.9442	1.2624	0.4970	1.3370	0.74792	2.012
32000	0.9368	1.2449	0.4901	1.3289	0.75249	2.040
32250	0.9295	1.2280	0.4835	1.3211	0.75693	2.068
32500	0.9224	1.2117	0.4770	1.3137	0.76124	2.096
32750	0.9153	1.1959	0.4708	1.3065	0.76543	2.124
33000	0.9084	1.1805	0.4648	1.2996	0.76950	2.152
33250	0.9016	1.1656	0.4589	1.2929	0.77346	2.179
33500	0.8949	1.1512	0.4532	1.2865	0.77731	2.206
33750	0.8882	1.1372	0.4477	1.2803	0.78106	2.234
34000	0.8817	1.1236	0.4424	1.2744	0.78471	2.261
34250	0.8753	1.1104	0.4372	1.2686	0.78826	2.288
34500	0.8689	1.0975	0.4321	1.2631	0.79172	2.314
34750	0.8627	1.0850	0.4272	1.2577	0.79509	2.341
35000	0.8565	1.0728	0.4224	1.2525	0.79838	2.368
35250	0.8504	1.0609	0.4177	1.2475	0.80158	2.394
35500	0.8444	1.0494	0.4131	1.2427	0.80471	2.420
35750	0.8385	1.0381	0.4087	1.2380	0.80775	2.447
36000	0.8327	1.0271	0.4044	1.2335	0.81073	2.473
36250	0.8270	1.0164	0.4002	1.2291	0.81363	2.499
36500	0.8213	1.0059	0.3960	1.2248	0.81646	2.525
36750	0.8157	0.9957	0.3920	1.2207	0.81922	2.551
37000	0.8102	0.9857	0.3881	1.2167	0.82192	2.577
37250	0.8048	0.9760	0.3843	1.2128	0.82456	2.602
37500	0.7994	0.9665	0.3805	1.2090	0.82713	2.628
37750	0.7941	0.9572	0.3768	1.2053	0.82965	2.654
38000	0.7889	0.9481	0.3733	1.2018	0.83211	2.679
38250	0.7837	0.9391	0.3697	1.1983	0.83451	2.705
38500	0.7786	0.9304	0.3663	1.1949	0.83686	2.730
38750	0.7736	0.9219	0.3629	1.1917	0.83916	2.755
39000	0.7687	0.9135	0.3597	1.1885	0.84141	2.780
39250	0.7638	0.9053	0.3564	1.1854	0.84361	2.806
39500	0.7589	0.8973	0.3533	1.1824	0.84577	2.831
39750	0.7542	0.8895	0.3502	1.1794	0.84787	2.856
40000	0.7494	0.8818	0.3471	1.1766	0.84994	2.881
40250	0.7448	0.8742	0.3442	1.1738	0.85196	2.906
40500	0.7402	0.8668	0.3413	1.1711	0.85394	2.930
40750	0.7356	0.8595	0.3384	1.1684	0.85587	2.955
41000	0.7312	0.8524	0.3356	1.1658	0.85777	2.980
41250	0.7267	0.8454	0.3328	1.1633	0.85963	3.005
41500	0.7224	0.8385	0.3301	1.1608	0.86145	3.029
41750	0.7180	0.8318	0.3275	1.1584	0.86324	3.054
42000	0.7138	0.8252	0.3249	1.1561	0.86499	3.078
42250	0.7095	0.8187	0.3223	1.1538	0.86670	3.103

Appendix

Parameter Tolerances

In determining the accuracy of the figures in the tables as a function of the tolerances of the parameters it is convenient to start with the general wavelength equation for the TE_{10} mode.

$$\lambda_g = \frac{\lambda}{\sqrt{\epsilon_r - \left(\frac{\lambda}{2a}\right)^2}} = \frac{1}{\sqrt{\epsilon_r\left(\frac{f}{c}\right)^2 - \left(\frac{1}{2a}\right)^2}}$$

where ϵ_r = dielectric constant of medium inside waveguide. After taking the natural logarithm

$$\ln \lambda_g = -1/2 \ln \left\{\epsilon_r\left(\frac{f}{c}\right)^2 - \left(\frac{1}{2a}\right)^2\right\}$$

and then its derivative, the following equation results

$$\frac{d\lambda_g}{\lambda_g} = -(1/2)h\frac{d\epsilon_r}{\epsilon_r} - h\frac{df}{f} + h\frac{dc}{c} - (h-1)\frac{da}{a}$$

where $h \equiv \epsilon_r(\lambda_g/\lambda)^2$.

As an illustration the following calculations are carried out for X-band waveguide. From various references the following are obtained.

$$\frac{\Delta c}{c} \doteq \frac{1}{75{,}000} \text{ error in velocity of light.}$$

$\epsilon_r = 1.0006$ for dry air at 0°C. and at sea level, thus

$$\frac{\Delta\epsilon_r}{\epsilon_r} \doteq \frac{1}{1700} \text{ by assuming } \epsilon_r = 1.00000000.$$

The accuracy of the better commercial frequency meters is approximately 1 part in 5000 or

$$\frac{\Delta f}{f} = \frac{1}{5000}.$$

The tolerance of the a dimension of commercial waveguide is about 0.003 of an inch so that for X-band waveguide

$$\frac{\Delta a}{a} = \frac{1}{300}.$$

For the usual operating frequency range of rectangular waveguide with air dielectric, the quantity h ranges from about

$$1.3 < h < 4.$$

Under the worst condition at the low frequency end ($h = 4$) of the waveguide band

$$\frac{\Delta\lambda_g}{\lambda_g} = 2\frac{\Delta\epsilon_r}{\epsilon_r} + 4\frac{\Delta f}{f} + 4\frac{\Delta c}{c} + 3\frac{\Delta a}{a}$$

$$= \frac{1}{850} + \frac{1}{1250} + \frac{1}{18{,}750} + \frac{1}{100} \approx 1 \text{ per cent error.}$$

Under the worst condition at the high frequency end ($h = 1.3$)

$$\frac{\Delta\lambda_g}{\lambda_g} = \frac{1}{2620} + \frac{1}{3850} + \frac{1}{58{,}000} + \frac{1}{1000} \approx 0.1 \text{ per cent error.}$$

Thus for X-band waveguide its dimensional tolerance introduces most of the error in λ_g over the entire bandwidth. As expected the effect due to a dimension tolerance is less significant at the high frequency end. In converting from centimeters to U.S. inches, an error of 1 part in 500,000 is introduced by assuming the factor of 2.54 but this is insignificant in relationship to the other tolerances.

Similarly the accuracy of λ_g/λ due to tolerances can be obtained by following the previous formulation which results in the following expression

$$\frac{d\left(\frac{\lambda_g}{\lambda}\right)}{\frac{\lambda_g}{\lambda}} = -(1/2)h\frac{d\epsilon_r}{\epsilon_r} + (h-1)\left\{\frac{dc}{c} - \frac{da}{a} - \frac{df}{f}\right\}.$$

For the example cited the effect due to a dimensional tolerance is again the main contributing factor to inaccuracy.

Interpolation

For most applications, a linear interpolation should result in good accuracy within the usual practical tolerances. However, where the tolerances are very small and high degree of accuracy is desired, a Taylor's series expansion will prove beneficial for interpolation. For waveguide wavelength interpolation,

$$\lambda_g\Big|_{f_2} = \lambda_g\Big|_{f_1} + \frac{\partial\lambda_g}{\partial f}\Big|_{f_1}\Delta f + \frac{1}{2!}\frac{\partial^2\lambda_g}{\partial f^2}\Big|_{f_1}(\Delta f)^2 + \frac{1}{3!}\frac{\partial^3\lambda_g}{\partial f^3}\Big|_{f_1}(\Delta f)^3 + \cdots$$

where

$$\frac{\partial\lambda_g}{\partial f} = -\frac{\lambda_g}{f}\left(\frac{\lambda_g}{\lambda}\right)^2$$

$$\frac{\partial^2\lambda_g}{\partial f^2} = \frac{\lambda_g}{f^2}\left(\frac{\lambda_g}{\lambda}\right)^2\left\{3\left(\frac{\lambda_g}{\lambda}\right)^2 - 1\right\}$$

$$\frac{\partial^3\lambda_g}{\partial f^3} = -\frac{\lambda_g}{f^3}\left(\frac{\lambda_g}{\lambda}\right)^4\left\{15\left(\frac{\lambda_g}{\lambda}\right)^2 - 9\right\}.$$

By letting $\Delta\lambda_g \equiv \lambda_{g2} - \lambda_{g1}$,

$$\Delta\lambda_g = -\lambda_g\left(\frac{\Delta f}{f}\right)\left(\frac{\lambda_g}{\lambda}\right)^2 + (1/2)\lambda_g\left(\frac{\Delta f}{f}\right)^2\left(\frac{\lambda_g}{\lambda}\right)^2\left\{3\left(\frac{\lambda_g}{\lambda}\right)^2 - 1\right\} - (1/6)\lambda_g\left(\frac{\Delta f}{f}\right)^3\left(\frac{\lambda_g}{\lambda}\right)^4\left\{15\left(\frac{\lambda_g}{\lambda}\right)^2 - 9\right\} + \cdots.$$

At the low frequency end of the band ($\lambda_g/\lambda \doteq 2.0$) where the table intervals in frequency are $\Delta f/f \doteq 1/90$,

$$\Delta\lambda_g \doteq \lambda_g\left(-\frac{4}{90}\right)(1 - 0.061 + 0.0042).$$

Thus the second and third terms contribute 6.1 and 0.42 per cent respectively to $\Delta\lambda_g/\lambda_g$. At the high frequency end of the band ($\lambda_g/\lambda \doteq 1.15$) where the intervals are $\Delta f/f \doteq 1/150$,

$$\Delta\lambda_g = \lambda_g\left(\frac{-1.3}{150}\right)(1 - 0.0097 + 0.00018).$$

Thus the second term adds about one per cent correction to $\Delta\lambda_g/\lambda_g$ while the third term is very much smaller.

Similarly Taylor's series expansion can be extended to the other functions of λ_g/λ, λ/λ_g, and $1/\lambda_g$.

INSTITUTIONAL LISTINGS

The IRE Professional Group on Microwave Theory and Techniques is grateful for the assistance given by the firms listed below, and invites application for Institutional Listing from other firms interested in the Microwave field.

AIRCRAFT RADIO CORPORATION, Boonton, N. J.
Airborne Electronic Equipment, Associated Test Equipment

CASCADE RESEARCH CORPORATION, 53 Victory Lane, Los Gatos, Calif.
Res., Dev., & Prod. Microwave Ferrite Devices, Backward Wave Oscillators & Microwave Test Equip.

COLLINS RADIO CO., Cedar Rapids, Iowa
Complete Industrial Microwave, Communication, Navigation and Flight Control Systems

ESPEY MFG. CO., INC., Congress and Ballston St., Saratoga Springs, N. Y.
Mfgrs. of X-Band and S-Band Wavemeters, Attenuators, Thermistor Mounts and Signal Generators

MARYLAND ELECTRONIC MANUFACTURING CORPORATION, College Park, Md.
Development and Production of Microwave Antennas and Waveguide Components

MEASUREMENTS CORPORATION, Box 180, Boonton, N. J.
Specialists in the Design and Development of Electronic Test Instruments

(Please see back cover for additional names.)

INSTITUTIONAL LISTINGS (Continued)

MICROWAVE DEVELOPMENT LABS., INC., 92 Broad St., Babson Park, Mass.
Design, Development & Production of Waveguide Components & Complete RF Assemblies

NATIONAL INSTRUMENT CO., INC., 23 E. 26 St., New York, N. Y.
Wide-Band Microwave Equipment, Simulated Flight Instruments, Lobe Switches, Custom Built Precision Apparatus

RAYTHEON MANUFACTURING CO., 148 California St., Newton, Mass.
Microwave Communications Systems, Radar, Missiles, Cooking Equipment, Tubes & Components

WEINSCHEL ENGINEERING CO. INC., Kensington, Md.
Attenuation Standards, Coaxial Attenuators and Insertion Loss Test Sets

WHEELER LABORATORIES, INC., 122 Cutter Mill Road, Great Neck, N. Y.
Consulting Services, Research & Development, Microwave Antennas & Waveguide Components

The charge for an Institutional Listing is $50.00 per issue or $140.00 for four consecutive issues. Applications for Institutional Listings and checks (made out to the Institute of Radio Engineers) should be sent to Mr. L. G. Cumming, Technical Secretary, Institute of Radio Engineers, 1 East 79th Street, New York 21, N. Y.